Volume 3
Number 5
7 March 2021
Pages 1155–1504

Nanoscale Advances

rsc.li/nanoscale-advances

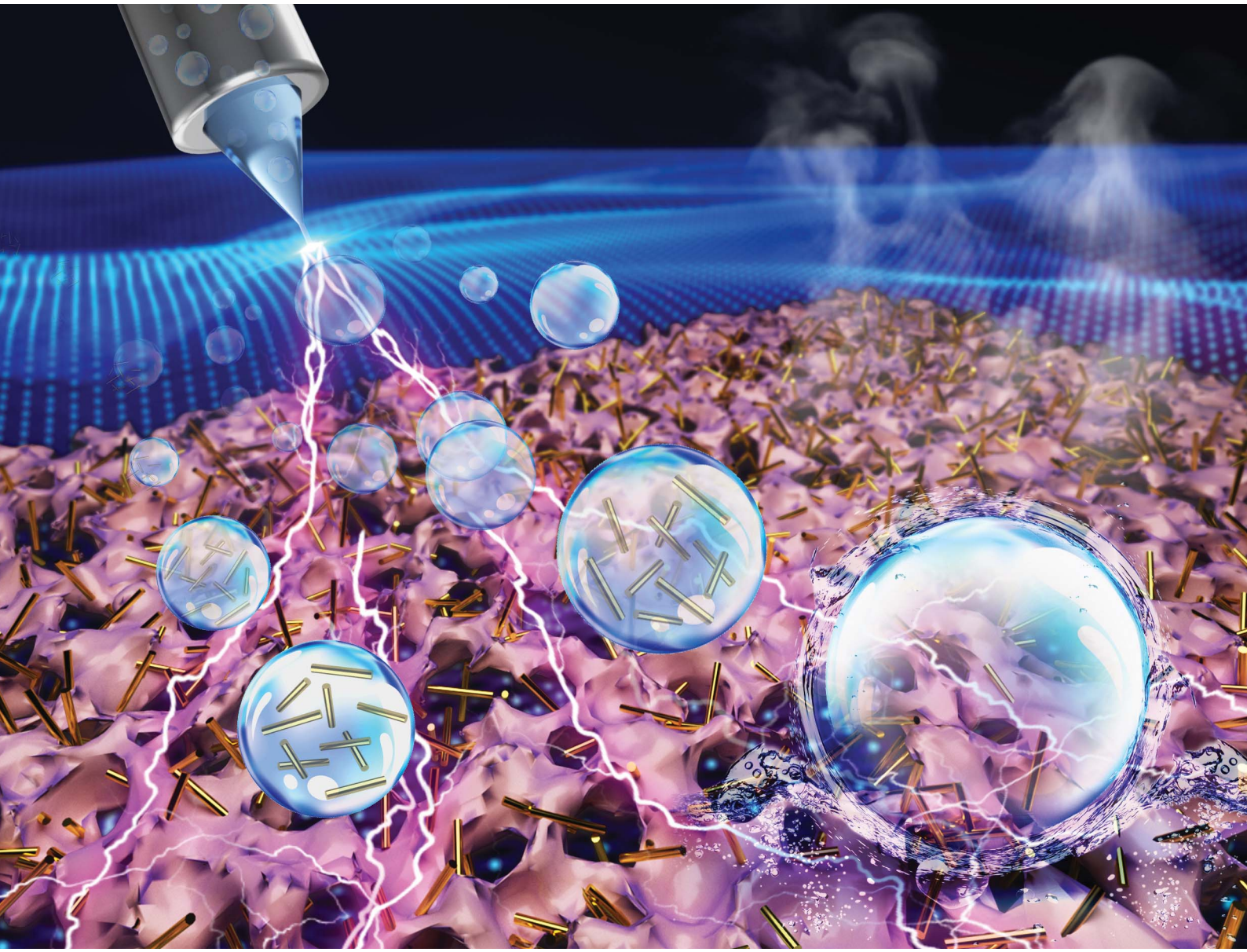

ISSN 2516-0230

ROYAL SOCIETY OF CHEMISTRY

REVIEW ARTICLE

Liang Ying Ee and Sam Fong Yau Li

Recent advances in 3D printing of nanocellulose: structure, preparation, and application prospects

NCNST

Nanoscale Advances

ROYAL SOCIETY OF CHEMISTRY

REVIEW

View Article Online
View Journal | View Issue

Cite this: *Nanoscale Adv.*, 2021, **3**, 1167

Recent advances in 3D printing of nanocellulose: structure, preparation, and application prospects

Liang Ying Ee and Sam Fong Yau Li *

Emerging cellulose nanomaterials extracted from agricultural biomasses have recently received extensive attention due to diminishing fossil resources. To further reduce the carbon footprints and wastage of valuable resources, additive manufacturing techniques of new nanocellulosic materials have been developed. Studies on the preparation and characterization of 3D-printable functional nanocellulosic materials have facilitated a deeper understanding into their desirable attributes such as high surface area, biocompatibility, and ease of functionalization. In this critical review, we compare and highlight the different methods of extracting nanocellulose from biorenewable resources and the strategies for transforming the obtained nanocellulose into nanocomposites with high 3D printability. Optimistic technical applications of 3D-printed nanocellulose in biomedical, electronics, and environmental fields are finally described and evaluated for future perspectives.

Received 20th May 2020
Accepted 26th December 2020

DOI: 10.1039/d0na00408a

rsc.li/nanoscale-advances

1. Introduction

The world is facing a grim environmental and ecological issue arising from the abuse of petroleum-based chemicals and materials, which calls for the quest to develop sustainable materials with green footprints. In this regard, cellulosic biomass has emerged as a suitable solution due to its ubiquitous abundance,[1] renewability, and high mechanical performance.[2] *Agricultural biomass* includes straws, husks, leaves, and animal waste byproducts from wood and agricultural activities; it represents 90% of industrial crops and approximately half the total forest biomass.[2,3] However, underutilized biomass has often been disposed of or incinerated en masse due to its undermined unique intrinsic properties that could otherwise allow interesting potential to be generated by processing into mechanically strong and sustainable materials.[4] To date, only 10% of the agricultural biomass has been used for processing and conversion into useful materials.

Cellulose is a noteworthy natural biopolymer and a constituent of sustainable materials existing in the cell walls of agricultural biomass together with hemicellulose and lignin,[5] which

Department of Chemistry, National University of Singapore, Lower Kent Ridge Road, Science Drive 4, S5-02-03, Singapore 117549. E-mail: chmlifys@nus.edu.sg

*Liang Ying Ee received his accelerated BSc (Hons.) in Chemistry from the National University of Singapore (NUS) in 2017. He has gained significant industrial work and research experience from Hyflux Pte. Ltd. and Agency for Science, Technology and Research (A*STAR), respectively. In August 2018, he was awarded the NUS Research Scholarship administered by the Singapore Ministry of Education to undertake the PhD program under Prof. Li at NUS. His research area involves the extraction of nanocellulose from agricultural waste and 3D printing of nanocellulosic desalination membrane.*

Sam Fong Yau Li is working as a Full Professor at the Department of Chemistry, National University of Singapore (NUS). He received both his BSc (Hons.) and PhD in Chemistry from the Imperial College and DSc from the University of London. Prof. Li has particular expertise and research interest in nanomaterials, 3D printing, environmental analysis and sensing, environmental remediation technologies, capillary electrophoresis, and metabolomics. To date, he has authored/co-authored over 400 papers in peer-reviewed journals (h-index = 53), with numerous papers on the preparation, analysis, and environmental toxicity of nanomaterials that are closely relevant to the reviewed field.

provide adequate strength and stability to the plant. Some examples of agricultural waste with their compositions are shown in Fig. 1. Despite being overshadowed by petroleum-based materials, cellulose has found important applications since its discovery by Anselme Payen in 1837 as mentioned by Hon (ref. 6) as evidenced by the considerable body of literature in this regard. Beyond its humble yet indispensable application in the production of paper and textiles, the huge annual production of 7.5×10^{10} tons of cellulose has been put into sophisticated use in food packaging, biomedical, filtration membranes, sensors, or as rheological modifiers and reinforcement composites[7–9] because of its mechanical strength, biodegradability, biocompatibility, and renewability. Globally, the cotton linters industry is expected to hit US$1.3 billion by 2025.[10]

The structure of natural cellulosic fiber can be described as a long linear polymeric chain of repeating β-D-glucopyranose units (the $C_6H_{11}O_5$ unit also known as β-1,4-D-anhydroglucopyranose) connected by acetal linkage between carbon atoms C-1 and C-4 in two different units upon the elimination of water, as shown in Fig. 2. Each building block of the framework consists of three hydroxyl groups positioned at carbon atoms 2, 3, and 6, contributing to the extensive intra- and intermolecular hydrogen bond network that determines its physical properties and accessibility toward reactions.[11,12] The terminal groups of the cellulose chain consist of asymmetrical reducing end and nonreducing end, which bear hemiacetal anomeric carbon atom and closed-ring structure, respectively. The cellulose polymeric fiber contains both amorphous and crystalline domains, for which both degrees of polymerization and crystallinity affect the mechanical properties.[13] Although harnessing low density as well as high strength and modulus, these characteristics are highly dependent on the origin and chosen extraction and treatment methods of the cellulosic fiber. Apart from that, the mechanical properties of the cellulosic fiber are greatly determined by the hierarchal organization of the amorphous and crystalline compositions.

The separation of cellulose fiber yields the cellulose nanomaterial, also known as nanocellulose with nanoscale dimensions. Normally, these nanocellulose will have a diameter smaller than 100 nm and length in micrometers accounting for the high aspect ratio.[14] This low-cost, abundant nanocellulose has received tremendous attention from both industry professionals and researchers due to its advantages such as improved and distinctive structural, physicochemical, and mechanical properties, biocompatibility, and ease of tunability and moldability into 3D models; because of these, it has high potential for applications in various fields such as cell scaffolds, bioprinting, food packaging, and environmental remediation.[15] Several studies have utilized the crosslinking of nanocellulose either intermolecularly or mediated by polymeric matrices to improve the hydrophobicity and compatibility with nonpolar components.[12] Alongside the capability to mold nanocellulosic material into complex 3D structures, additive manufacturing (also known as 3D printing) techniques could be employed. Currently, 3D printing is a growing research topic of interest to fabricate the 3D structure of compatible materials at a fast speed and high resolution for industrial applications. Nonetheless, the limited availability of printable biocompatible and environmentally friendly nanomaterials remains a huge challenge in the biomedical and environmental field as a synthetic polymer exhibits the problem of biocompatibility, degradability, and release of potentially toxic additives.[16] Fortunately, these limitations could be overcome with the development of functional nanocellulosic composite materials.

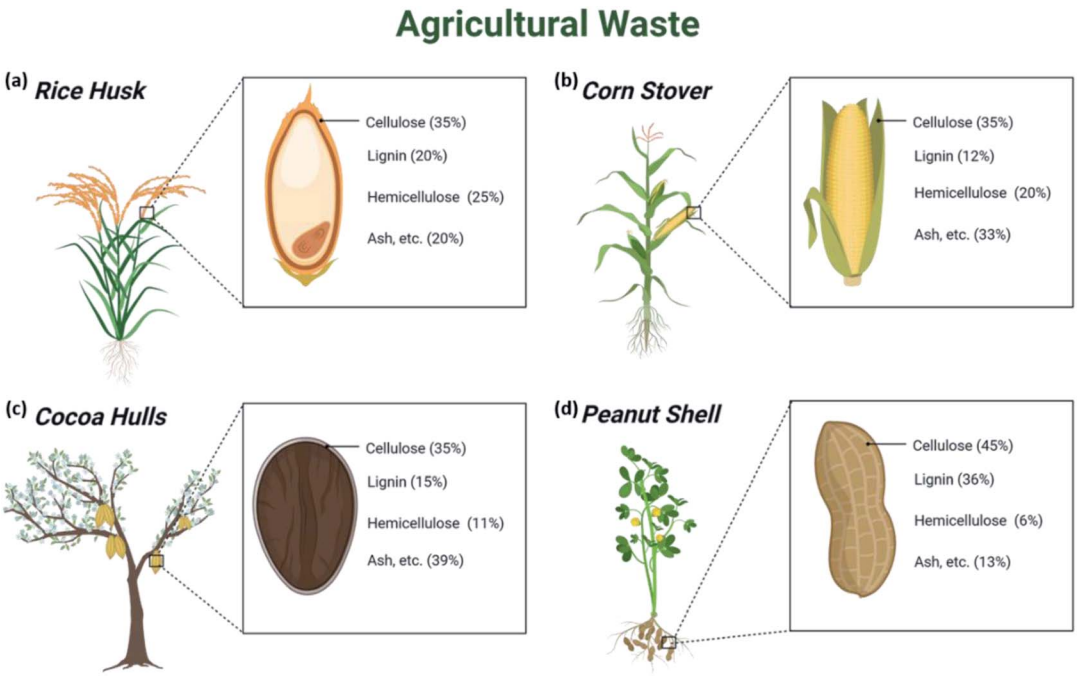

Fig. 1 Examples of (a) rice husk, (b) corn stover, (c) cocoa hulls, and (d) peanut shell with their respective compositions.

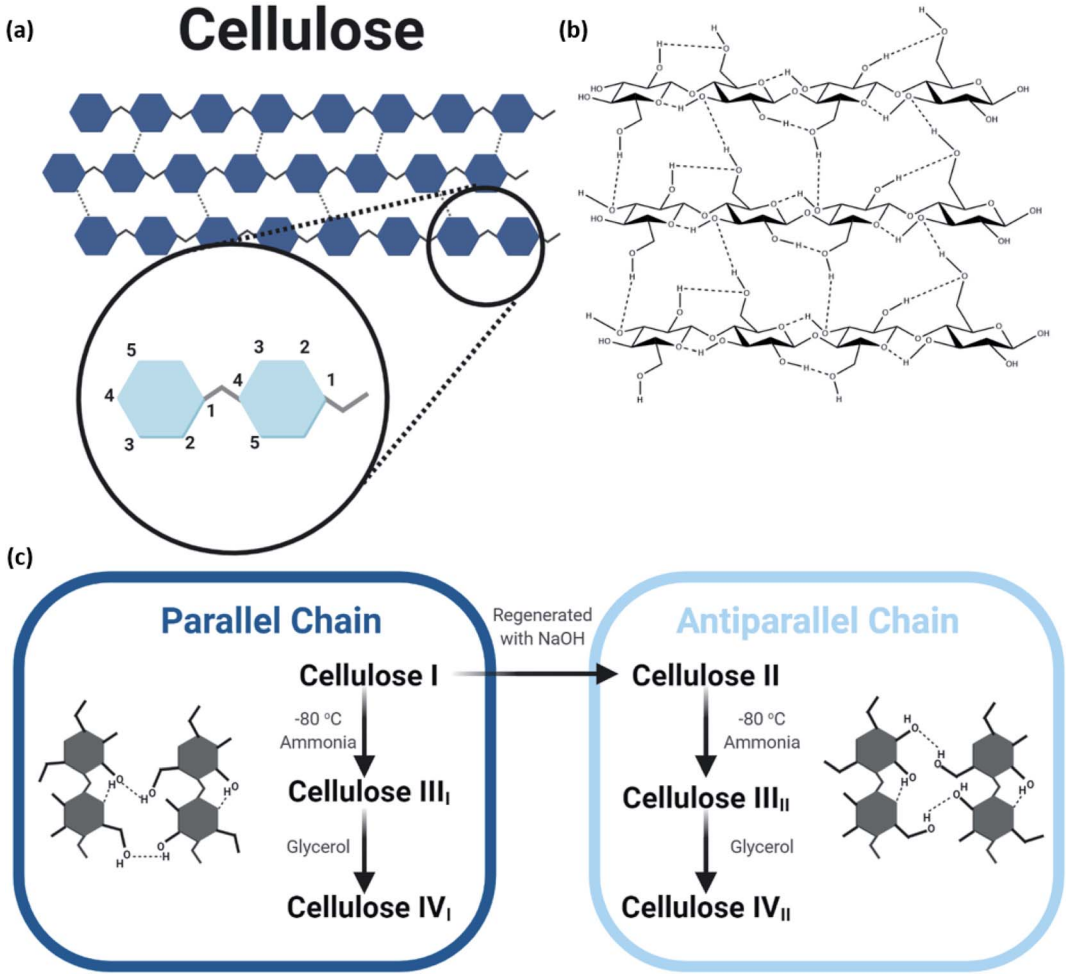

Fig. 2 (a) Molecular structure of cellulose; (b) extensive hydrogen bond network within and between cellulose molecules; (c) schematic of the steps to obtain the various polymorphs of cellulose.

This comprehensive review paper is the first attempt to present the recent advancements in isolation techniques of nanocellulose from agricultural biomass and development of nanocellulose-based materials, with an emphasis on the functionalization and incorporation into nanocomposites. Thereafter, additive manufacturing (also known as 3D printing) technologies will be covered in subsequent chapters to find the extended practical applications of 3D-printable functional nanocellulosic materials in biomedical, electronics, and environmental fields. Most importantly, the growing global interest in green and sustainable materials has prompted the author to critically review the research limitations in the current state of the art and provide insights into the outlook toward the research and development of nanocellulosic functional materials in corresponding chapters.

2. Structure of nanocellulose obtained from biomass

The two main families of nanocellulose, namely, cellulose nanofibers (CNFs) and cellulose nanocrystals (CNCs), can be isolated from agricultural biomass sources by means of the disruption of the extensive hydrogen bond network and amorphous regions within cellulosic fiber.[17] On the other hand, bacterial nanocellulose (BNC) can be produced from a variety of aerobic bacteria such as *Komagataeibacter hansenii*, *Acetobacter xylinum*, and *Sarcina*.[1,4,13] This is a different approach of production known as the "bottom-up approach" compared with the former CNF and CNC produced *via* the "top-down approach". Nanocellulose has great diversity in its morphology, spanning from rod-like to ribbon-like structures that are influenced by the raw material source and preparation methods.[4,5] Today, most of the nanocellulose is derived from agriculture and waste sectors, whilst some is obtained from bacterial cultivation.

Several methods have been presented in the literature to address issues such as the lack of transparency, viscosity, mechanical strength, or even hydrophilicity, by incorporating nanocellulose as the composite that has considerable practicality and can improve the materials for high-end applications.[3,4,7,9,15] Fig. 3 shows a summary of the discovery milestones in the structural elucidation and preparation of cellulose nanomaterials.

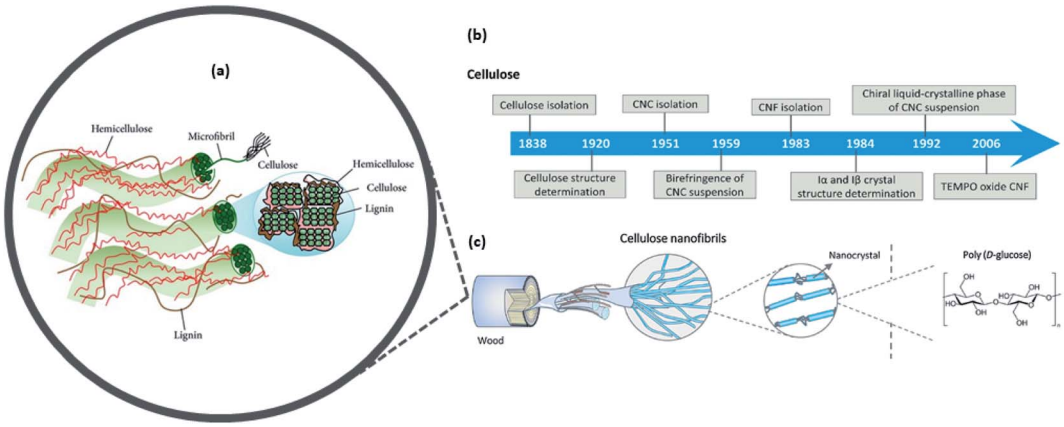

Fig. 3 (a) Illustration of the plant cell-wall structure where cellulosic fibers are intertwined within the hemicellulose and lignin matrices; (b) timeline of the cellulose and nanocellulose structural characterization and preparation; (c) hierarchal structures and types of nanocellulose that can be obtained from woody biomass [reproduced with permission from Lee *et al.* 2014 & Ling *et al.* 2018,[18,19] Copyright © Hindawi & © Elsevier Limited].

Cellulose from all the biomass sources consists of alternating amorphous and crystalline regions. The former is more easily accessible and relatively easy to disrupt and break by mechanical, chemical, or enzymatic treatment, while the crystalline portion has limited accessibility.[20–23] Apart from the source of cellulose, it is important to investigate the structural details of the nanoscale cellulose to elucidate the inherent mechanical, physicochemical, and biological characteristics of the two types of nanocellulose to find their potential applications. In the next two sections, we will investigate the types of nanocellulose, namely, CNF and CNC, that could be obtained from the agricultural biomass source.

2.1. CNFs

CNFs contain both amorphous and crystalline domains, with lengths in several micrometers and diameters in the nanometer range (10–100 nm), accounting for the high aspect ratio[4] along

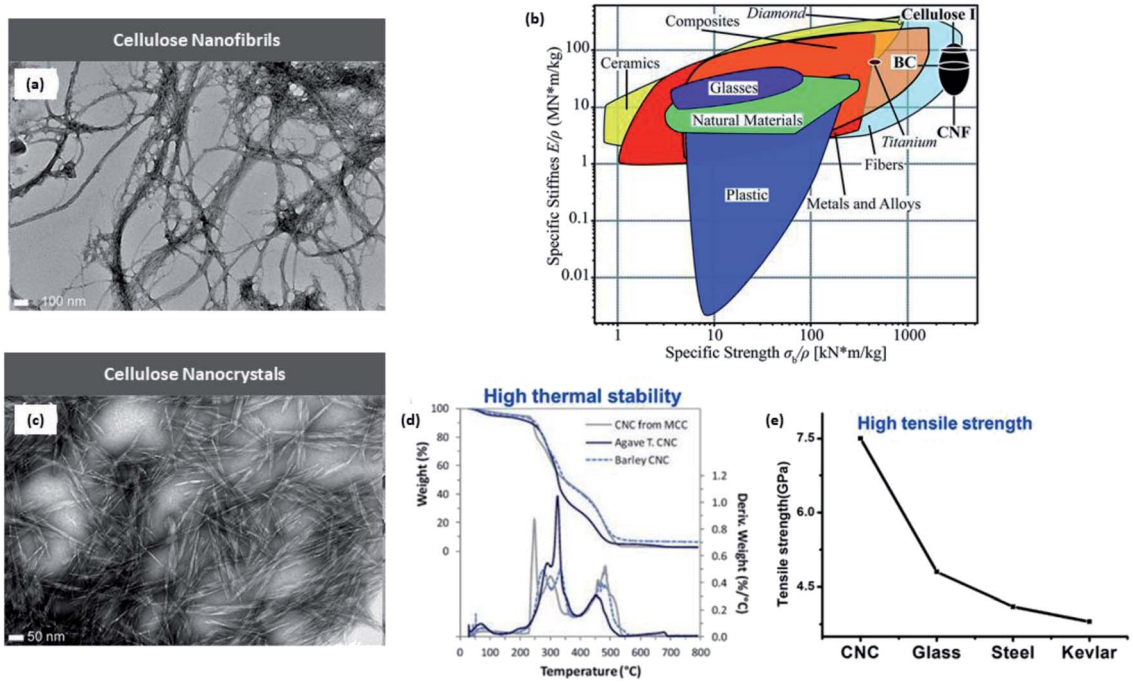

Fig. 4 (a) High-resolution TEM images of CNFs (scale bar: 100 nm); (b) comparison of specific mechanical properties including stiffness (E/ρ) and strength (σ_b/ρ) of CNFs against a variety of common materials in the Ashby plot. CNF is shown in the top right corner, exhibiting excellent stiffness and strength-to-weight ratio; (c) high-resolution TEM images of CNCs (scale bar: 50 nm); CNC exhibiting (d) high thermal stability and (e) tensile strength compared with other materials [reproduced with permission from Xu *et al.* 2013, Benitez *et al.* 2017 & Thomas *et al.* 2018,[7,20,32] Copyright © American Chemical Society & © The Royal Society of Chemistry].

with other desirable physical properties such as low density (1.6 g cm^{-3}) and huge surface area (estimated to be 1000 m^2 g^{-1}) for useful applications.[24] Four cellulose crystalline allomorphs (cellulose I, II, III, and IV) exist due to the differences in the positioning of intra- and intermolecular hydrogen bonds. There are two types of native cellulose I (I_α and I_β), with the latter being predominately present in agricultural biomass, which are considered within the framework of this paper. The relative displacement of cellulose accounts for the distinctive difference in the features between these two cellulose crystals along the (110) triclinic lattice plane for I_α and the (200) monoclinic lattice plane for I_β in the chain axis direction.[25] On the other hand, the structure of cellulose III can be attained *via* ammonia treatment under −80 °C of either cellulose I or II. Finally, with the addition of glycerol to cellulose III, numerous authors have successfully achieved the cellulose IV structure.[26,27]

The long-entangled network of CNF is considerably disordered with amorphous domains, with the ratio of crystalline to amorphous regions affecting the overall stiffness, which was explained by Benítez *et al.* to be between 29 and 36 GPa.[20] Additionally, the strength of CNF stands beyond 1000 MPa like its preceding native cellulose I. From Fig. 4, it is evident that CNF offers strong and mechanically stiff characteristics due to the extensive hydrogen bond interactions compared with common materials such as plastics and other composites.[28] Because of this, CNF has promising applications as a rheological modifier when dispersed in water as well as the fabrication of flexible nanofilms or the formulation of 3D-printing ink for optimal rheology.[20,29] However, CNF is intrinsically hydrophilic and susceptible to swelling when exposed to moisture that could compromise the structural fidelity of the printed structure. Due to the interfibrillar network, it is challenging to use drying techniques such as air drying, freeze drying, or spray drying to remove the bounded water content.[30] This issue can be resolved by Soni *et al.*'s findings that a combination of 2,2,6,6-tetramethylpiperidine-1-oxyl (TEMPO)-oxidized CNF with hydroxypropyl starch could enhance the tensile strength to 7 MPa and reduce the swelling in wet conditions.[31]

2.2. CNCs

Compared with CNFs, CNCs are highly ordered without any amorphous region, accounting for the length and width within the nanometer range.[3,21,32] Consequently, Oun *et al.* explained that the purely crystalline structure results in a much higher stiffness between 135 and 155 GPa and an estimated strength of 7500 MPa.[29] As evident from Fig. 5d and e, CNC stands out as a rigid and strong structure with high thermal stability and Young's modulus comparable with those of glass and steel. In addition, CNCs do not have as many carboxyl groups along their surface in comparison to their nanofibril counterpart.[33] The rod-like or needle-like nanocrystal is widely accepted to have inherently attractive characteristics such as high rigidity and crystallinity because of which CNC is a top choice as a reinforcement filler in composite materials within the polymer matrix; consequently, the stress transfers from the polymer

$$Cu^{2+} + H_2O_2 \rightarrow Cu^{1+} + {}^{\bullet}O_2^{-} + 2H^{+} \quad (1)$$

$$Cu^{1+} + H_2O_2 \rightarrow Cu^{2+} + {}^{\bullet}OH + OH^{-} \quad (2)$$

$$2{}^{\bullet}O_2^{-} + 2H^{+} \rightarrow H_2O_2 + O_2 \quad (3)$$

$$RCH_2OH + {}^{\bullet}OH \rightarrow R{}^{\bullet}CHOH + H_2O \quad (4)$$

$$R{}^{\bullet}CHOH + H_2O_2 \rightarrow RCHO + {}^{\bullet}OH + H_2O_2 \quad (5)$$

$$RCHO + 2{}^{\bullet}OH \rightarrow RCOOH + H_2O \quad (6)$$

Fig. 5 Suggested mechanism of H_2O_2 oxidative delignification in the presence of a copper-ion catalyst [adapted with permission from Koshani *et al.* 2018,[41] Copyright © American Chemical Society].

matrix to the extensive hydrogen bonds among the CNCs.[17,32] It is also well known that the evaporation of CNC under meticulous conditions above the critical concentration yield iridescent films due to the preservation of the chiral nematic and lyotropic liquid crystalline phases,[33] finding applications in anti-counterfeit currency notes.

Being able to differentiate between the two types of nanocellulose materials on the basis of their physical properties is vital in choosing a suitable material for a specific application. Table 1 summarizes the differences in length, cross-sectional width, degrees of polymerization, and crystallinity between CNF and CNC, while Fig. 4 shows the high-resolution transmission electron microscopy (TEM) images of both the nanocelluloses for ease of comparison. The academic community has extensively explored and characterized the source of cellulose fiber that influences the chemical compositions and fibril structures affecting the physical properties of the obtained nanocellulose.[34] Yet, the preparation methodologies should also be taken into consideration. In addition, dimensions, self-assembly, and other mechanical properties could vary due to different treatment methods and conditions.[35] Therefore, the next chapter will focus on the different pretreatments and treatments (mechanical, chemical, and enzymatic) to prepare nanocellulose from agricultural biomass sources.

3. Preparation of nanocellulose

Today, there is a wide choice of commonly employed top-down approaches in the preparation of nanocellulose from agricultural biomass such as fruit peels, wheat straw, and wood pulp available in the literature. Jyoti and Adhikari prepared a comprehensive review on the different methods of extraction and preparation of nanocellulose from biomass, which can be categorized into chemical, enzymatic, and mechanical processes.[35] These processes are envisioned at separating and purifying cellulose content in lignocellulosic biomass from their lignin and hemicellulose counterparts.[18,35,36] The percentage of the main components in some of the lignocellulosic agricultural biomass is summarized in Table 2. Aside from the three main components, agricultural biomass can include ash, wax, and other sugar and moisture content that have to be

Table 1 Comparison of the physicochemical properties of nanocellulose from plant biomass [reproduced with permission from Klemm *et al.* 2018,[21] Copyright © Elsevier Limited]

Nanocellulose type	Length (nm)	Cross-section (nm)	Degree of polymerization	Degree of crystallinity
Cellulose nanofibers (CNF)	100–2000	5–60	≥500	Low
Cellulose nanocrystals (CNC)	100–250	5–70	500–15 000	High

removed in order to obtain cellulose.[2,14] Generally, the isolation of nanocellulose from agricultural biomass follows (1) pretreatment or purification step for fractionation and (2) the extraction of nanocellulose from purified cellulose pulp.[34]

3.1. Chemical pretreatment of biomass

Lignin exists as a crosslinked amorphous biopolymer, consisting of a dendritic network of three different phenylpropane monomers (*p*-cournaryl, sinapyl alcohols, and coniferyl), and its ratio is dependent on the biomass source. Lignin can crosslink to hemicelluloses, such as xylan, which are heteropolymers comprising different types of pentoses and hexoses.[37] Then, hemicellulose adheres to the cellulosic fibers through hydrogen bonding as well as van der Waals interactions.

The presence of lignin and hemicellulose creates a protective structure around the cellulose fibers in the biomass, contributing to hydrolytic stability *via* their ester and ether linkages. This provides the cell wall with the strength to remain in the structured form.[36] However, this eventually leads to biomass recalcitrance where the cellulose has low accessibility due to the high lignin content. In order to successfully derive nanocellulose, the raw lignocellulosic biomass requires mechanical treatment such as grinding with high shear to reduce its size before chemical pretreatment for the purpose of fractionating cellulose out of the biomass. Often, eventually, a unified preparation system with multiple pretreatment methods has appeared to ensure the higher removal rate of the non-cellulosic constituents.

3.1.1. Alkaline pretreatment. The pretreatment of biomass with alkalis is one of the most commonly used methods for delignification in the industrial production of cellulose. Despite decades of research on this method of pretreatment, its degradative characteristic continues to be debated. Alkaline pretreatment promotes the breakage of the cell wall and the removal of lignin to access the cellulosic fiber.[38] In most cases of alkaline delignification, the β-aryl ether linkages are cleaved to aid solvation.[39] At the optimum temperature, the biomass is soaked in 4–10% (w/v) alkaline solutions such as NaOH, KOH, or NH_4OH to effectively disrupt and remove the lignin content along with the partial solvation of hemicellulose.[37] As a consequence of the effective removal of non-cellulose constituents (79–84%) *via* the alkaline pretreatment of the brewer's spent grain (BSG), dos Santos *et al.* successfully documented the preparation of carboxymethyl cellulose (CMC) with the highest measured degree of substitution at 1.46.[40] The scanning electron micrograph (SEM) analysis revealed pristine BSG with diameters between 150 and 350 μm, while the alkali-pretreated BSG exhibited a rougher surface with a reduced diameter in the range of 80–200 μm. The BSG was pretreated with NaOH in the presence of isopropanol and subsequently bleached to obtain highly pure cellulose and α-cellulose containing less than 5.97 ± 0.92% hemicellulose and 3.23 ± 0.03% lignin.

In several other research papers, the prevailing alkaline pretreatment method has been adopted to isolate cellulose fibers from sisal fibers, rice, and oat husks, as well as fruit shells.[42–44] With the elimination of amorphous hemicellulose and lignin to overcome cellulose recalcitrance, the crystallinity of the extracted cellulosic material should be expected to have a higher degree of crystallinity. X-ray diffraction (XRD) analysis at two angles of 2Θ values of around 16° and 22.8° that correspond to the (101) and (200) planes in the native cellulose crystal indicates relative crystallinity at 84.2% for sisal fibers,[43] 93% for rice and oat husks,[42] and 72% for fruit shells.[44] Correspondingly, Mariño *et al.* determined a high crystallinity of 77% with regard to the preparation method of cellulose nanomaterials from orange bagasse with multistep 2% NaOH treatment.[45] On the contrary, a longer period of exposing the biomass in an alkaline pretreatment solution of high concentration can potentially lead to a slight reduction in the crystallinity as the crystalline cellulose structure is disrupted and degraded.[46] Despite having shown that it is highly effective when combined with other pretreatment methods, a drawback of the alkaline pretreatment of biomass is the high operational cost and the tendency to result in the decrystallization of cellulose that we are interested to extract.[46,47] Hence, these limitations of conventional alkaline maceration have created the need for alternative effective pretreatment methods that are mild toward the degradation of cellulose.

Table 2 Chemical composition of common lignocellulosic biomass [reproduced with permission from Lee *et al.* 2014,[18] Copyright © Hindawi]

Type of Biomass	Cellulose (%)	Hemicellulose (%)	Lignin (%)
Barley straw	33–40	20–35	8–17
Wheat straw	30	50	15
Nut shells	25–30	25–30	30–40
Fruit peels	41	24	21.2
Hardwood stems	40–55	24–40	18–25
Switch grass	45	31.4	12

3.1.2. Oxidative delignification. Strong oxidizers such as hydrogen peroxide and ozone can be used to convert lignin copolymer into carboxylic acids. Oxidative delignification can

be successfully created with effective enzymatic hydrolysis since lignin is being removed in this case to ease the penetration of hydrolytic media.[35,37] Earlier research done by Mussatto and Rocha reported a 95.7% (w/w) cellulose obtained from BSG using alkaline and oxidative delignification pretreatments. In another instance, Khan *et al.* pretreated dunchi fiber with alkali and bleached with hydrogen peroxide followed by sulfuric acid hydrolysis to finally obtain CNC with the aspect ratio of 10.45 ± 3.44 nm and crystallinity index of 66.7%.[48] The considerably attractive approach of chlorine-free bleaching with hydrogen peroxide has succeeded in reducing the kappa number to 11.2, which corresponds to a low lignin content.[49] However, the optimization of bleaching conditions is essential to ensure that the pulp strength is not being compromised by the peroxide radical degradation of cellulose.

Hydrogen peroxide unquestionably represents a cheap and effective delignification reagent that has been widely used on woody biomass until today.[41,50,51] Moreover, it is considered to be a greener and milder bleaching medium in comparison with harsh acid–chlorite pretreatment for which the latter poses a detrimental effect on the degree of polymerization in pretreated cellulose due to the oxidative cleavage of the biopolymeric chain.[52] Comparatively, a one-step catalyst-assisted hydrogen peroxide oxidation of softwood pulp has been developed to isolate carboxylated CNCs, with 30% hydrogen peroxide added with copper(II) sulfate pentahydrate as the catalyst in an acidic medium. Koshani *et al.* proposed the possible mechanisms from this one-step preparation of carboxylated CNCs, as shown in Fig. 5, which shows that the generated hydroxyl-free radical (eqn (3)) reacts with cellulose, *i.e.*, introducing the aldehyde and carboxyl groups along the framework, as described in eqn (4)–(6).[41]

Meanwhile, previous studies have promoted the adoption of TEMPO-mediated oxidative pretreatment on softwood kraft pulp, rice straw, and cotton linters.[53–56] Isogai and Zhou corroborated the effectiveness of this pretreatment method by preparing diverse nanocellulose with controllable morphologies upon undergoing the TEMPO-mediated oxidation of woody biomass.[53] The anionic carboxylation of C-6 carbon in cellulose occurs without a significant change in the crystal structural characteristics and crystallinity of cellulose I, as shown in Fig. 6.

Despite the aforementioned advantage, this study does not identify that the formed TEMPO-oxidized nanocellulose cannot

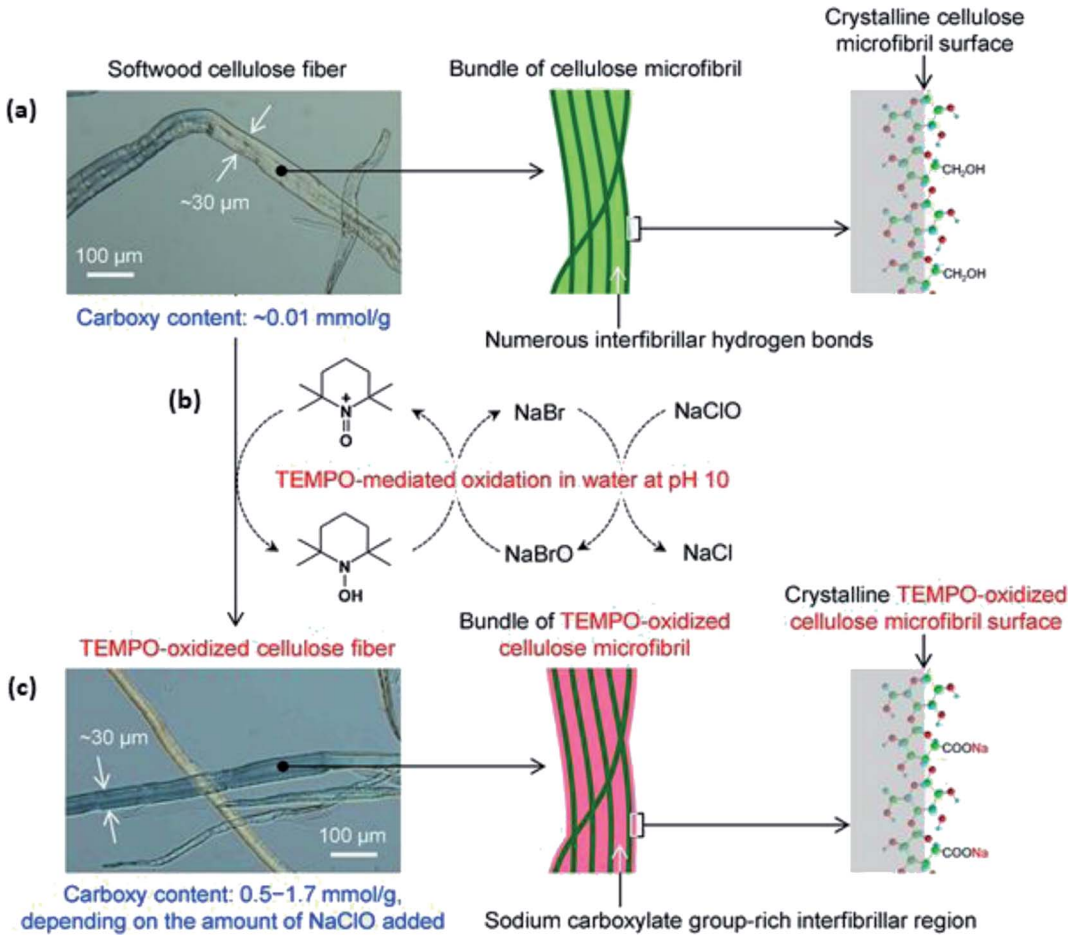

Fig. 6 (a) SEM image and illustration of softwood cellulose microfibril surface (scale bar: 100 μm); (b) TEMPO-mediated oxidation of softwood cellulose fibers by the position-selective formation of sodium C6–carboxylate group on the fiber surface; (c) SEM image and illustration of TEMPO-oxidized cellulose microfibril surface with the retained morphology (scale bar: 100 μm) [reprinted with permission from Isogai & Zhou 2019,[53] Copyright © Elsevier Limited].

recover to the solid phase with a higher yield.[53,56] In short, oxidative delignification could simultaneously introduce surface modification with the pretreatment process. However, this method could effectively remove only lignin but not the hemicellulose content to obtain pure cellulose. In addition, oxidizing agents such as TEMPO and hydrogen peroxide are expensive and would require more demanding reaction conditions.

3.1.3. Ionic liquids (ILs). ILs exist as molten salts at room temperature and atmospheric pressure. Generally, they possess low vapor pressure, low melting point (<100 °C), and comprise poorly coordinated bulky organic cations and anions (*e.g.*, quaternary ammonium cations and halides).[36,37] Some typical cations and anions of ILs are shown in Fig. 7.[57] It is possible to tune the IL to either target the dissolution of lignin and hemicellulose or just cellulose to ensure efficient fractionation with the following: (1) highly selective and specific dissolution capability for the targeted fiber by carrying an organic cation; (2) low viscosity; and (3) high chemical and thermal stability.[58–60]

Discussions on IL pretreatment have dominated research since 2002, describing the dissolution of cellulose—without derivation—in various ILs such as 1-butyl-3-methylimidazolium chloride ([BMIM]Cl) and 1-allyl-3-methylimidazolium chloride ([AMIM]Cl) that are hydrophilic in nature. In general, cellulose can be easily regenerated as a precipitate in the presence of water in the IL solution, while other organics, such as lignin, remain dissolved.[61–63] It was found that halides such as chlorides act as an excellent hydrogen bond acceptor due to their small size, and hence, they are highly effective in dissolving cellulose together with the hydrogen bond donor[62] by disrupting the extensive hydrogen bonding in the cellulosic network. Fig. 7b shows how the hydrogen bond donor and acceptor in the IL disrupt the cellulose hydrogen bond network.

Various agricultural biomasses such as wood chips, bagasse, rice straws, and tree wood have been examined for the fractionation and extraction of cellulose by ILs.[65–68] According to Jiang *et al.*, the addition of 1.5 g steam-exploded dried rice straw to 20 g [AMIM]Cl stirred at 40–60 °C for approximately 3 h under anhydrous condition yielded cellulose with 74% crystallinity and 95.58% purity with an average degree of polymerization of 484.[65] In a timely study, Lan *et al.* conducted the complete dissolution of bagasse with [BMIM]Cl followed by 3% NaOH treatment and have reported obtaining pure cellulosic fraction of over 92%.[66]

With the aim to screen the IL that affords the best cellulose dissolution, Koel *et al.* subsequently carried out a comparative examination on the solubility of cellulose with 11 different types of ILs to make a 10 wt% solution.[64] Table 3 lists a summary of the extent of the dissolution of cellulose and the form of solution experimented. Correspondingly, Singh *et al.* advanced into the crystallinity characterization of deconstructed water hyacinth biomass after pretreatment with imidazolium-based ILs.[69] A range of crystallinity increments between 11 and 41% with reference to the untreated biomass have been observed with 1-octyl-3-methylimidazolium bromide ([Omim][Br]) and 1-ethyl-3-methyl imidazolium bromide ([Emim][Br]), respectively. Although a variety of green ILs for the preparation of cellulose fiber are available, the degree of polymerization of cellulose is drastically lowered when dissolved due to violent degradation. Fortunately, the inclusion of L-arginine in the dissolution system was shown to increase the yield of purified cellulose fiber with the inhibition of the degradation effect of IL.[70]

Although research has revealed that ILs are recyclable and reusable for a couple of times,[58,64,71,72] only a few studies till date have successfully been able to examine the costs and implication of environmental conditions on the effectiveness in regenerating the IL dissolution capability. Moreover, the dissolution of cellulose in ILs requires high temperature and shearing so that it can penetrate the protective layers of the cell wall. The high sensitivity of IL toward environmental conditions, particularly moisture, hinders the dissolution ability of the target fiber.[10] Furthermore, the process to separate IL from water is expensive and energy-intensive. The high viscosity associated with the presence of halide anions also creates difficulty for the dissolution process, particularly at the industrial scale. Finally, the expensive synthesis of ILs that often involves strict conditions dramatically shaped the industry to be more inclined toward the cheaper, conventional alkaline pretreatment.[59,63]

3.1.4. Deep eutectic solvents (DES). DESs are considered to be a new generation of ILs that eliminate the high cost of preparation and possess similar physicochemical characteristics as ILs. To date, a limited number of studies and knowledge is available to garner a clearer understanding of the cellulose dissolution ability in DESs. By customizing the molar ratio of

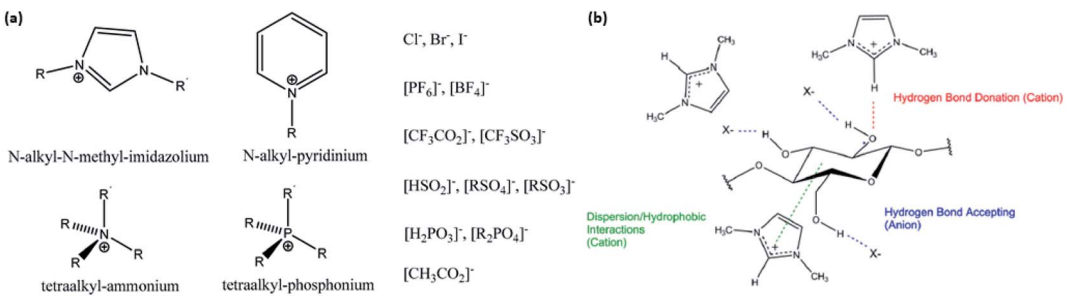

Fig. 7 (a) Examples of cations and anions in ILs; (b) interactions between IL and cellulose in disrupting its hydrogen bond network [reproduced with permission from Lopes *et al.* 2017 & Holding 2016,[57,63] Copyright © MDPI].

Table 3 Dissolution of microcrystalline and microfibrillated cellulose in ILs and solution form [reproduced with permission from Koel *et al.* 2016 (ref. 64)]

Ionic liquid	Microcrystalline cellulose	Microfibrillated cellulose
1-Allyl-3-methylimidazolium chloride (AMIMCl)	Soluble (liquid)	Soluble (liquid)
1-Ethyl-3-methylimidazolium chloride (EMIMCl)	Soluble (non-liquid)	Partially soluble (non-liquid)
1-Butyl-3-methylimidazolium chloride (BMIMCl)	Soluble (non-liquid)	Partially soluble (non-liquid)
1-Butyl-3-methylpyridinium chloride (BMpyCl)	Soluble (non-liquid)	Soluble (non-liquid)
1-Ethyl-3-methylimidazolium acetate (EMIMAc)	Soluble (liquid)	Soluble (liquid)
1-Butyl-3-methylimidazolium acetate (BMIMAc)	Soluble (liquid)	Partially soluble (non-liquid)
1,3-Dimethylimidazolium methyl sulfate ($DMIMMeSO_4$)	Insoluble (non-liquid)	Partially soluble (non-liquid)
1-Butyl-3-methylimidazolium methyl sulphate ($BMIMMeSO_4$)	Insoluble (liquid)	Partially soluble (liquid)
1-Ethyl-3-methylimidazolium diethyl phosphate (EMIM DEP)	Soluble (liquid)	Partially soluble (non-liquid)
1-Butyl-3-methylimidazolium hexafluorophosphate ($BMIMPF_6$)	Insoluble (non-liquid)	Insoluble (liquid)
1-Butyl-3-methylimidazolium bis(trifluoromethylsulfonyl)imide ($BMIMTf_2N$).	Insoluble (liquid)	Insoluble (non-liquid)

binary components in the DES, the physicochemical properties could be altered and designed according to the requirement.[73] An example is the eutectic mixture of choline chloride (ChCl) and urea at a molar ratio of 1 : 2 having a melting point of 12 °C, with ChCl acting as the hydrogen bond acceptor, while the latter acts as the donor having melting points of 302 and 133 °C in their individual states, respectively.[73–75] Examples of other hydrogen bond acceptors and donors used in the formation of DESs are shown in Fig. 8.

Studies on the DES extraction of cellulose are well documented and the importance to optimize the DESs' ability for cellulose dissolution within the solvent system in the DES preparation procedure is also well documented.[74–77] Sirviö *et al.* subjected bleached birch pulp to ChCl/urea DES pretreatment before the mechanical nanofibrillation of cellulose through a microfluidizer. Unlike the previously discussed pretreatment processes, no change in the degree of polymerization between pristine pulp and DES-pretreated pulp was observed.[75] With DES that shows favorable and analogous degree in the dissolution of cellulose as the IL, further studies have been carried out to screen the most suitable class of DESs that could be used to effectively pretreat biomass.[78–80] A synergistic pretreatment effect has been established by Liu *et al.* using ChCl/oxalic acid dihydrate DES coupled with high-intensity ultrasonication to disintegrate cotton cellulose fiber into CNCs.[78] The cotton fiber was pretreated under 800 W ultrasonication in DES at 80 °C for 3 min before cooling and ultrasonication for another 30 min at 1200 W that eventually produced 74.2% yield of CNCs with 82% crystallinity and degradation temperature of more than 320 °C. ChCl-based DES has become the most popular choice in the dissolution of cellulose and has been reported in various other papers in the literature.[80–83] Using the same class of deep eutectic mixtures, Yu and her co-workers prepared a CNF film from ramie fibers, but have instead observed a lower tensile strength of 52.0 MPa in comparison to 89.5 MPa that was not treated with DES.[84] Hence, this useful study potentially opens

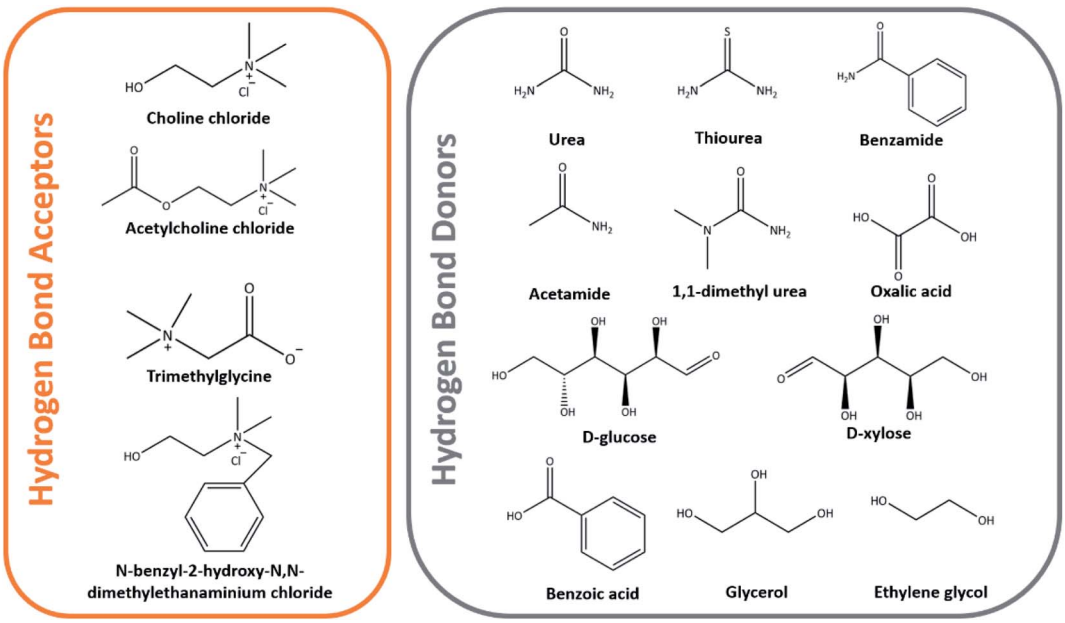

Fig. 8 Examples of some DESs as hydrogen bond acceptors and donors.

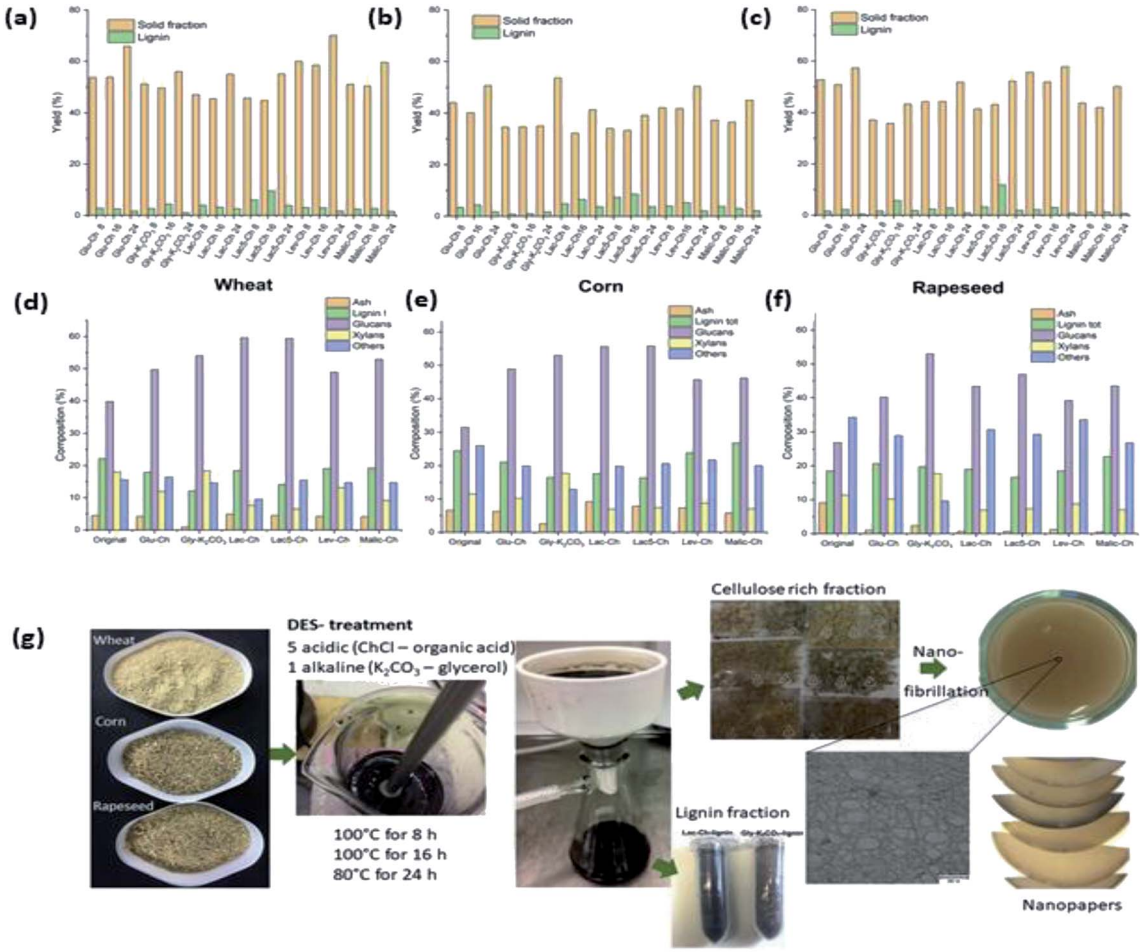

Fig. 9 Compositional analyses on the solid and lignin fractions after DES treatments of (a) wheat, (b) corn, and (c) rapeseed over 8, 16, and 24 h; compositions of solid fractions of (d) wheat, (e) corn, and (f) rapeseed before and after the DES treatments at 100 °C for 16 h; (g) illustration of the experimental procedure to obtain CNF nanopapers from DES-treated raw materials [adapted with permission from Suopajärvi *et al.* 2020,[89] Copyright © Elsevier Limited].

questions about the effect of DES dissolution on the physicochemical and mechanical properties of the cellulose and nanocellulose materials produced. For this reason, more recent in-depth studies have been conducted to unearth the interactions between DES and cellulose and how they could affect the physicochemical properties of pretreated cellulose.[85–88] Ling *et al.* revealed the structural variations in the cellulose crystal when it underwent pretreatment with ChCl/oxalic acid DES, for which they proposed a detailed mechanism of CNC preparation from cotton biomass.[85] The proposed mechanism of structural variation in the cellulose crystalline structure following the DES pretreatment and ultrasonication disintegration is as follows: the oxalic acid content was critical as it disrupted the hydrogen bonding of glucose residues on the hydrophobic (200) and (110) planes, thereby leading to smaller crystallite sizes due to the loosened surface layer.[85] Subsequent mechanical fibrillation and freeze drying recrystallized the glucose resulting in an enlarged crystallite size and preserved the CNC crystalline structure.

In addition to targeting cellulose dissolution, a series of seminal contributions have been made by several authors in preparing DESs designed for the dissolution of non-cellulosic materials to finally produce pure cellulose pulp for further treatment. Kumar and his co-workers observed that the pretreatment of rice straw with ChCl/lactic acid at a molar ratio of 1 : 5 is effective at removing 68.1 ± 4 mg g^{-1} of lignin; the DES treatment of rice straw left behind only 3.8 ± 0.5% lignin content, and the lowest compared with alkaline treatment (6.5 ± 0.6%) and acidic treatment (8.1 ± 0.2%).[90]

Apart from the ChCl-based DES, researchers have also performed lignocellulose pulping and pretreatment of cellulose with other classes of DESs such as acidic sulfamic acid/urea and alkaline potassium carbonate DESs.[91–93] Lim *et al.* predicted and analyzed the use of alkaline K_2CO_3/glycerol DES at a molar ratio at 1 : 7 for lignocellulose pulping on rice straw. It was found that the crystallinity of the pretreated pulp distinctly increased from 52.8 to 60.0% upon 100 min of pretreatment with DES at 140 °C. Additionally, it was revealed that the DES-pretreated cellulose pulp has high thermal stability with an onset temperature of 277.2 °C.[92] More recently, numerous studies have differentiated the benefits of alkaline DES over their acidic counterpart.[89,94] Suopajärvi and co-workers compared the

performance of delignification between alkaline K_2CO_3/glycerol DES and five other ChCl/organic acid DES on various agricultural sources such as wheat, corn, and rapeseed raw materials. Fig. 9 shows the charts of the compositional analysis results of the original samples and treated samples with the above-mentioned DES at 100 °C over different time intervals (8, 16, and 24 h). According to the results shown, a higher solubility of ash content was observed in alkaline K_2CO_3/glycerol DES in wheat and corn samples with remaining 0.9–2.5% compared with 4.5–7.8% upon acidic DES treatment. On the other hand, the lignin content measured from solid fractions, as shown in Fig. 9d–f, was slightly lower with the alkaline DES, indicating a slightly lower delignification efficiency than that of the ChCl/lactic acid DES. Nonetheless, the lactic-acid-type acidic DES was prone to evaporation and has reduced thermal stability when heated at 100 °C over a long period.

A new class of nontoxic and cheap IL, known as DES, has been recently discovered for the fractionation of lignocellulosic biomass. The ease of customizing and designing the DES could bring about many benefits such as the functionalization of cellulose in addition to dissolution pretreatment. It is imperative to perform more comprehensive and deeper mechanistic studies into the interaction between different types of DESs and cellulose. This pre-treatment process is still underemployed as it has been hampered by the poor specificity in dissolution and lack of research in demonstrating its intrinsic advantages over conventional pretreatment processes. Although results from binary DESs are promising for pretreatment, researchers have also started exploring ternary DESs to improve the performance, specificity, and recyclability.[95]

With reference to Table 4 summarizing the comparison among the four chemical pretreatment processes, we understand that DES is a benign and effective reagent to yield pure cellulosic content from agricultural biomass. On the other hand, it is essential to note that process complexity and product requirement are important factors to put into consideration. Therefore, the amalgamation of various methods could be potentially the best pretreatment for producing the cellulose of desired properties. Although the ability to obtain purified cellulose is the primary consideration to decide on the pre-treatment method, it is essential that the efficiency, environmental cost, energy consumption, and practicality be taken into account before introduction for industrial applications.[39]

3.2. Nanocellulose isolation

The appropriate treatment methods to choose for converting the extracted cellulose into nanosized cellulose largely depends on the type of nanocellulose (*i.e.*, CNF and CNC) to be prepared. Different methods yield altered crystallinity as well as different degrees of depolymerization due to the extent of hydrogen bond disruption.[47] The preparation of nanocellulose from biomass is typically difficult because of the extensive hydrogen bond network and stiffness of the chains in the lignocellulosic structure.[98] Nevertheless, nanocellulose isolation can be achieved by mechanical, chemical, or enzymatic treatment upon overcoming the biomass recalcitrance through pretreatment methods mentioned in the previous sections.

3.2.1. Mechanical treatment. The mechanical treatment of cellulose fibers into nanocellulose is the most energy-intensive process as it aims to overcome the interfibrillar hydrogen bond network, which is estimated to range between 19 and 21 MJ kg^{-1} mol^{-1}. As an example, approximately 30 kW h kg^{-1} of energy is consumed to produce CNFs from bleached eucalyptus pulp. The bleached and purified cellulose pulp is grounded into fine particles using a commercial stone grinder.[99] Hence, mechanical treatment is often coupled with pretreatment to reduce the energy required for the disintegration of cellulose.[100] Bharimalla and co-workers reported a significant reduction of 3510 kJ in the energy required for 1 kg of pretreated cellulose ground using a stone grinder.[99] Fig. 10 shows a summary of the various conventional and modern mechanical processes to prepare nanocellulose from the extracted cellulose fibers.

Other traditional mechanical treatments include the use of high-pressure homogenization, where pretreated biomass is passed several times through a homogenizer at a specified pressure. This method was incorporated with the IL pretreatment of pineapple lead by Wang *et al.* to prepare nanocellulose particles with diameters ranging from 4 to 10 nm after 45 cycles

Table 4 Comparison of the various chemical pretreatment methods for cellulose

Type of pre-treatment	Effectiveness	Cost	Toxicity/ environmental impact	Recoverable	Effect on pre-treated cellulose
Alkaline	Highly effective with catalyst	High operational and catalyst cost	Unfriendly to environment	Not recoverable	Could reduce crystallinity of cellulose
Oxidative delignification	Only removes lignin	Some oxidizers are expensive (*e.g.* Ozone and TEMPO)	Toxic to environment	Not recoverable	Cellulose dispersed unable to recover in high yield
Ionic liquids (IL)	Effective with selectivity	Synthesis of IL and starting materials are expensive	Toxic	Can be recovered and reused	Could affect the morphologies of cellulose crystalline
Deep eutectic solvents (DES)	Effective with selectivity	Low cost	Non-toxic and natural ingredients	Can be recovered and reused	Readily designed to requirement

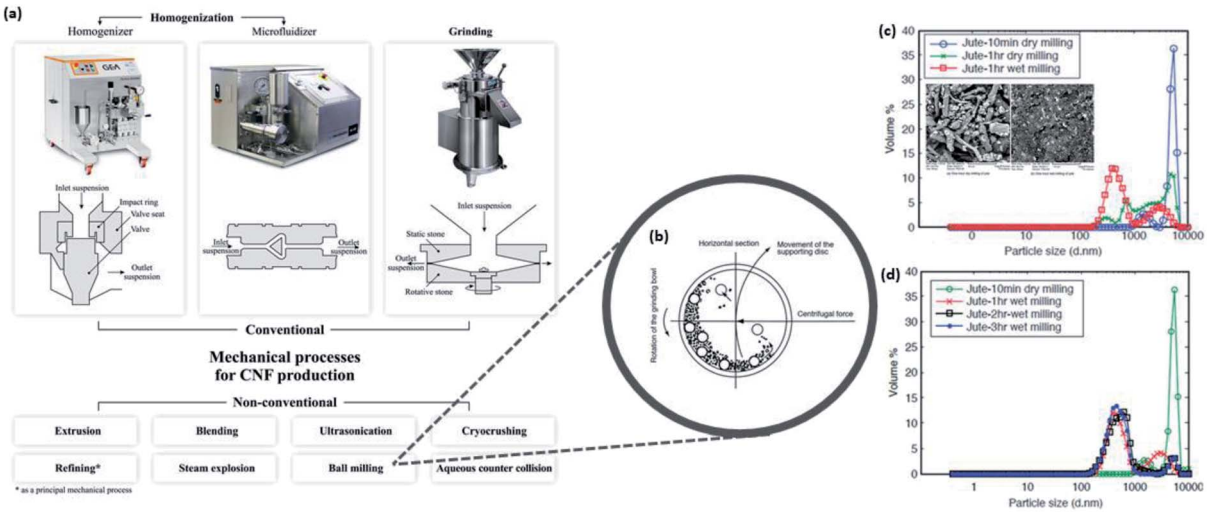

Fig. 10 (a) Conventional and nonconventional mechanical treatment processes for nanocellulose production; illustration of the (b) working principle of planetary ball milling and the influence on particle size distribution by (c) dry and wet milling and (d) duration of milling [reproduced with permission from Nechyporchuk *et al.* 2016, & Abbasi & Baheti 2018,[96,97] Copyright © Elsevier Limited & © MedCrave Group].

of high-pressure homogenization at 100 MPa and room temperature.[101]

On the other hand, there have been numerous recent studies in recognizing the need to reduce energy consumption. Hence, some authors have driven the further development of mechanical isolation and evaluated the efficiency and effectiveness of preparing nanocellulose using nonconventional mechanical treatments such as high-speed blending, steam explosion,[102] ball milling, and high-intensity ultrasonication.[97,103–110] Khawas and Deka revealed that the introduction of high-intensity ultrasonication assisted the reduction in the size and diameter of CNFs, which enhanced the thermal stability with increased degradation temperature from 260.81 to 295.33 °C when coupled with the ultrasonication power of 1 kW.[105] The effectiveness of this approach has been further investigated by Zhang *et al.* and Yazdanbakhsh *et al.* who have successfully optimized a combination of chemical–mechanical processes. They have demonstrated the induced breaking of the cell wall through high shear force and cavitation to obtain CNFs with diameters ranging between 20 and 56 nm with increased crystallinity from the original agricultural materials such as wheat bran.[102,110] However, the yield of nanocellulose obtained from ultrasonication remains low as this method has little or no selectivity in eliminating both amorphous and crystalline regions.[34] Naturally, the relevant question is whether the selectivity of high-intensity ultrasonication could be enhanced by controlling the environmental conditions and the frequency and output power. Meanwhile, Abbasi and Baheti investigated the influence of planetary ball milling on the particle size of nanocellulose produced from jute fiber waste.[97] Fig. 10b–d show the schematic of the working principle of ball milling as well as the particle size distribution of nanocellulose produced under various conditions. As shown in Fig. 10d, it is confirmed that approximately 180 min of wet milling can adequately prepare the powder dispersion form of nanocellulose from jute fiber waste with a particle size below 500 nm.

Despite the effectiveness of mechanical treatment toward the preparation of nanocellulose, the huge energy consumption, duration of treatment, and size homogeneity remain a huge challenge, which has given the impetus to researchers at the forefront to investigate alternatives to nanocellulose isolation methods.

3.2.2. Chemical treatment. With the purpose of conserving energy and the production of CNC, chemical treatments have been adopted. Bharimalla *et al.* indicated that paper fibrillation *via* oxidation reactions only requires around 2.1 kW h per kg of nanocellulose produced.[99] Several chemical treatment techniques have been developed to produce nanocellulose from cellulosic materials. Nevertheless, acid hydrolysis remains the main chemical process to extract CNC since the disordered amorphous region could be easily hydrolyzed, leaving the ordered crystalline region intact, as shown in Fig. 11; here, the oxygen in glycosidic bonds is protonated by the acidic hydronium ion to cleave out the amorphous regions.[34] The use of 62–65% (w/w) sulfuric acid as the hydrolytic media has been a well-known effective way for extracting CNCs from lignocellulosic biomass, which is included in many reports in the literature.[112–121]

Under controlled time and distinction in kinetics, CNC is successfully obtained from different rates of hydrolyzing the amorphous and crystalline regions. In a study to extract CNC from tea leaf waste fibers under hydrolysis with 65 wt% sulfuric acid at 45 °C for approximately 45 min has managed to increase the crystallinity of CNCs in bleached fibers from 74.4% to 83.1%, indicating the successful removal of non-cellulosic substances.[112] Fig. 11b–f show the XRD and electron microscopy characterizations of the cellulose and nanocellulose at each point of treatment. Nonetheless, the rapid decrease in the degree of polymerization upon acid hydrolysis over a long

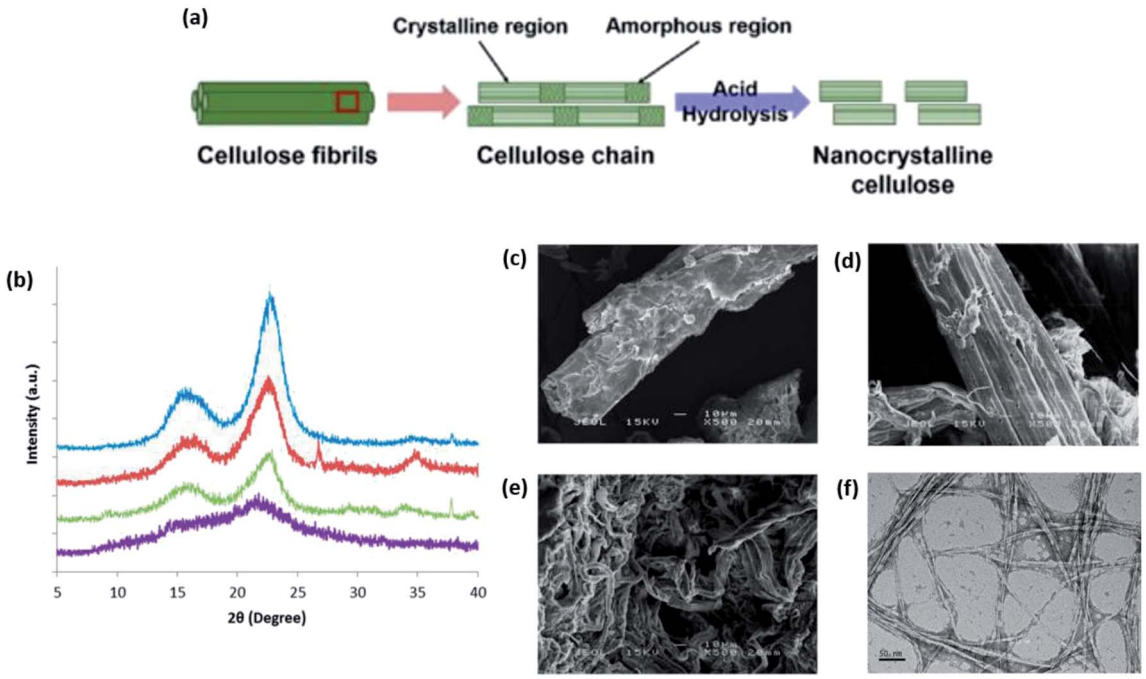

Fig. 11 (a) Schematic of the CNC produced from cellulose chains using the acid hydrolysis treatment method; (b) XRD diffractograms of raw tea leaf waste fiber (purple), alkaline-pretreated tea leaf waste fiber (green), bleached tea leaf waste fiber (red), and extracted CNC (blue); SEM micrographs of (c) raw tea leaf fiber, (d) alkaline-pretreated tea leaf waste fiber, and (e) bleached tea leaf waste fiber (scale bar: 10 μm); (f) TEM micrograph of the extracted CNC (scale bar: 50 nm) [adapted with permission from Phanthong *et al.* 2018 & Abdul Rahman *et al.* 2018,[111,112] Copyright © Elsevier Limited & © MDPI].

period often results in the degradation of CNC, affecting its thermal stability. Therefore, many researchers have turned to using milder acids such as hydrogen chloride and formic acid.[34]

The esterification of the hydroxyl group in the cellulose by a negatively charged sulfate anion accounts for colloidal stability when dispersed in solution because of the strong electrostatic repulsion.[111] However, the presence of anionic groups compromises the thermostability of the final nanocellulose product that was characterized by thermogravimetric analysis (TGA) by Yang and co-workers.[122] Conversely, the thermal stability would be improved if the cellulose had undergone acid hydrolysis with hydrochloric acid (HCl), but the CNC tends to aggregate more due to poor dispersibility and surface charge.[123] Moreover, the difficulty to control the crystal polydispersity and morphology has presented challenges in both quantitative characterization and ensuring the reproducibility of work.[124] Recent studies have attempted to prepare less polydisperse CNC samples through asymmetrical flow field-flow fractionation, which dramatically improved the ability to characterize the CNC crystal size and other physical properties. However, many open questions remain unanswered on how the particle size distribution and polydispersity influence the behavior of CNC in terms of diffusivity in composite matrices and the physicochemical properties of the final product.

On the other hand, the application of TEMPO for surface modification on cellulose could introduce carboxylate and aldehyde functional groups.[47] It works in the same way as acid hydrolysis by introducing negatively charged groups for electrostatic repulsion,[125] which eases nanofibrillation through improved colloidal stability and elimination of cellulose aggregation *via* hydrogen bonds. Fig. 12 shows the chemical and position selectivity in the biomass fractionation for better understanding the various chemical treatments that are proposed. In addition to the preparation of well-dispersed nanocellulose, their physical properties could be more easily controlled by TEMPO oxidation in comparison to acid hydrolysis.[125] Wakabayashi *et al.* managed to prepare a TEMPO-oxidized nanocellulose film with versatile porosity,

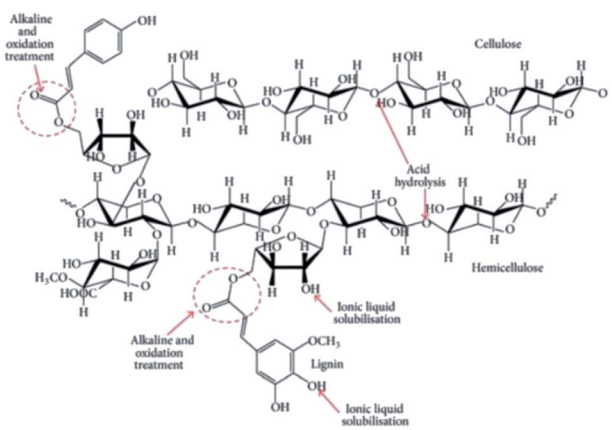

Fig. 12 Schematic of the selectivity of chemical treatments toward biomass fractionation [reprinted with permission from Lee *et al.* 2014,[18] Copyright © Hindawi].

mechanical and optical properties, and oxygen permeability by controlling the degree of fibrillation.

A similar method was employed by Soni *et al.* in isolating oxidized CNFs from cotton stalks *via* TEMPO-mediated oxidation for producing CNFs of uniform sizes (width: 3–5 nm; length: 10–100 nm) with a high yield of 90%.[126] The mechanism of cellulose undergoing TEMPO oxidation with the grafting of the carboxylate group was proposed, as shown in Fig. 6b, illustrating the regioselective oxidation of cellulose at the C-6 primary hydroxyl group into the carboxylate.[127] A recently published article by Oun and Rhim developed another strategy to oxidize isolated nanocellulose from rice straw by using 1.0 M ammonium persulfate (APS) at 75 °C for 16 h.[128] It is imperative to note that TEMPO-mediated oxidation dramatically differs from APS oxidation as the latter produces CNC with higher crystallinity and thermal stability even though its diameter (14 ± 7.0 nm) is larger.

3.2.3. Enzymatic treatment. Enzymatic treatment is another alternative to reduce the overall energy consumption while facilitating effective nanocellulose production.[99] Hydrolysis using an enzyme, particularly cellulase, provides another alternative to obtain nanocrystals of cellulose from biomass.[129] The active constituents of cellulase include endoglucanase, cellobiohydrolases (I and II), and β-glucosidase. Endoglucanase aims to randomly eliminate the amorphous domain of cellulose, leaving most of the product crystalline.[102] Cellobiohydrolases I and II destroy the crystalline region from the ends of the linear cellulose chain; finally, β-glucosidase breaks them down into glucose.[130,131] Subsequently, it is important that these three constituents be separated in the cellulase enzyme so that the latter two components could be avoided to preserve the nanocrystalline cellulose.[129,130]

Lignin, being one of the main constituents of woody biomass, constructs the major barrier to enzymatic hydrolysis[132] and many research papers have focused on a combined process with pretreatments to overcome biomass recalcitrance and enhance the effectiveness of enzymatic hydrolysis.[133–136] Moreover, mild agitation and exposure to the air–liquid interface could inhibit the activity of the enzyme.[137] Lou and his coworkers demonstrated the enhancement of the enzymatic hydrolysis of cellulose using nonionic surfactants (PEG4600) to reduce this deactivation, wherein the surfactant competes with cellulase at the air–liquid interface shielding it from exposure to reduce the deactivation of enzymatic activity. PEG4600 also forms a hydration shell around cellulase through hydrogen bonding to lubricate the effect of shear force on the enzyme. Enzymatic treatment, in comparison to others, is known to reduce water consumption by approximately 67% and presents a more sustainable process compared with chemical treatment for their toxic effluent.[138] A critical open question is whether enzymatic treatment is the most selective and effective method over other reported strategies to prepare CNCs.

Nevertheless, a limitation of these pretreatment methods is that they do not always guarantee improved performance of enzymatic hydrolysis as inhibitory byproducts could be generated, which may lead to the unproductive adsorption of enzymes, as disregarded by many studies.[139] Furthermore, Ribeiro *et al.* underlined the high costs and slow process of enzymatic hydrolysis, which has hindered the upscaling of this treatment for nanocellulose production.[140] Table 5 summarizes some of the latest publications on the preparation of CNF and CNC with various characteristics for comparison. In order to find commercial value in industrial applications, surface modifications or functionalization including silylation, acetylation, carbonylation, or polymeric grafting are the most practical methods that have been comprehensively reported thus far.[13]

4. Fundamentals of 3D printing

3D printing is the state-of-the-art manufacturing technique underpinning a remarkably infinite prospect of customizability, flexibility, and sustainability in the production of newly developed materials. While the emergence of 3D printing is revolutionizing the global manufacturing system, some authors have suggested that the current understanding of its cost modeling and applicability still lags behind.[168,169] Over the past decades, 3D printing has found a wide range of applications in different fields, particularly biomedical and biotechnology.[170–172] In addition, different methods of 3D printing have been summarized and compared in the subsequent segments.

4.1. Fused deposition modeling (FDM) and direct ink writing (DIW)

The FDM and DIW 3D-printing techniques have been developed as bottom-up processes, where the material fed into the print head gets pneumatically deposited in a layer-by-layer manner. The materials used here include thermoplastic filament made of polymers[173] for FDM and liquid print inks[174,175] for DIW that are heated at the nozzle into a flowable semiliquid state that solidifies after printing and conductive cooling.[176] Further, numerous authors have employed this technique to bio-print nanocellulose for implants and cell scaffolds.[177,178]

Wang and her co-workers utilized polylactic acid (PLA) filled with nanocellulose and polyethylene glycol (PEG) as the filament for FDM printing.[180] The inclusion of nanocellulose improved the thermal stability, mechanical strength of the PLA composite filament, and provided synergistic effect with PEG on the crystallization rate with the semi-crystallization time shortened from 12.2 min at 120 °C for a pure PLA filament to 1.5 min at 100 °C for nanocellulose-incorporated PLA/PEG composite that is used as the filament in FDM printing. Ambone *et al.* also demonstrated the improvement in the 3D-printed PLA structure in tensile strength and modulus by 84% and 73%, respectively, with just 1 wt% CNFs extracted from the sisal fiber. Moreover, crystallinity also increased by 14% with an addition of 14 wt% CNF, which contributes to the accelerated nucleation of the 3D-printed PLA structure.[181] In another instance, Giubilini *et al.* fabricated biodegradable reinforced poly(3-hydroxybutyrate-*co*-3-hydroxyhexanoate) (PHBH) with acetyl-functionalized CNC with FDM printing into a complex design.[182] The acetylation of CNC enhanced the dipole–dipole interactions with the carbonyl groups of PHBH for solvent-free

Table 5 Summary of the different preparation processes of CNFs and CNCs

Source material	Pre-treatment	Treatment	Post-treatment	Characteristics of nanocellulose	Reference
Cellulose nanofibers					
Corncob cellulose	(Commercially available corncob cellulose)	Ball milling with *N*,*N*-dimethylformamide (DMF) and hexanoyl chloride (HC)	Solvent-exchanged to *t*-butyl alcohol and freeze-dried	– Esterified CNF obtained with 54% crystallinity degree upon 6 h of ball milling – TEM images show typical fibril width of 1.5–2.8 nm width after 6 h of ball milling	141
Hemp stubs (*Cannabis sativa* L. subsp. *Sativa*)	Peeled and grounded into rough powder, followed by alkaline treatment with 4 w/v% NaOH and bleaching with 1.7 w/v% $NaClO_2$	Dispersion of suspension using high-speed blender before defibrillation by microfluidizer	Freeze-dried for further analysis	– CNF of diameter 10–50 nm was obtained upon maximum 120 min of defibrillation – Degree of polymerization of obtained CNF was 1371 and crystallinity index of 78.25% after 120 min of defibrillation – Onset degradation temperature was 279 °C	142
Sisal fibers	Washed, dried and macerated with 2 w/v% NaOH, followed by bleaching with 1.7 w/v% $NaClO_2$; fibers dried and crushed	Acid hydrolysis with 64 v/v% H_2SO_4	Dialyzed and sonicated	– CNF with mean length of 302.3 ± 29.2 nm and width of 12.7 ± 1.6 nm – Zeta potential on the surface of each CNF particle was −23.6 ± 2.1 mV in water suspension – Decomposed between 257.46 °C and 352.81 °C	143
Bamboo leaf	Grounded and sieved through 60-mesh before removing wax under soxhlet with benzene/ethanol solution	Dispersed in water and ultrasonicated at 1800 W	Oven-dried and solvent-exchanged to ethanol for further functionalization	– TEM shows average fibril diameter of 53.2 nm with high aspect ratio of 5600 – CNF crystallinity was 55.0% – TGA shows onset degradation temperature at 194 °C	144
Olive tree (*Olea europaea*) pruning (OTP) residue	Cooked in sealed reactor at high temperature and then disintegrated at 1200 rpm; further delignification upon treatment with oxygen using same reactor	TEMPO-oxidation of extracted pulp followed by defibrillation using microfluidizer	Washed and stored in refrigerator	– Crystallite size of 3.1 nm observed by XRD with 82% crystallinity index – High carboxylate content at 1038 μmol g^{-1} – Fibrillation yield of 48%, considerably low	145
Soybean hull; wheat straw; pine wood flour	Disintegrated using high-speed grinder at 25 000 rpm followed by sieving through 100-mesh; macerated in 2 w/w% NaOH and bleached with $NaClO_2$	TEMPO-oxidation followed by fibrillation using microfluidizer	Aqueous suspension homogenized using high-speed homogenizer	– Onset degradation temperature at approximately 205 °C – AFM shows average diameters of 5 nm (soybean hull), 3 nm (wood flour) and 6 nm (wheat straw) CNFs – Treatment yield of 22.1% (soybean hull), 70.8% (wood flour) and 41.4% (wheat straw)	146

Table 5 (*Contd.*)

Source material	Pre-treatment	Treatment	Post-treatment	Characteristics of nanocellulose	Reference
Bamboo pulp	Alkaline treated with NaOH and bleached with $NaClO_2$	Cellulase treatment followed by ultrasonic homogenization	Dispersed as aqueous suspension (0.1 wt%) for further analysis	– TEM analysis shows CNF length of several micrometers and diameter of 20–30 nm	147
Softwood kraft pulp sheets	Torn into pieces before immersing into oxalic acid dihydrate to obtain cellulose oxalate	Dispersed in water and pH adjusted to 9–10 for full dissociation, followed by disintegration using microfluidizer	Diluted suspension and dispersed using high-speed homogenizer	– Treatment yield of 85.6% with 0.97 mmol g^{-1} free carboxyl content upon 60 min of reaction time with oxalic acid dihydrate – Estimated degree of substitution at 0.17 – Onset thermal degradation at 176 °C – Average length reported to be 0.34 μm and diameter of 3.2 nm after 35 min reaction	148
Hybrid aspen *Populus tremula x tremuloides*	Grounded into powder and dewaxed with acetone/methanol soxhlet extractor before alkaline treatment with 2 wt% NaOH and bleaching with $NaClO_2$	TEMPO-oxidation before disintegration using high shear fluid homogenizer at 1000 bar	Diluted to 0.2 wt% consistency before further characterization	– Yield of CNF after TEMPO-oxidation was 47.4 ± 0.7% – Main degradation temperatures at approximately 220 °C and 315 °C – Fine grade CNF at toughness height of 2 nm while coarse grades height between 2 nm and 100 nm	149
Hardwood kraft pulp	Grounded using high-power grinder and swelled with glycerol before extruding cellulose fibers	Swelled mixture added with 72% H_2SO_4 and agitated before neutralization with 10 w/w% NaOH; neutral mixture deep grinded with colloid mill at 6000 rpm	Mixture dialyzed to remove glycerol completely	– With 1.28% H_2SO_4 added in treatment of swelled mixture and stirred for 2 h, CNF fibril width falls within 80 nm – High treatment yield of 85%	150
Acetobacter xylinum	Incubated to obtain bacterial cellulose (BC) pellicles	Purified through 2 wt% NaOH and mechanically compressed without heat to remove excess water	Made into five different aligned nanofibril bacterial cellulosic film samples from draw ratios of 0%, 5%, 10%, 15% and 20%	– Estimated intrinsic birefringence at 0.09	151
Strain *G. xylinus*	Cultivated in Hestrin–Schramm medium and 4.0% mannitol	Starter cell culture prepared using stock solution of glycerol for incubation	Bacterial cellulose membrane was harvested and rinsed continuously in 0.5 M NaOH before washing, cutting into small pieces and freeze-dried for further analysis	– Degree of crystallinity was at 92% – SEM micrograph shows fibril diameter at around 70 nm forming nanoporous matrix – Tensile test shows BC film with 16.4 ± 0.84 GPa	152

Table 5 (*Contd.*)

Source material	Pre-treatment	Treatment	Post-treatment	Characteristics of nanocellulose	Reference
Ginger tubers	Raw ginger was soaked and dewaxed in toluene/ethanol soxhlet extractor before drying; subsequently immersed into 5% NaOH and bleached with mixture containing $NaClO_2$ and CH_3COOH	Suspension hydrolysed with 5 M HCl before washing and hydrolyzation; ultrasonic homogenization at 600 W for 60 min	Samples dried in oven overnight before characterization	– CNF length falls within 100 nm from FESEM micrograph – Crystallinity index was 67% after acid hydrolysis but decreased to 48% upon ultrasonication – Maximum decomposition temperature at 353 °C after ultrasonication treatment – Moisture absorption of sonicated CNF film was 7.4 ± 0.6%	153
Komagataeibacter hansenii	Cultured in fermentation medium for 14 days; BC harvested and rinsed with running water overnight before soaking into 0.1 M NaOH	Disintegration with high-speed blender at 15 000 rpm, before being hydrolysed by 2.5 M HCl	Washed until neutral before storing in refrigerator until analysis	– BC nanofiber with 40–80 nm in diameters and 100 nm to several micrometers in lengths – With 4 wt% of B-CNF, AFM analysis has shown roughness (R_q) at 61.80 ± 4.55 – Main degradation at 180–210 °C and 280–330 °C for different B-CNF content (0–3 wt%)	154
Hardwood kraft pulp	Fiber treated with DES (choline chloride/imidazole) and washed	DES pre-treated pulp diluted to 0.5 wt% and premised with high-speed homogenizer at 10 000 rpm; nanofibrillated with microfluidizer	Freeze-dried for further characterization	– TEM shows CNF average fibril diameter from 10–18 nm – Onset thermal degradation happened at 273–278 °C	155
Cellulose nanocrystals					
Cotton fibers	Soxhlet pre-treatment with benzene-alcohol and ground into fine grains sieved through 20-mesh	Mixed with 63.9 w/w% H_2SO_4 and quenched	Dialyzed for 2 days before freeze-drying for further tests	– Average length of CNC at 125.6 nm upon acid hydrolysis for 55 min – Crystallinity of 90.72% was observed for CNC hydrolysed for 55 min – Specific surface area was at 118 $m^2\ g^{-1}$ and total charge density at −0.314 meq. g^{-1} after 55 min of acid hydrolysis	156
Sugarcane bagasse pulp (bleached)	Cut into small pieced by crusher	One-step ammonium persulfate (APS) oxidation	Freeze-dried for further characterization	– With 2 mol L^{-1} APS used, the carboxyl content in cellulose was at 0.99 mmol g^{-1} – CNC length was 140–500 nm and width 8 nm–20 nm when treated with 2 M APS – Relatively high crystallinity of 76.5% for APS-treated CNC – Onset degradation temperature at 277 °C, higher than TEMPO-CNC at 227 °C	157

Table 5 (*Contd.*)

Source material	Pre-treatment	Treatment	Post-treatment	Characteristics of nanocellulose	Reference
Gelidiella aceroso red seaweed	Dried and ground into powder using ball miller; pre-treated using 2.5 M NaOH with simultaneous microwave irradiation (360 W); bleached with 32% H_2O_2	Acid hydrolysis with 1 M H_2SO_4 solution and 1 M EMIM(Cl) assisted by ultrasonication at 450 W	Samples freeze-dried for further characterization	– Average diameter of CNC obtained reported between 10 nm–21 nm – AFM analysis has observed CNC length at 408 nm – Crystallinity was at 60% with crystallite size of 4.57 nm – Final CNC yield was calculated to be 30%	158
Cotton cellulose fiber	Ground into fine powder using milling machine and sieved through 0.5-mesh	Acid hydrolysis with oxalic acid and ultrasonicated at 30 kHz	Final suspension with pre-determined concentration prepared for subsequent tests	– Lengths of CNC concentrated between 300 nm and 400 nm; average diameter at around 10 nm – Crystallinity index of obtained CNC was found to be 70.7% – Peak thermal degradation occurred at approximately 310 °C, lower than original fiber	159
Maize plants (*Zea mays* L.) from hybrid Supremo Viptera	Stem of maize plant used; cut into small pieces and dried in oven before crushing in rotor cutting miller; alkaline treatment and bleaching	Acid hydrolysis with 64–66 w/w% H_2SO_4	Dialyzed to neutral pH before characterization	– CNCs obtained have mean dimensions of 66.7 nm (length) and 2.7 nm (diameter); aspect ratio at 24 – Onset degradation temperature at 199.3 °C and maximum degradation at 358.6 °C – Crystallinity of CNC was at 66.8%	160
Jackfruit peel	Three methods: (1) Dewaxed with water then ethanol; bleached with 1.5 w/v% $NaClO_2$; alkaline treatment (2) Dewaxed biomass treated with 5 w/v% NaOH; bleached with 10 v/v% hydrogen acetic acid and 65% nitric acid (3) Pre-treated with 3 v/v% H_2O_2 and 10 w/v% NaOH; added 20% formic acid and 10% H_2O_2	Acid hydrolysis with 65% H_2SO_4	Dialyzed to neutral pH and ultrasonicated in bath sonication; suspension concentrated with rotary evaporator and dried	– Produced spherical CNC has diameter of 130 nm and average zeta potential of −11.6 mV (method 1 pre-treatment) – Isolated CNC has crystallinity index of 83.42% – Maximum degradation linear range observed at 312–350 °C	161

Table 5 (*Contd.*)

Source material	Pre-treatment	Treatment	Post-treatment	Characteristics of nanocellulose	Reference
Scoured cotton fiber	Washed with ethanol and dried in oven	Hydrolysis with DES (choline chloride/oxalic acid); dissolved cellulose in DES dispersed in ultrapure water and placed in high-pressure homogenizer at 100 MPa	Recycling of DES: permeated solution subjected to distillation using rotary evaporator and reused	– Average diameter observed at 300 nm after 30 min cycle in homogenizer – Obtained CNC has crystallinity index of 77.6% – Onset degradation of isolated CNC occurred at 304.3 °C and maximum degradation at 343.14 °C	162
Cotton powder	Cotton powder milled using laboratory milling machine	Milled powder introduced into microwave pressure vessel with 1 M APS added; heated with 850 W microwave power	Suspension of CNCs undergo centrifugation-washing for purification and remove excess acid using deionized water; freeze-dried for further characterization	– Average CNC length of 153 nm and width 7 nm observed – Treatment yield at 45% – Dispersed nanoparticles in water have zeta potential of −0.040 V – Maximum degradation temperature occurred at 343.16 °C	163
Seaweed biomasses (*Laminaria japonica*, *Sargassum fluitans*, *Palmaria palmata*, *Porphyra umbilicalis*, *Ulva lactuca*, *Arthrospira maxima*)	Pulverized into powder form; depolymerization with 0.2 M HCl followed by 4% NaOH; bleached with 5% KOH and then 30% H_2O_2	Acid hydrolysis with 51% H_2SO_4 and quenched after 30 min	Centrifugation-washing with deionized water followed by homogenization with ultrasonicator	– Crystallinities of all CNCs extracted fall within 66.97%–98.89% – Highest aspect ratio of 11.50 ± 3.66 was obtained with *Laminaria japonica*; with average length at 239.43 ± 38.57 nm and width at 22.45 ± 6.51 nm	164
Hardwood kraft pulp cellulose	(Commercially available kraft pulp)	Acid hydrolysis with concentrated 64% H_2SO_4	Dialyzed to neutral pH and sprayed dried into powder form by emulsification with hempseed oil; re-dispersed at predetermined concentration in deionized water through stirring and sonication	– Zeta potential of obtained CNCs was found to be −51.7 ± 0.5 mV – Dimensions of approximately 200–250 nm (length) and 10–15 nm (width) – Onset degradation temperature for the CNCs was at 280 °C	165
Rice husk biomass	Washed and dried, before grounding in a knife mill to sieve through 14-mesh; alkaline pre-treatment with 5 w/v% NaOH in controlled temperature jacketed reactor; bleached with solution of H_2O_2, NaOH and magnesium sulfate	Acid hydrolysis with 64 w/w% H_2SO_4 and quenched after 30 min	Centrifugation-washing with deionized water and dialyzed; ultrasonic homogenization of dialyzed suspension before lyophilizing	– Chlorine-free preparation of the CNC has yielded a degree of crystallinity at 77.45% – Isolation yield was at 52.8% – Onset thermal decomposition temperature was found to be at 226 °C – DLS analysis has shown hydrodynamic diameter of CNC to be of 220 nm	166

Table 5 (*Contd.*)

Source material	Pre-treatment	Treatment	Post-treatment	Characteristics of nanocellulose	Reference
Wastepaper	Cut into small pieces and shredded	One-step APS oxidation	Freeze-dried to obtain powdered CNCs	– CNC obtained has aspect ratio of 30; 130 ± 15 nm (length) and 4 ± 2.5 nm (width) – Crystallinity was found to be 72.45%, but with low yield of 22.42% – Maximum decomposition temperature at 324 °C, higher than acid hydrolysed CNC at 207 °C – 0.57 mmol g^{-1} of carboxyl content was introduced upon decomposition of APS to H_2O_2	167

melt compounding. This revealed the necessity of functionalizing CNC to minimize the aggregation of pristine CNC that could create difficulties in melt compounding. With the inclusion of 20 wt% acetylated CNC, the storage modulus of composites observed a 150% enhancement.

The DIW of nanocellulose composites was demonstrated by Müller and co-workers with a controllable Young's modulus based on the composition of anisotropic CNC.[183] These CNCs were made to be photoresponsive by grafting photocrosslinkable cinnamates on their backbones before inclusion into a polyurethane acrylate matrix. They were extruded into a modeled 3D structure and photo-stiffened under UV irradiation at 410 nm. Notably, the limited compatibilities of hydrophilic nanocellulose with a normally hydrophobic polymer matrix is necessary for successful compounding.[184,185] Hence, the functionalization or grafting of nanocellulose is usually required for the compatibilization and stabilization of the nanocellulose–polymer mixture before 3D printing.

4.2. Digital light processing (DLP) and stereolithography (SLA)

DLP and SLA print out a photo-polymeric resin in the top-down (can also be bottom-up) approach that can be selectively cured and polymerized by light or laser illumination. The degree of curing and shape fidelity can be controlled by the type and formulation of the photo-initiator and photo-absorber. The print platform can immerse into the liquid resin and the first layer can solidify onto it upon light-initiated curing by a digital light projector or UV laser according to the 2D-patterned layer in a 3D CAD model.[186]

This technique has been demonstrated on fabricating a CNF composite material for bio-adhesion and optics by Sun and co-workers.[187] A hybrid poly(*N*-isopropylacrylamide) (PNIPAm)/CNF hydrogel was fabricated *via* inverted SLA with a tuned bio-adhesive and optical properties. An impressive 8 °C reduction in the lower critical solution temperature was achieved with the incorporation of just 2.0 wt% CNF, possessing controllable bio-adhesion in response to a change in temperature. Despite having a faster print time, 3D parts printed using DLP have compromised the print resolution and surface finish.[188,189] In addition, the porosities of the printed construct have been difficult to control with light-mediated printing.[184]

4.3. Inkjet 3D printing

As shown in Fig. 13c, inkjet 3D printing prints analogously as a normal inkjet printer. It can be used to print a complex structure with advanced materials such as ceramic powder suspension.[186] A final heat treatment is necessary to strengthen the bond between the substrate and binding powder while removing the unbound ones.[173]

The utilization of the inherent features of the nanochitin–nanocellulose material, including biocompatibility and high surface area for cell adhesion, for inkjet printing into the cell culture substrate has been explored in prior studies by Teramoto.[190] Mouse fibroblast cell line L929 micropatterned and

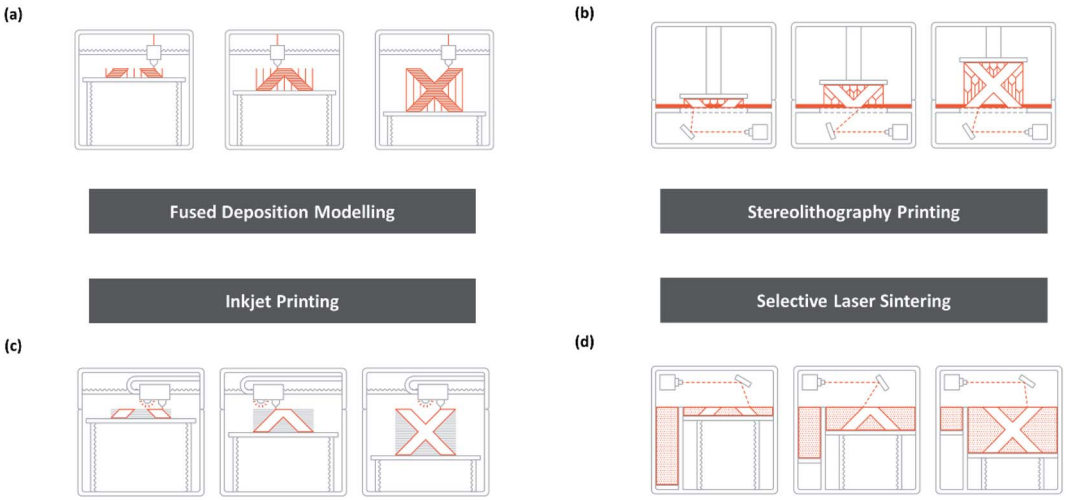

Fig. 13 Schematic of (a) FDM, (b) SLA, (c) inkjet printing, and (d) SLS [adapted with permission from 3D HUBS 2019 (ref. 179)].

cultivated onto the printed material was found to be more susceptible to bio-adhesion and therefore proliferation compared with a polystyrene (PS) substrate.

4.4. Selective laser sintering (SLS)

Similarly, using a powder at a low sintering temperature is called SLS, also known as powder bed fusion, which fuses each layer of the powdered material with the thermal energy from a focused laser to the building part. The surface of each layer is partially liquefied to initiate the binding. The build stage subsequently lowers and spreads another layer of powder on top for binding, finally removing the excess by a vacuum. This technique is adept to fabricate 3D structures from an array of polymeric, metallic, or alloy powders. Different from FDM and SLA, SLS does not require a support structure since the sintered layers are supported by the residues.[189] Moreover, the residual powders could be recycled and reused, minimizing wastage.[188]

Table 6 Summary of materials, print resolution, strengths, and weaknesses of different 3D-printing methods

3D-printing method	Materials	Resolution range (μm)	Strength	Weakness	References
FDM	Thermoplastic filament (photopolymer, biopolymer, *etc.*)	50–200	- High speed – Simple to operate – Huge availability of thermoplastics – Good surface finish	– More expensive than SLA & DLP – Brittle product – Clogging of nozzle	173, 176 and 191
DIW	Viscous liquid ink or paste that solidifies	1–100	– High speed – Simple to operate – Wide range of viscous ceramic or polymeric materials	– Easy to collapse and limited to 2D stacking – Requires strict optimization on rheology of ink	173, 176 and 191
SLA & DLP	Photopolymer resin	10	– Fine resolution with smooth surface finish – High quality – Low cost	– Very limited photopolymer resin material – Toxic photoinitiators – Slow speed	173, 176, 179 and 191
Inkjet printing	Concentrated suspension (ink or paste) of ceramic, concrete, *etc.*	5–200	– High speed – Large structure printable	– Coarse surface with low resolution – Lack strong adhesion between layers	173, 179 and 186
SLS	Thermoplastic powder	80–250	– Can print object with hollow design – Fine resolution	– Expensive – Slow speed – Coarse surfaces that require post-processing	176, 179 and 191

It should be noted that the extrusion-type FDM and DIW printing techniques are most commonly employed for the ease of functionalization, mechanical reinforcement, and favorable rheological properties of nanocellulosic materials. Table 6 lists a summary of the various 3D-printing techniques by comparing the type of materials used, resolution of printing, as well as the strengths and weaknesses of each method.[173,176,186,191,192]

4.5. Nanocellulose as a viable 3D-printable material

With the introduction of 3D printing that allows the production of complex structures relying on the user's 3D computer-aided design, a plethora of materials have been developed but still not widely used due to the lack of robust properties.[189] Therefore, this calls for a new class of 3D printable material that is highly sustainable, biocompatible, green, and customizable for achieving the desired mechanical and physicochemical properties.[193,194] The advent of a biopolymer such as nanocellulose opens a new paradigm toward the discovery of a new generation of materials that could be safely and effectively put into real-life applications.

3D printability strongly relies on the materials' rheological properties as well as consistency in gelation of the polymer. Even though there is currently no reported standardized method of evaluating the printability, visual observation and measurements using photographs taken after printing have been prevalently practiced.[195,196] Dai *et al.* proposed that the favorable physicochemical and mechanical properties of cellulose nanomaterials such as high strength and ease of surface functionalization greatly contribute toward its potential as a 3D-printing material.[197] Due to the extensive fibril entanglement and hydrogen bonding, CNF could readily form a hydrogel with high zero shear viscosity that is appropriate for 3D printing.[197,198] Even so, the change in the rheological properties within the gel should be minimized during gelation to promote high shape fidelity and volume production.[199] It is also found that CNC with a length of 13 nm and a width of 0.3 nm was observed to have a permanent structural alteration above the maximum 25% viscosity change, complexly influenced by shear stress, temperature, and concentration.[200]

Various researchers have investigated the relationship between the 3D-printed structure and rheological properties of the biomaterial hydrogels.[201–203] Two conditions must be achieved before studying the effect of the rheological behavior: (1) components of the hydrogel to obtain proper and consistent extrusion and (2) ability to hold the structure upon crosslinking. The viscoelasticity and shear thinning effect of nanocellulose provides better control over the print resolution and accuracy, wherein the injection of the print ink is eased even at higher concentrations and retaining an increased viscosity upon extrusion with high shape fidelity.[204] Ma *et al.* successfully quantified the shear-induced particle alignment of CNC with atomic force microscopy (AFM) and 2D wide-angle X-ray scattering (2D-WAXS) upon 3D printing as composite hydrogels.[203] They revealed that an optimal print resolution and shape fidelity was achieved with 20 wt% CNC that ensures a high degree of CNC particle alignment along the 3D-printed

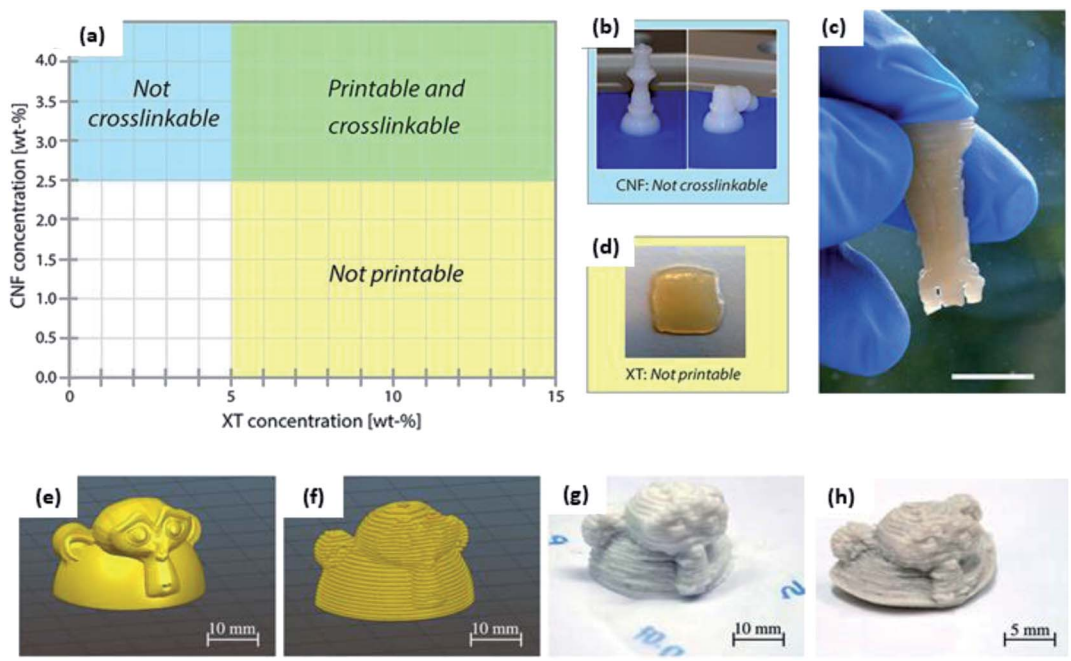

Fig. 14 (a) Plot of print ink composition with varied CNF:xylan–tyramine (XT) concentrations for the prediction of printability and crosslinking ability; (b) 3D-printed chess piece with 100% CNF and collapsed due to no cross-linkability; (c) printed queen chess piece with optimal composition of CNF:XT ink, held upside down; (d) unsuccessful grid printed with pure XT, showing poor printability; (e) CAD model of elephant head to be printed; (f) rendering of CAD model to be printed with 0.84 mm-diameter nozzle; (g) wet-printed structure and (h) deformed dried printed structure [reproduced with permission from Markstedt *et al.* 2017 & Klar *et al.* 2018,[212,217] Copyright © American Chemical Society & © Springer Nature Limited].

direction, with orientation at 72%. This can be explained by the anisotropic crystallization of CNC when the solvent evaporated upon extrusion, inducing an ordered self-assembly of the nanocrystals. This quantification provides a strong basis for the optimal concentration of CNC to be considered during extrusion-type 3D printing for future studies.

Another critical property that governs 3D printability in nozzle-based printing is the dispersibility of nanocellulose within the liquid ink. Nanomaterials are highly likely to agglomerate due to their poor surface zeta potential and could therefore clog up the nozzle.[205] To overcome this problem, most researchers have relied on the deposition of highly charged nanoparticles such as carbonate-stabilized gold nanoparticles onto functionalized CNC surfaces with the help of surfactants. The increase in electrostatic repulsion would facilitate the diffusion and prevent the agglomeration of nanocellulose in the print ink.[206] In addition, solvent compositions to improve the dispersibility and stability of nanocellulose dispersion should be investigated as it has a critical influence on the rheology of ink and viscoelasticity of the printed construct.[185,188]

Numerous publications since 2017 have investigated the preparation of UV-crosslinkable nanocellulose gels for 3D printing, particularly for DLP and SLA.[178,207,208] Tang *et al.* developed a methodology that prescribed the use of polyethylene glycol diacrylate (PEGDA) to prepare UV-crosslinkable hydrogel based on nanocellulose composites, where the former component induced photosensitivity in the aqueous dispersion of nanocellulose containing a photoinitiator, namely, Irgacure 2959.[208] From the FT-IR spectroscopic analysis of the hydrogel, it was noted that nanocellulose does not have any influence on the photopolymerization since there is no difference between the spectra of nanocellulose/PEGDA and pure PEGDA hydrogels. However, Tang *et al.* makes no attempt to provide sufficient consideration to the cytotoxicity of the photoinitiator used in this study for application in the printing cell scaffold. The findings would have been more persuasive if the authors had conducted a cell viability analysis on the relevant mammalian cells.

Lately, CNCs have also been extensively proven to enable the 3D printability of thermoset elastomers *via in situ* polymerization to enhance the interfacial adhesion force among the 3D-printed layers.[209] The presence of CNC slows down the solidification of the thermoset rubber upon printing, allowing interlayer diffusion to happen. Tang *et al.* further investigated the benefit of nanocellulose inclusion into the hydrogel and manifested its contribution to improving the compressive modulus from 0.7 MPa without nanocellulose to 0.91 MPa containing 1.8% nanocellulose.[208] This improvement was accounted for by the ability of the nanocellulose toward self-alignment and restricted mobility in the hydrogel. The gradual *in situ* gelation has created less time to mobilize and reorient.[199,210]

Besides SLA/DLP, nanocellulose has been integrated as both a rheological modifier[211,212] and a reinforcer[213–216] for inkjet printing and extrusion-based FDM, respectively. Markstedt *et al.* proposed a 3D-printable ink that completely comprised forest-based components such as xylan and CNF functionalized by tyramine to be crosslinkable, extrapolating the development of printable materials beyond synthetic polymers.[212] Fig. 14 shows the predicted printability of the composition (CNF:xylan–tyramine) and the cases when pure components were individually printed. We understand that crosslinking is fundamental to prevent the collapse of the printed object, keeping it intact during handling. Therefore, this paper exemplifies the printability and crosslinking ability of the natural CNF and xylan–tyramine, respectively, exhibiting promising potential as bio-inks for tissue engineering.

Despite having cellulose as its precursor, huge research work has been conducted to incorporate nanocellulose into papermaking as it can contribute toward overcoming the limit of mechanical strength and barrier properties of the current paper products.[193] Other than its excellent mechanical properties, nanocellulose in the composites with other materials exhibits versatility in terms of their forms such as powder, hydrogel, aerogel, or films depending on its combination and composition. This flexibility of controlling the form could be beneficial in 3D-printing applications, easing the choice of printing technique, and design of experiments.

Admittedly, much attention has been paid toward the study of the fabrication process for high structural complexity,[198] controlled print resolution, and quality and characterization of mechanical properties,[218] which is equally important as the development of 3D-printable and compatibilized materials (resins, gels, filaments, *etc.*).[219] Anisotropic volumetric deformation and shrinkage have been observed for the enzymatically produced high consistency nanocellulose because of the substantial water content within the printed structure, as shown in Fig. 14e–h.[217]

In order to properly study the issue on shape fidelity, Klar *et al.* reported that the consistency, printing parameters, and post-treatment are extremely critical; therefore, high consistency (25 wt%) coupled with slow air drying (25 °C with 50% relative humidity) after printing yielded a systematic improvement in the structural integrity. An impressive study by Hausmann provided evidence that the quantification of the dynamics of CNC alignment during extrusion printing helps the user in deciding on the optimal design of printing conditions, nozzle size, and rheological properties to fine-tune the local properties of the printed structure.[220]

A double strategy based on physical and chemical enhancement was employed by Wang *et al.* to enhance the 3D printability and construction fidelity of the reinforced cellulose nanocomposite with the SLA technique.[221] CNC reinforcement induced physical enhancement to the mechanical properties where the tensile strength was increased from 32.9 to 45.9 MPa with 0.5 wt% CNC and glass transition of the reinforced compound additive increased from 119.8 to 126.9 °C. Esterification was conducted for chemical enhancement due to the formation of percolated and robust network in the post-cured structure to induce a stronger interaction between the filler and resin.

There is a high incentive to obtain a deeper understanding of the ink formulation requirements and relevance of different parameters for the design of experiment in 3D printing. With that in mind, additional studies to more comprehensively

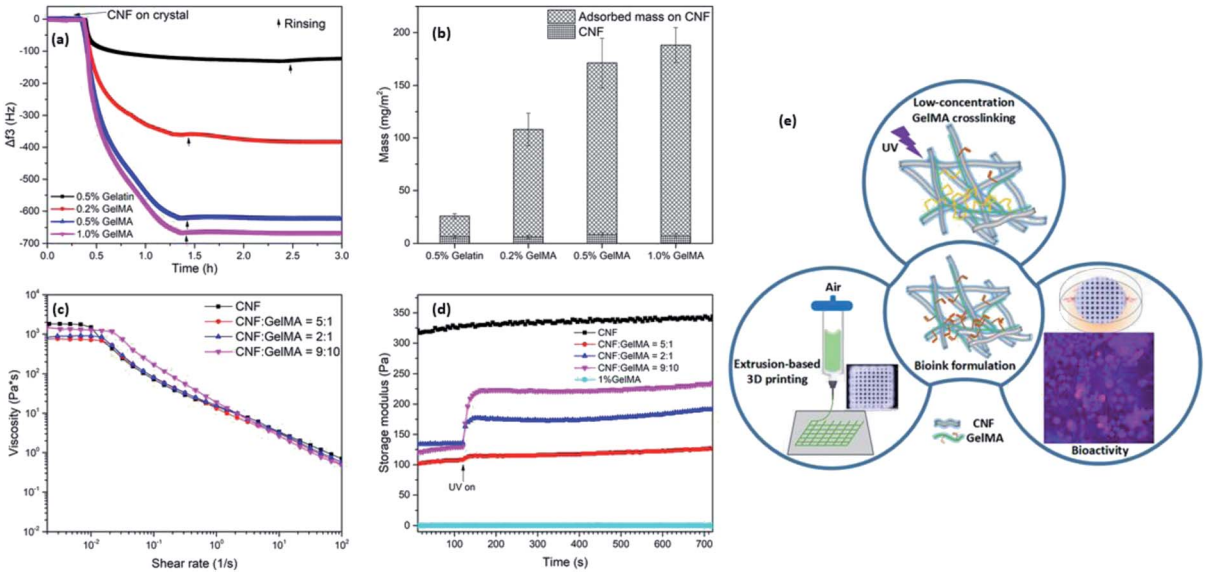

Fig. 15 QCM-D analysis of (a) demonstrating the adsorption–desorption cycle of 0.5 w/v% gelatin or GelMA (0.2–1.0 w/v%) onto the CNF substrate; (b) mass of CNF adsorbed onto the crystal support and GelMA onto the CNF substrate on the basis of per unit area; (c) Rheometer results as a function of the shear rate for CNF (1.0 w/v%) and CNF/GelMA hydrogel bio-inks with different mass ratios of 5 : 1, 2 : 1, and 9 : 10; (d) plot of the storage modulus as a function of time for the formulated CNF bio-inks under UV irradiation; (e) illustrations of the 3D-printing procedure with UV crosslinking and confocal image of 3T3 cell proliferation in printed scaffold using CNF/GelMA at a compositional ratio of 5 : 1, indicating high bioactivity [adapted with permission from Xu *et al.* 2018,[232] Copyright © American Chemical Society].

understand the key tenets of printing CNC-type supports are required to be further materialized so that researchers do not limit themselves to the CNF's long and flexible nanoscale properties for the preparation of a deformable and viscous network. One of the tough challenges for all researchers in this domain is to control the nanocrystalline size such that they can ensure high reproducibility and ability to elucidate the relationship between the nanocrystal size and properties of the final printed product. Moreover, there is a limit of nanocellulose content that can be added into the matrix material as exceeding concentrations could lead to nozzle clogging and greater variations in the fiber distribution.[176]

5. 3D-printing applications of nanocellulose

5.1. Biomedical applications

Considering the biocompatibility,[222] biodegradability, and nontoxicity,[223] the use of nanocellulose in 3D printing or bioprinting is desirable for applications in the biomedical field, encompassing cell scaffolds, tissue engineering, and wound

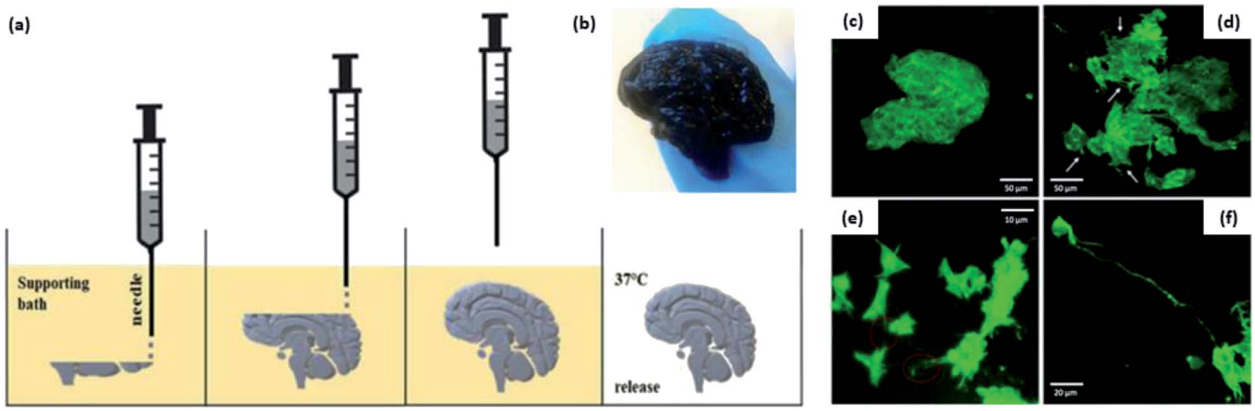

Fig. 16 (a) Schematic of the FRESH 3D-bioprinting technique; (b) FRESH 3D-bioprinted brain scaffold with an intricate structure; confocal imaging of (c) neural cells cultured on the brain scaffold printed with 100% CNF without any observed differentiation; (d) cells cultured on a conductive brain scaffold without any observed differentiation but more neurites; (e) visible interaction within the cells cultured on a conductive ink; (f) differentiation between the cells cultured on a conductive ink observed with a long neurite [adapted with permission from Bordoni *et al.* 2020,[240] Copyright © MDPI].

dressing.[177,224,225] Many hydrogel bio-inks formulated for bio-printing a robust architecture are mechanically weak with poor crosslinking in the network.[226] Various gels and inks that are based on nanocellulose have been prepared and reported, exhibiting great viscoelasticity and conductivity.[227–231] Jessop *et al.* derived a unique bio-ink formulated with alginate and nanocellulose that could be printable and capable of maintaining the printed complex macrostructure for cellular proliferation.[230] Research suggests that bio-ink containing both CNF and CNC, with alginate and 0.5 M crosslinker $CaCl_2$ was biocompatible with human nasoseptal chondrocytes, and could be printed out with the highest resolution of 1.01 mm and smallest volumetric shrinkage of 62.3 mm^3 compared with bio-ink containing pure CNF or CNC. Binders are particularly important with regard to retaining the shape of the materials printed upon fabrication. Although crosslinking is vital to prepare printable bio-inks and ensure shape fidelity, excessive crosslinking can lead to adverse effects on the brittleness of the structure due to the formation of a heterogeneous network.[226] Furthermore, reproducibly controlling the degree of crosslinking is arguably an important question to be addressed.

Another study has introduced the preparation of hydrogel comprising 1.0 w/v% TEMPO CNF with up to 1.0 w/v% of gelatin methacrylate (GelMA) for FDM 3D printing.[232] The bio-ink was characterized by quartz crystal microbalance with dissipation (QCM-D) to scrutinize the macromolecular interaction between the CNF and GelMA, as shown in Fig. 15. A homogeneous ink is necessary to achieve good printability and the findings suggested that a GelMA concentration of less than 1.0 w/v% can prevent phase separation with the CNF suspension. Furthermore, the molar ratio of CNF/GelMA of 5 : 1 has afforded outstanding adhesion and proliferation of human fibroblasts, finding promising potential as an approach for wound healing. The FDM technique enables a widely interconnected network of nanofibers and pores, where the porosity can be altered by the concentration of the nanofillers.[233] However, most studies on 3D-printed scaffolds were only able to verify the cellular proliferation on the surfaces but not the bulk of the fabricated scaffold to account for the culture media and oxygen diffusivities.

Additionally, several publications have investigated the fabrication of complex structures including organs and tissue cellular architecture.[234–238] Li and co-workers proposed the use of photo-polymerizable and curable polymer resin containing PEGDA, glycerol 1,3-diglycerolate diacrylate (DiGlyDA), and Irgacure 819, incorporated with CNC for DLP 3D printing of a highly complex 3D structure, where they printed an ear model.[238] The hydrogel material, with reinforced mechanical properties by CNC, was successfully printed out with highly defined features, including intricate contours and valleys from the CAD design of the ear model with high shape fidelity. The inclusion of DiGlyDA with many hydroxyl groups is one example of overcoming the frequent problem of CNC aggregation that resulted in a compromise of the mechanical properties. The resulting scaffolds showed a favorable improvement in the Young's modulus by 80.2 MPa when CNC was added at 5 wt%.[184]

Apart from optimizing the physical parameters to achieve high-resolution printing of an intricate structure, it is crucial to formulate print inks that have optimally high viscosity to ensure the structural integrity upon being 3D printed.[239] This stringent requirement has been overcome by Bordoni *et al.* who have successfully introduced the 3D bioprinting of freeform reversible embedding hydrogel (FRESH) that allows the use of low-viscosity liquid ink.[240,241] A simplified schematic of the workflow of the FRESH 3D bioprinting technique is shown in Fig. 16. Briefly, a highly viscous gelatin supporting bath was used, wherein the liquid bio-ink was pumped through the nozzle for printing the crosslinked scaffold. Thereafter, the gelatin was melted in incubation and removed before seeding the cells onto the structure. In this case, a realistic shape of a brain with an intricate surface was bio-printed with a composite ink; it contained highly conductive 10% single-walled carbon nanotubes (SWCNTs), alginate, and CNF aqueous dispersion, allowing the

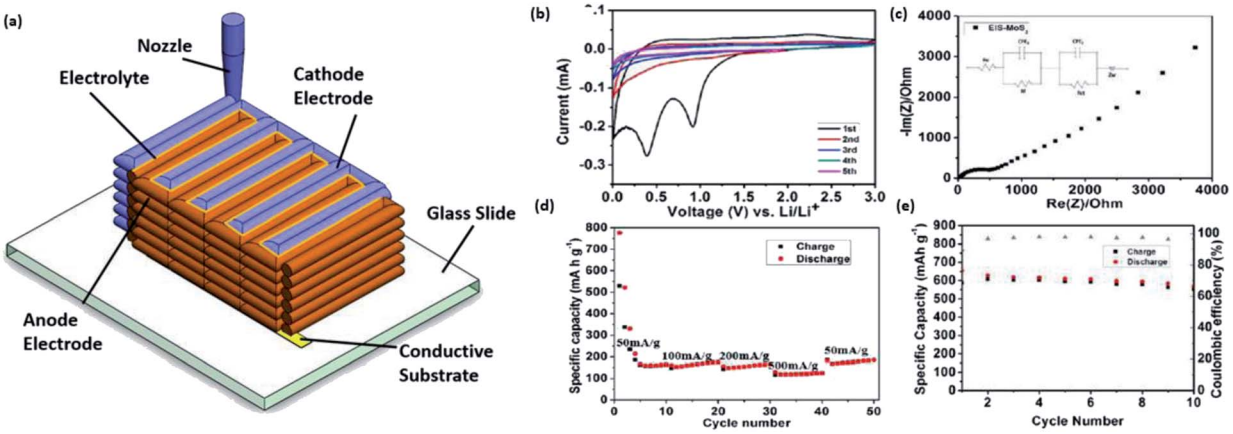

Fig. 17 (a) 3D illustration of printed electrodes on a glass slide; (b) cyclic voltammetry (CV) of printed CNF/MoS_2 electrode for first five cycles at 0.1 mV s^{-1}; (c) Nyquist plot of the printed electrode at frequencies between 100 kHz and 10 MHz; (d) retention of specific capacity as a function of cycles at different current rates (50, 100, 200, 500, and 50 mA g^{-1}); (e) coulombic efficiency of the printed electrode at a current density of 100 mA g^{-1} [adapted with permission from Xing 2017 (ref. 246)].

generation of a complex neural network with highly proliferated SH-SY5Y cells.

Nanocellulosic material has shown low cytotoxicity and high porosity in their printed scaffolds, which has been studied by many researchers.[242] It plays a vital role in enhancing the mechanical strength of the cellular scaffold that can affect the interactions between the cultivated cells and scaffold, where a cell–scaffold interaction is favored over cell–cell interactions.[176,233] It has been reported that the smaller particle size of a nanofiller provides higher mechanical strength and shape fidelity. This inclusion of nanocellulose can considerably reduce the formation of voids in the printed products, which adversely affect the physical properties. In addition to these advantageous properties, the printed cellular scaffold must be biodegradable wherein *in vitro* experiments have shown that the initial rapid degradation of approximately 70% cellulose is followed by a slower biodegradation, leaving behind non-resorbable components.[233]

Many reports in the literature have been directed toward the biomedical application of the 3D printing of nanocellulose since it can ensure structural and mechanical stability,[222,223] as well as to efficiently support cell proliferation due to its high moisture retention equating to porosity upon freeze drying,[239] thereby enabling ideal functions in drug release and tissue engineering. Most importantly, to be 3D printed successfully, cellulose nanomaterial should exhibit a shear thinning behavior that promotes the smooth extrusion of print inks without clogging the nozzle.[222] The self-alignment ability of CNC can also be exploited for the contact guidance of bio-inks that control the cellular alignment upon extrusion, which can provide the capability to carefully design scaffolds with a higher extent of cellular differentiation.[184] Again, the nanoscale structure allows huge opportunity for the introduction of intricate morphologies and topographies to effectively enhance the proliferation and differentiation of specific cells of interest.

The huge abundance of hydroxyl groups and large surface area of cellulose nanomaterials further allow the biochemical design for enhanced tissue formation. Furthermore, antibacterial properties have been highly sought after for improved cultivation quality in cell scaffolds (due to the highly nutritious broth) and wound dressing application.[185] Several studies have exploited the ease of chemical surface modifications that include aldehyde-modified, carboxyl-modified, amine-modified, and sulfate-modified techniques, as well as cationization with quaternary ammonium compounds or quaternized halamine for inhibition efficiency against both Gram-positive and Gram-negative bacteria.[243,244] Finally, the fabrication of patient-specific scaffolds could be combined with the potentiality of biomimetic 4D printing, which has been scrutinized for additional dimensions with response to external stimuli, which could be used for drug release and smart actuators.[245]

5.2. Electronics application

Today, researchers are focusing on miniaturizing electronic products with multifunctional materials that can eliminate the heat accumulation problem. The self-assembly and orientation of nanocellulose reveal a highly ordered structure that enhances the thermal conductivity of its composite film.[247] Both degrees of amorphous and crystallinity of the nanocellulose must be controlled as the former provides the structure with flexibility while the latter is the main contributor to thermal conductivity. The high degree of crystallinity also alters the polarization density with dielectric properties. Being hygroscopic has also made moisture as an electrical conducting solvent, affecting the dielectric property.[248]

As previously reported in the literature, to explore the applications of CNF and CNC in electronics, Tuukkanen *et al.*

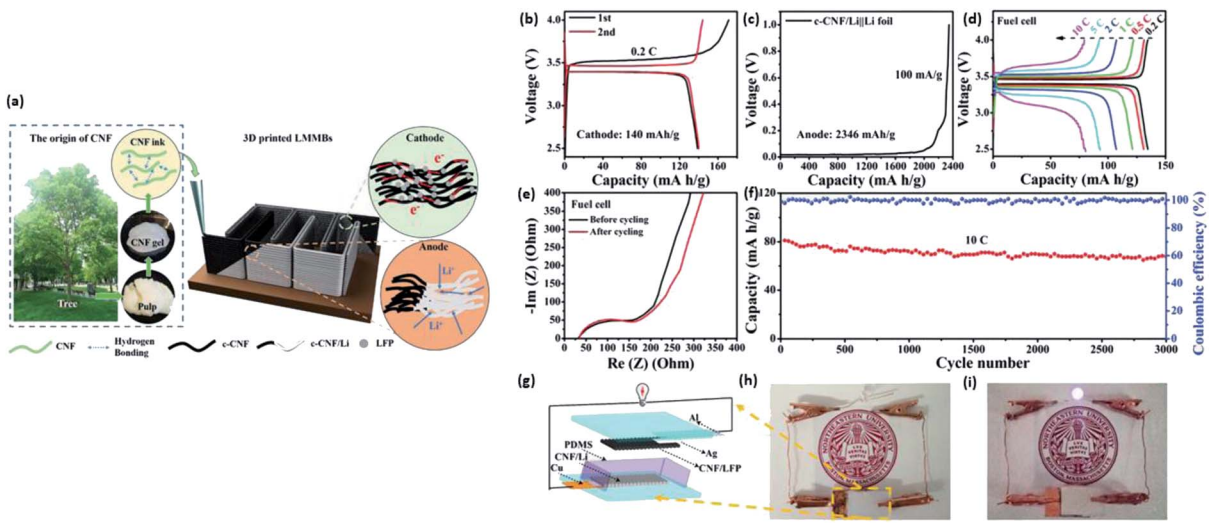

Fig. 18 Schematic of (a) 3D printing using CNF composite ink for the fabrication of lithium batteries; (b) charge–discharge profile of a fuel cell with CNF/LFP cathode and Li foil anode; (c) Li stripping behavior of CNF/Li anode; (d) voltage profiles of fuel cell at different charges from 0.2C to 10C; (e) Nyquist plots depicting the states before and after cycling and (f) retention of capacity over many cycles at 10C for the fuel cell; (g) schematic of the fuel cell with 3D-printed electrodes; images of packaged Li batteries in (h) open and (i) closed circuits [adapted with permission from Cao *et al.* 2019,[252] Copyright © John Wiley and Sons, Inc.].

demonstrated the fabrication of a flexible and disposable printed supercapacitor based on carbon nanotube (CNT) nanocomposite electrodes and nanocellulose separator on a poly(ethylene terephthalate) (PET) substrate.[249] The printed supercapacitor has a high capacitance ranging within 14.9–16.5 mF, retaining it even after 2000 cycles of charge/discharge.

More recently, a novel technique for making a 3D-printed microbattery has been developed with electrodes at a high aspect ratio to facilitate electron and ion transportation.[246] Xing made use of TEMPO CNF as both a rheology modifier as well as a source of carbon for electrical conductivity[250] when bound with molybdenum disulfide (as-MoS_2) gel to be 3D printed as the anode. Fig. 17 shows the CV analysis and other performance characterizations of the shown 3D-printed electrode. From this figure, it is evident that the CNF/MoS_2 electrode has poor cycling stability with a charge–discharge capacity reduction within ten cycles. Despite the poor stability, it has been successfully established by numerous reports in the literature that the incorporation of TEMPO CNF initially accounted for a high specific capacity and therefore validating its potential in energy storage applications.[251–253] However, much of the research in the literature up to now has been descriptive of the properties in nature, but the overall feasibility of replacing current marketed materials with cellulose nanomaterials has not been considered.

Despite the difficulties presented in printing batteries due to the use of metals such as lithium, the manufacturing technique has inherent advantages with regard to miniaturizing the product with customizable structural properties and shapes. Cao *et al.* employed CNF as a (1) viscosity modifier, (2) effective surfactant, (3) electrical conducting material, (4) mechanical strength reinforcer, and (5) a material with a superior water retention property in printing CNF/$LiFePO_4$ (LFP) cathode and CNF/Li anode, as shown in Fig. 18.[252] Firstly, the CNF structure was 3D printed into the illustrated micropattern and cauterized at 700 °C to yield the electrical conducting and strong scaffold. Lithium-ion solution or molten lithium was then uniformly infused and distributed within the highly porous scaffold since the CNF structure had water retention of 92%. The printed electrodes were assembled into a fuel cell and found to derive a high energy density of 80 mA h g^{-1} and retaining 85% capacity even after 3000 cycles at 10C, as shown in Fig. 18b–i. The excellent fuel cell performance due to the enhanced ion accessibility and customized design was enabled by the 3D-printing technology and the highly sought-after properties of CNFs.

The emerging challenges for the application of 3D printed nanocellulose composite material in electronics and batteries were proposed by Zhang and co-workers.[254] In spite of the inherent unique structures of nanocellulose, giving it great potential to be transformed into energy storage products, current research is still unable to resolve the heat accumulation issue for the use of this material.[254,255] Notwithstanding the challenge to reduce the thermal resistance of the nanocellulose–substrate interface in the composites, nanocellulose has been demonstrated to possess high thermal stability above 300 °C and lower thermal expansion in comparison to other polymeric materials.[247] Inevitably, the most challenging limitation would be to expand the production of nanocellulose of high

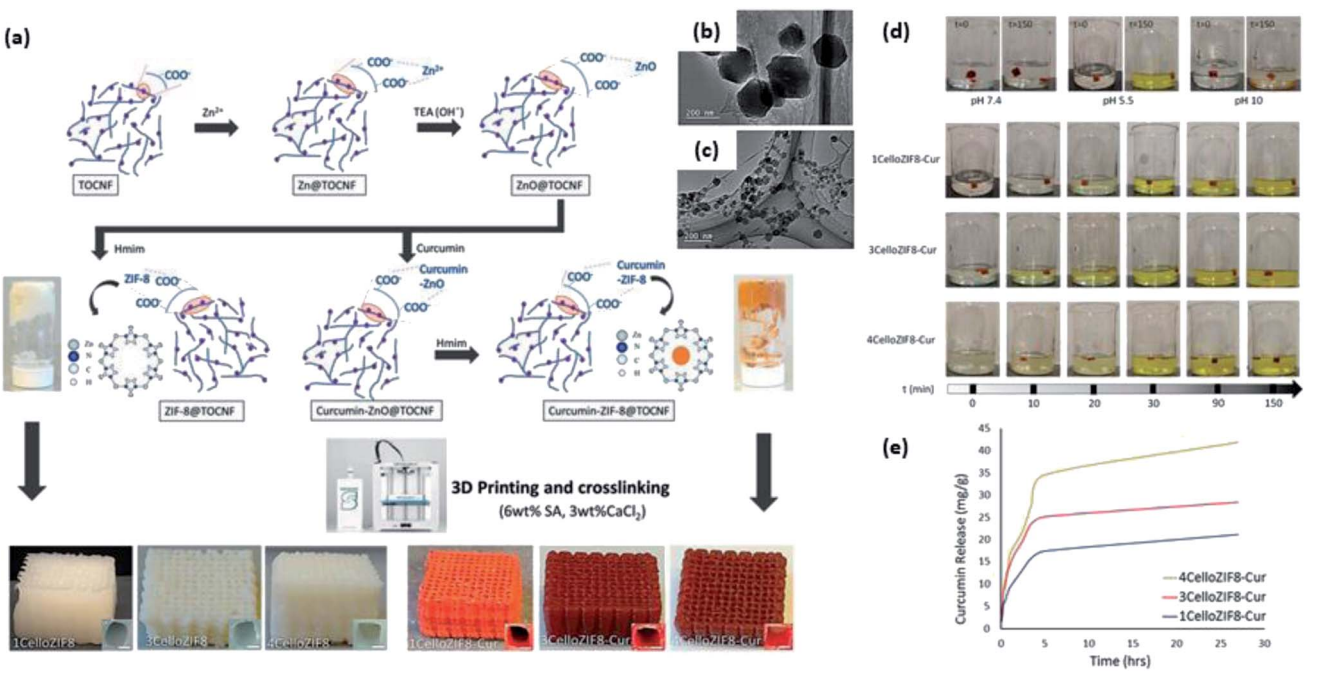

Fig. 19 (a) Illustration of the preparation procedures and 3D printing of CelloMOF ink and in the presence of curcumin. Scale bar = 0.5 mm; high-resolution TEM images of (b) 1 mg and (c) 5 mg of CelloZIF8–curcumin (scale bar: 200 nm); (d) images of curcumin release at different pH values (5.5, 7.4, and 10) over 150 min; (e) curcumin release rate from a printed structure over a 30 h period [adapted with permission from Sultan *et al.* 2019,[263] Copyright © John Wiley and Sons, Inc.].

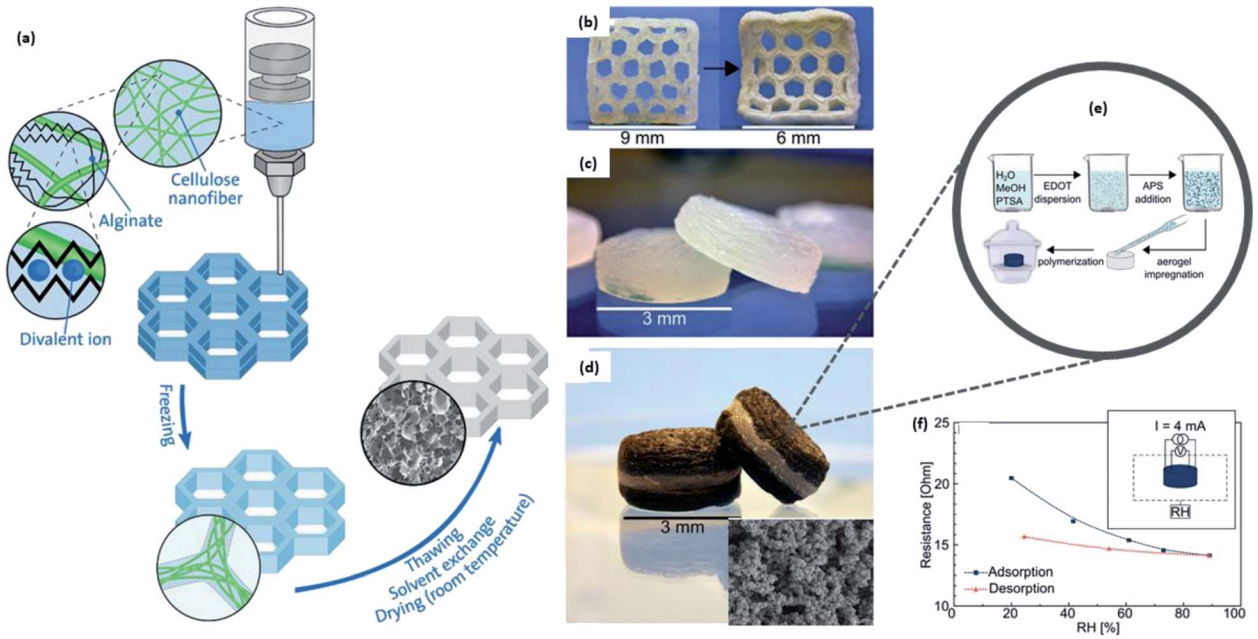

Fig. 20 Schematic of the (a) workflow of 3D-printed CNF/alginate aerogel and images of (b) 3D-printed aerogel structure shrinks after freeze drying; (c) 3D-printed cylindrical-shaped aerogel and (d) 3D-printed layered aerogel with a dark layer functionalized with PEDOT:PSS, with the SEM micrograph of its internal surface (scale bar: 5 μm); (e) schematic of the *in situ* polymerization of EDOT in the fabricated aerogel; (f) resistance of the 3D-printed layered aerogel in relation to the relative humidity in the environment [adapted with permission from Françon *et al.* 2020,[268] Copyright © John Wiley and Sons, Inc.].

purity considering the environmental and processing costs. Hence, an effective electronic and energy storage technology could only be sustained with global efforts to develop thermal management techniques and to search for the cheapest way for producing cellulose nanomaterials from agricultural waste.[256]

5.3. Environmental applications

Besides the widely reported application of 3D-printable nanocellulosic materials in biomedical use and electronics, there have been limited reports in the literature on environmental applications. The rampant emergence of bionanomaterial has shown a great fit for environmental remediation given its non-toxicity, ease of chemical modifications, and larger surface area or porosity for removal and sensing contaminants.[257] Unfortunately, the overabundance of hydroxyl groups along the nanocellulose chain can become unsuitable for wastewater remediation since it is susceptible to aggregation.[257,258] At present, functionalized nanocellulose systems have been found to have superior performance to traditional materials for fabrication into a selective water filtration membrane or adsorbent in water remediation.[259–262] When prepared *via* acid hydrolysis, the introduction of negatively charged sulfate or phosphate groups along the backbone of nanocellulose has been favored for utilization to remove cationic dyes through electrostatic attraction.[244] Nevertheless, poor specificity and cost-effectiveness in scaling up are dire limitations to be addressed for commercial realization.

Gaining popularity in recent years, a new class of compounds known as metal–organic frameworks (MOFs) have been widely explored for their advanced application in environmental remediation as they can reach a specific surface area as high as 10 000 $m^2 g^{-1}$, outshining conventional zeolites and other commonly known porous materials. Although 3D printing ensures high reproducibility and ability to fabricate complex structures, the printing of MOFs has greatly been limited by the requirement of existing composites with binder, plasticizer, and photo-polymeric matrices, which often demands high temperature or intense ultraviolet light for curing. Sultan and his co-workers employed a one-pot synthesis of ZIF-8 (Zn) and MIL-100 (Fe) onto TEMPO-oxidized CNF (TOCNF) facilitated by the coordination between the carboxylate group of TOCNF and metal divalent ion.[263] Fig. 19 shows the synthesis process of the print ink with or without the encapsulation of naturally antibacterial curcumin. A modest concentration of sodium alginate was added into the hybrid ink for co-crosslinking and yielding a 3D structure. This technique of printing CelloMOF could be extended to environmental applications such as water or air purification, offering great surface area and porosity for the uptake of targeted pollutants. Other studies have reported utilizing a cellulose nanomaterial for adsorbing heavy metals such as chromium, arsenic, and lead. In addition, such a nanoscale material can be easily regenerated in an acidic medium and reused with an adsorption capacity comparable to the initial state.[264]

In light of huge global investment into environmental sensing solutions, researchers have worked round the clock to search for effective sensing materials, and in this case, the application of CNF as a potential material as a humidity sensor.

Table 7 Nanocellulose composite materials for 3D printing and its applications

Preparation of nanocellulose	3D printing material	Printing approach	Printed structure	Application & mechanism(s)	Advantage(s)	Limitation(s)	Reference
Biomedical application							
High-pressure fluidizer to disintegrate bleached birch wood fiber	Aqueous suspension of acetylated CNF	Direct ink writing (DIW) with 0.84 mm nozzle	Porous monolithic scaffolds with high surface charge and axial aspect	Cardiac myoblast cell scaffold for effective proliferation and high cell viability	– Does not need any crosslinker for stable structure – Fast and cheap fabrication having dimensional stability without need for crosslinking	– Swelling problem still exist in AceCNF although it has reduced hydrophilicity – Dried structure shows slight collapse, indicating need for stronger composition	177
TEMPO-mediated pre-treatment of bleached hardwood kraft pulp	Hydrogel of TCNF, alginate and glycerin formulation crosslinked with Ca^{2+}	Microextrusion based on nScrypt technology with 0.20 mm tip	Flexible grid structured hydrogel crosslinked by UV. Dimension 14×14 mm^2 grid with 2 mm squares	Covalent conjugation of avidin protein to printed TCNF gel for wound dressing	– Excellent capability for bio-functionalization with application in therapeutic release of drug	– Poor structural stability – Composite hydrogel absorbs water faster than pure TCNF hydrogel	227
TEMPO/ NaClO /NaBr pre-treatment and oxidation of CNF	Ink formulation containing TCNF and gelatin methacrylate (GelMA) crosslinked with Ca^{2+}	Extrusion-based 3D bioprinting	Scaffold model crosslinked with UV. 10 mm wide, 10 mm long and 3 mm height printed with 1 mm filament grid and 0.2 mm layer thickness	Promotion of fibroblasts proliferation in the hydrogel scaffold with tuneable mechanical strength	– High resolution printing, with high shape fidelity and structural stability – Improved Young's modulus and stiffness of composites	– Compromised cell proliferation activity – High swelling ratio of freeze-dried scaffold – Need for optimized alignment in printing of GelMA with CNF fiber for well-defined struts in the scaffold	232
Acid hydrolysis of abaca pulp fibers to obtain CNC	Reinforced CNC-PEGDA hydrogel with lithium phenyl (2,4,6-trimethy-lbenzoyl)-phosphinate photoinitiator	SLA 3D printing with laser wavelength at 405 nm	Complex human ear structure crosslinked by PEGDA–PEGDA interaction upon UV irradiation	Tissue engineering application with reinforced physicochemical and thermo-mechanical properties	– Enhanced toughness and strength of printed structure with CNC loading (1.2 ± 0.3 MPa) – Improved thermal stability with CNC (around 400 °C)	– Flexibility of structure has been compromised and limits the application – Much longer printing duration as compared to extrusion-based printing	234
TEMPO-mediated oxidation pre-treatment of bleached	TCNF/Alginate hydrogel crosslinked with Ca^{2+}	Paste extruder 3D printing with 0.5 mm nozzle	Bone scaffold structure with dimensions $30 \times 30 \times 20$ mm	Bone tissue engineering scaffold with biomimetic mineralization	– Improvement in cell attachment with successful mineralization of 20.1% hydroxyapatite	– Viscosity recovery (66%) is still considered low	236

Table 7 (*Contd.*)

Preparation of nanocellulose	3D printing material	Printing approach	Printed structure	Application & mechanism(s)	Advantage(s)	Limitation(s)	Reference
bagasse pulp for CNF				process using body fluid		for optimized formulation, resulting in potential collapse of weaker layers printed	
TEMPO-mediated pre-treatment of CNF followed by high-pressure homo-genization	Unmodified concentration TCNF and 1*H*,1*H*,2*H*,2*H*-perfluorooctyl-trichlorosilane (PFOTS) modified TCNF	Direct ink writing with 800 μm nozzle, followed by freeze-drying	Porous aerogel structure of complex human ear crosslinked using Kymene, with high deformability and shape recovery	Tissue engineering with good hydrophobicity and shape recovery after deforming	– Modified hydrophobicity of aerogel surface with PFOTS – Freeze-drying results in minimal shrinkage and damage of aerogel structure – Can achieve shape recovery to above 90% after 5 cycles of compression-release	– Printed aerogel has inferior specific storage modulus and strength in comparison to pure CNF or other polymers	237
Acid hydrolysed CNC derived from wood pulp	Ink formulation containing CNC, PEGDA, DiGlyDA, Irgacure 819 and Sudan I photoinitiator	DLP 3D printing with curing layer thickness of 100 μm	Highly defined human ear model with enhanced mechanical properties	Tissue engineering fabrication with tuneable property and structural customizability	– DLP printing technique enables tuneable mechanical properties and swelling behaviour such as by changing curing layer thickness – Great shape fidelity exhibited with complex structure	– Although swelling could be minimized, the hydrogen bond interactions between CNC, PEGDA and DiGlyDa are highly likely to be disrupted by the moisture uptake	238
Mechanical and enzyme pre-treated pulp followed by microfluidizer to obtain CNF (noncharged and carboxy-methylated)	Bioink containing SWCNTs, CNF and alginate co-crosslinked with Ca^{2+}	FRESH bioprinting technique in highly viscous biocompatible supporting bath	Intricate and electrically conductive structure of brain scaffold	Scaffold containing 10 wt% SWCNTs utilized for proliferation of SH-SY5Y cells and differentiate into complex neural cellular network	– FRESH bioprinting enables printing of intricate and complex structure with great resolution with liquid bioink of low viscosity – SWCNTs account for electrical stimuli for the high proliferation of neural cells	– Cells were not able to generate realistic neural network in absence of medium – Crosslinking of alginate has resulted in obstruction of SWCNTs inter-connectivity and hence loss of conductivity	240

Table 7 (*Contd.*)

Preparation of nanocellulose	3D printing material	Printing approach	Printed structure	Application & mechanism(s)	Advantage(s)	Limitation(s)	Reference
Electronics application							
Acid hydrolysis of wood pulp to obtain CNC; mechanical homogenizing process to obtain CNF	Aqueous nanocellulose dispersion and viscous carbon nanotube (CNT) ink	Screen printing	Fabricated flexible supercapacitor on cross-linked polydimethy-lsiloxane (PDMS) substrate	Solution-processable nanomaterials for short-life powered application in electronic devices	– Cheap and easy fabrication of supercapacitor with high capacitance (14.9–16.5 mF) – Capacitance maintained after 2000 cycles of charge/discharge	– Gravimetric specific capacitance is lower than other papers reporting on CNT electrode – Limited application as further optimization required due to large equivalent series resistance (74–155 Ω)	249
TEMPO-mediated pre-treatment followed by microfluid-ization to obtain CNF	Ink formulation containing CNT and CNF composite dispersion	Direct ink writing with 150 μm needle, with solvent exchange	Flexible and conductive 3D-printed pattern with good adhesion between layers	High-performance microfiber material with high conductivity for application in wearable electronics	– Great mechanical strength (247 ± 5 MPa) and electrical conductivity (216.7 ± 10 S cm^{-1}) – Improved 3D printability due to CNF ability to disperse CNT leading to high viscosity	– Solvent exchange and evaporation decrease the diameter of 3D printed fiber drastically, thus requiring optimization	250
Mechanical disintegration of wood microfibers following TEMPO pre-treatment	CNF/$LiFePO_4$ (LFP) ink for the cathode; CNF-based ink for the anode	Extrusion-based 3D printer with 150 μm nozzle	3D printed LFP cathode with CNF-based inks as surfactant and viscosifier; and Li anode with 3D printed carbonized CNF scaffold	Lithium metal microbatteries with improved ion accessibility enabled by porous CNF gel	– CNF as rheological modifier enhanced 3D printability and strongly negative zeta potential enable it to be a suitable surfactant for improving LFP dispersibility – High water retention of CNF result in highly porous aerogel for excellent ion accessibility – CNF/Li anode with high specific capacity, and retains 85% efficiency after 3000 cycles of charge/discharge	– A high system printing pressure of 551 kPa is used for the extrusion-based 3D printing – Lithium dendrite could potentially grow on the anode foil surface and within the pore due to massive volumetric change during cycling	252
Environmental application							
Alkaline and TEMPO pre-treatment followed by high-pressure	Bio-composites of TCNF and PEG	Flatbed screen printing	Biocomposite film printed with carbon electrode	CNF/PEG film with good oxygen barrier property and exhibiting high impedance	– Impedance change over three order magnitude without PEG plasticizer, with excellent repeatability	– Due to CNF hydrophilicity, water desorption from within CNF matrix is slow and result in slow response recovery	265

Table 7 (*Contd.*)

Preparation of nanocellulose	3D printing material	Printing approach	Printed structure	Application & mechanism(s)	Advantage(s)	Limitation(s)	Reference
homogenizer of bagasse fibers				change for humidity sensing	– Simple design of sensor based on CNF film and printed carbon electrodes	– Oxygen barrier properties compromised with introduction of PEG	
TEMPO oxidation of cellulose fiber from hardwood bleached kraft pulp followed by ultrasonic homo-genization	Combination of TOCNF aqueous dispersion, metal divalent ion (Zn^{2+} or Fe^{2+}) and curcumin	Extrusion 3D printing and crosslinking with 6 wt% sodium alginate and 3 wt% $CaCl_2$	Patterned and porous scaffold for application in cartilage regeneration	Release of encapsulated curcumin, natural chemotherapeutic compound, from MOF in printed scaffold under different pH	– One-pot *in situ* growth of MOF onto TOCNF upon 3D printing without demanding processing conditions – Demonstrated stimuli-responsive release of drug initially encapsulated within cavity of MOF – Huge potential in environmental remediation (*e.g.* water purification, air purification and sensors)	– Due to the drastic increase in viscosity upon inclusion of MOF, there is a limit to the extrusion resolution in printing intricate structure – Uptake performance of ions or molecules by embedded MOF not yet examined	263
Carboxy-methylated pulp fibrillated in high-pressure microfluidizer to produce CNF	Hydrogel comprising of CNF, alginate and concentrated solution of NaCl or $CaCl_2$	3D bioprinting of hydrogel followed by functionalization with PEDOT:PSS through *in situ* polymerization, following freeze-drying	3-Layered aerogel prepared (PEDOT:PSS functionalized layers act as electrode while CNF/alginate layer acts as insulation)	Potential application in fabrication of aerogel supercapacitors with change in resistance as indicator in measurement of relative humidity	– Wet-stable aerogel successfully prepared using highly hygroscopic and mechanically strong CNF – Relatively high specific capacitance of 78 F g^{-1} observed, showing potential as energy storage materials – Absorption of moisture from environment induces change in resistance due to swelling and increase in contact area	– Upon desorption of moisture, resistance is not reproducible as function of relative humidity – Rate of absorption or desorption of moisture is slow (more than 30 min conducted in this research) before resistance reaches equilibrium – Further studies need to be conducted to accelerate the rate of absorption or desorption for effective humidity sensing performance	268

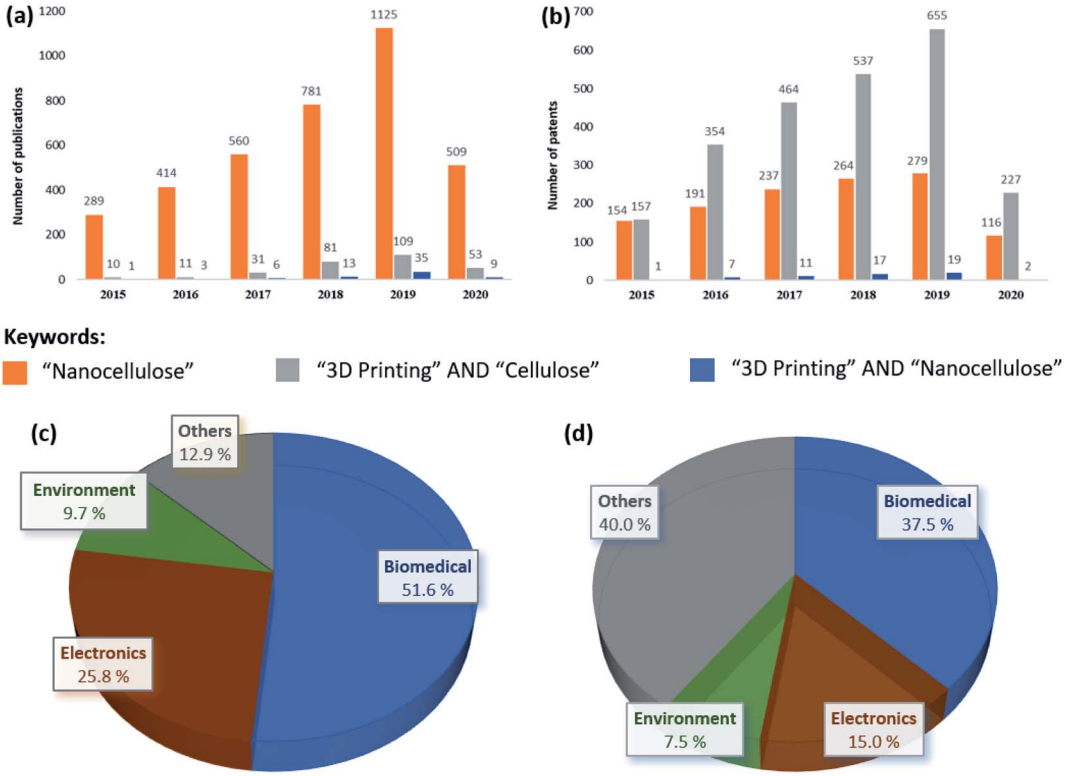

Fig. 21 Utilizing Scopus with keywords ("Nanocellulose"), ("3D Printing" and "Cellulose"), and ("3D Printing" and "Nanocellulose") to generate the (a) number of publications and (b) number of patents from 2015 to 2020; pie charts by field of application for (c) publications and (d) patents (others refer to food & packaging, automotive, novel materials, printing methods, *etc.*).

Syrovy *et al.* explored the printability of CNF/PEG biocomposite film for sensing the humidity and discussed the mechanical profile of the printed sensor and its sensory characteristics.[265] The printed CNF-based sensor responded within 4 orders of magnitude with a change in the impedance. In addition, the recovery time was cut by half by the integration of a PEG plasticizer that facilitated the faster desorption of water molecules out of the CNF.

The potential use of a 3D-printed CNF aerogel functionalized with a conducting polymer, *i.e.*, poly(3,4-ethylenedioxythiophene) polystyrene sulfonate (PEDOT:PSS), have also been described by Francon *et al.*, as shown in Fig. 20, wherein the CNF/alginate composites were mixed with the metal divalent ion as a hybrid ink for printing the patterned structure before freeze drying into an aerogel. Cellulose, being a hygroscopic material, is expected to change its physical properties and dimensions according to the amount of water absorbed.[266,267] This favorable change makes cellulose a suitable moisture or humidity sensor. In Fig. 20d–f, it could be observed that the three-layered aerogel with a dark layer being functionalized with PEDOT:PSS had a gradual decrease in resistance from 20 Ω at 20% relative humidity to 15 Ω at 90% relative humidity. In light of the reported change in resistance as shown in the plot, it is conceivable that an increase in the contact area upon swelling with increased moisture was the dominant contributing factor. It is important to note that the change in resistance that varies with the relative humidity could be utilized as a parameter for designing a sensing capability. The question now is how well is moisture desorbed to regenerate the hydrogel back to its initial state, which can be used to explain its effectiveness as a viable humidity sensor.

To advance the growing interest of utilizing nanocellulose as a sustainable precursor material in a composite for environmental remediation and sensing, Zhu and co-workers formulated colloidal probe techniques and molecular dynamics simulations to better understand the interaction mechanisms and forces between the metal pollutants in water and nanocellulose.[262] It has both been experimentally proven and confirmed that the electrostatic interaction between nanocellulose and metal ions is dominant. With regard to organic dye pollutants, Zhu disclosed their flat adsorption and stacking (clustering) around nanocellulose mainly directed by its functional sites. This approach of elucidating the structure–property–mechanism relationships is of central interest that could be extended to studying the nanocellulose interactions with other environmental pollutants.

A list of 3D-printing applications of nanocellulose composite materials, with a focus on isolation and preparation strategies, is tabulated in Table 7 to compare their respective advantages and disadvantages.

6. Trends and outlook

6.1. Publications and patent trends

Growing research efforts have been directed toward the development and study of the 3D printing of nanocellulosic materials, as shown in Fig. 21. By searching using the keywords

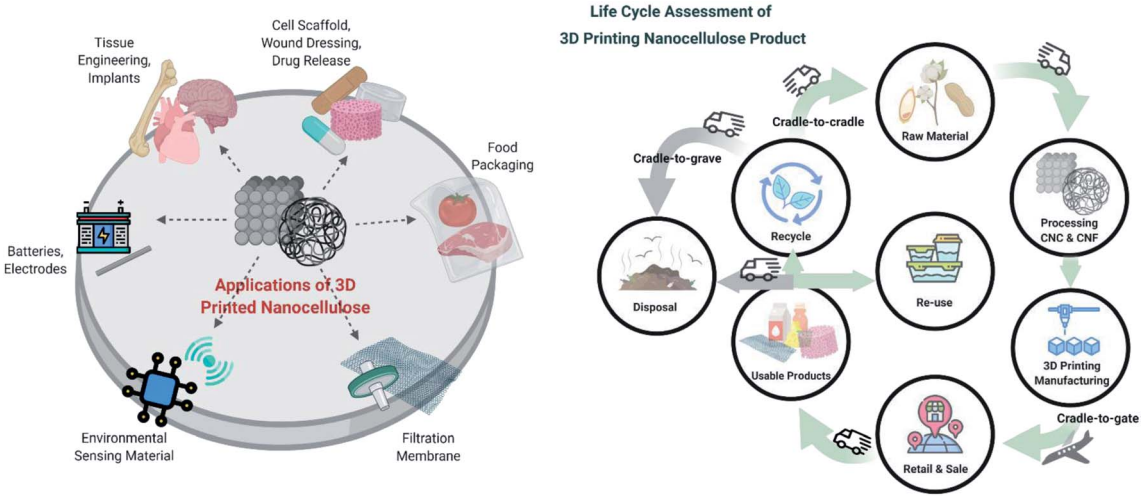

Fig. 22 Applications and LCA of 3D-printed nanocellulose.

"nanocellulose" and "3D printing" in the Scopus database, both research publications and patents are still scanty, standing at 73 and 85, respectively, from 2015 to 2020.

Lux Research further corroborated that companies have yet to produce nanocellulose at the industrial scale, unlike incumbent materials.[269–271] Moreover, there have been a few instances of the actual applications of nanocellulose, taking full advantage of its properties.[263,272] The state-of-the-art technology does not stagnate with 3D printing as another promising line of research would be its merger with stimuli-responsive materials to achieve a temporal behavioral change in the morphology, geometry, or color in response to external stimuli in the environment.[273] This is also known as four-dimensional (4D) printing, opening up the next generation of manufacturing with complex functional structures programmed with response to changes in the pH, temperature, humidity, light, electric, and magnetic field.

These temporal changes are reversible as the materials are tuned in terms of chemical composition as well as geometrical and origami-based designs to enhance the shape memory performance.[274] This fabrication technique has emerged in biomedical applications as cell scaffolds, self-expendable vascular stents, tracheal stents, bone scaffolds, and other medical devices that help to cut down the risk and need for invasive surgery.[274,275] These shape memory materials can be engineered to either permanently retain their new shape upon external stimuli or can return to their initial shape. Their response rate toward the stimulations are affected by the physicochemical properties of the material, environmental conditions, density, and thickness of the printed structure.[275] Tang *et al.* reported a self-healing stimuli-responsive CNC/sodium alginate–polyacrylamide hydrogel prepared through a one-pot *in situ* polymerization process. Notably, the prepared hydrogel could self-heal within several hours after being cut into pieces, with no cracks observed after healing at room temperature.[276] Moreover, the system became highly responsive to thermal stimuli within 20 s with the incorporation of oligoethylene glycol methacrylate. This is an excellent example illustrating the huge potential of nanocellulose composites as biocompatible smart materials for applications in the biomedical field. The grafting of nanocellulose before incorporation into the polymeric matrix plays a huge role to offer a stimuli-responsive system. Many researchers have demonstrated that nanocellulose can be responsive to temperature, pH, and mechanical changes, which can be useful in biomedical and environmental applications.[277] The abundance of hydroxyl groups along the backbone of nanocellulose enables the ease of functionalizing the hydrophobic group or the introduction of ionic and π–π-stacking system for various usages. With the advance in technology, 4D printing is believed to promote the rapid manufacturing of products with good quality and real usability if it can realize an integrative creation of an intelligent and autonomous process to eliminate the need for post-printing treatment.[275,278]

6.2. Insights from life-cycle assessment (LCA) of scale-up nanocellulose production

Several LCA studies have been discussed in the literature for the scale-up production of nanocellulose and its environmental impact on either cradle-to-grave[279] or cradle-to-gate[280–283] situation. Fig. 22 shows the differentiation among the different types of LCA analyses. These studies are conducted on the basis of making a thorough comparison between the lab-scale production process and existing commercial production processes.[13] Unfortunately, existing LCA studies have many problems in representing the real industrial process due to the lack of risk-associated information and immature adoption of the production technology, making them inadequate to be conclusive.[13,280,282] Nonetheless, the results from the LCA analysis provide beneficial insights and predictions on the environmental and health issues at an up-scaled production stage.

The majority of prior research has involved the use of harsh acids for the generation of CNFs or CNCs from agricultural biomasses, which is both energy consuming and harmful to the

environment when the industrial effluents are released. Moreover, pretreatments are responsible for the huge amount of chemicals expended even though they can reduce the energy input by a factor of ten during nanocellulose production from agricultural biomass.[284] Gu *et al.* carried out a cradle-to-gate analysis on the pilot-scale production of CNC from hardwood pulp based on the conventional bleach removal of recalcitrant fibers followed by acid hydrolysis.[280] They calculated that the whole process incurs 992.7 MJ of energy to produce 1 kg of CNC, 17 times greater than that of producing 1 kg of steel. Sodium hydroxide, determined to contribute dominantly in this LCA study, was also used in this process to neutralize the acid solution for hydrolysis. The research team suggested that the acid solution could be recycled in the industrial process to reduce the energy and alkali consumption.

With regard to the LCA study on the production of CNF by mechanical treatment together with ethanol/isopropanol and carboxymethylation pretreatments, the energy input was reported to be 20 MJ kg^{-1}, much lower than the production of carbon nanotubes at 1000 MJ kg^{-1} to as high as 1 million MJ kg^{-1}.[281] This theoretically low energy consumption was accompanied by the reduced use of solvents in the carboxymethylation pretreatment step that introduced electrostatic repulsion and facilitated separation into nanofibrils.[13] Many other studies in the literature have only considered the effect of producing nanocellulose on the environment and human health,[285] but they have failed to address the impact associated with the usage of nanomaterials as well as their waste during end of life.

In contrast with CNFs and CNCs, many researchers have considered bacterial cellulose to be the most promising production route for nanocellulose since it does not require the pretreatment of biomasses for the fractionation of fibers. However, this process is time-consuming and requires alternative carbon sources without impeding food production.[279] The production of nanocellulose is highly energy consuming and the high probability of aggregation during process worsens the situation, creating more hotspots.[283,286] Hence, a considerable facet along with the exhaustion of natural resources and energy may include the minimization of harsh acid and alkali consumption, encouraging solvent recovery, improvement in trade effluent filtration efficiencies, and reduction in the transportation cost of produced nanocellulose since it is highly hygroscopic and the water content tremendously contributes to its weight.

6.3. Research gap and future perspective

The rapidly advancing state of knowledge in nanocellulose and 3D-printing technologies make research focusing on the in-depth insight into the effective and green preparation of 3D-printable nanocellulosic material imperative. A closer look into the studies presented in earlier sections on nanocellulose and 3D printing, however, reveals a number of research gaps and shortcomings, as summarized below:

(1) There is a lack of low-cost and sustainable preparation of nanocellulose from agricultural biomass that lowers the green and blue footprints.

(2) The inherent hydrophilicity of nanocellulose can hinder its use in packaging and other applications. Little focus has been put into reducing this hydrophilicity or developing composite materials between the nanocellulose and hydrophobic materials for novel applications.

(3) Many researchers have failed to elucidate the process–structure–property relationships of 3D-printed nanocellulosic materials.

(4) 3D printing of CNF is more extensively studied in comparison to CNC due to the former having more extensive fibrillated bonds, affording higher printability. However, the desired mechanical properties of CNCs encourage the study into how to transform it into a 3D-printable and viable material.

(5) There is still insufficient evidence and investigation into the benefits of 3D printing functional nanocellulosic materials for applications other than biomedical and electronics.

The production of nanomaterials from biorenewable resources can serve many variations in their final properties. Since a fast, convenient, and sensitive production method is required to reproduce a nanomaterial of desired properties, further studies and development on optimal extraction and nanoprocessing should be conducted. The dewatering process has been reported as the main determinant that limits the commercialization of nanocellulose, without compromising its final physicochemical properties and their redispersibility after drying.[287]

The emergence of nanocellulosic materials for additive manufacturing has brought significant attention, offering a cheap alternative and solution to modify materials to be 3D printable with desirable rheological and physicochemical properties. However, more studies are required for the inclusion of hydrophilic cellulose nanomaterials into the hydrophobic polymer matrix, particularly at the loading limits of 5 and 20 wt% for CNF and CNC, respectively.[184,266,288] Moreover, the tendency of nanocellulose aggregation that compromise reinforcement and mechanical properties should be further investigated. Furthermore, solvent components and compositions are particularly important for 3D-printing techniques using print inks such as 3D bio-plotting, DIW, and inkjet printing.

The solution to degradability limitation of nanocellulose is lacking due to the difficulty of breaking up the β-(1,4)-glycosidic linkages in cellulose and high crystallinity. Hence, the extent of the application of 3D-printed nanocellulosic material should be carefully studied and filtered. The methods to enhance biodegradability, either environmentally or in the human body, along with control over its rate of degradation plays an elaborate role in expanding the application of nanocellulose. Some studies have shown that oxidized nanocellulose materials are susceptible to hydrolysis and hence could be degraded in the human body.[289]

With regard to applications in electronics, thermal resistance between the nanofiller and substrate in 3D-printed constructs should be carefully designed to provide effective thermal conductivity and dissipation of heat.

While 3D printing offers low-cost fabrication with minimal waste production and allows customized shape and properties,

challenges including anisotropic attributes, nozzle clogging due to nanomaterial aggregation, and difficulty to identify critical printing parameters have been narrowly addressed.[176,189] In a thorough investigation by PricewaterhouseCoopers (PwC), a majority of the manufacturing companies are skeptical and uncertain with regard to the quality of product being 3D printed.[290] The survey results reveal that data underpinning the mass-produced 3D-printed product quality is still not readily available, confining the fabrication technique to prototyping and modeling.[176] Therefore, the author hopes that researchers and industrial partners can successfully work together for the integration of 3D printing with novel nanocellulosic materials, thereby confirming complex functions for applications in biomedical, electronics, and environmental fields with indicative advantages on the fabricated product and LCA over conventional production methods.

7. Conclusions

In this review, the authors have critically assessed research papers on the isolation of nanocellulose and the preparation and applications of 3D-printable nanocellulosic materials. Great progress has been achieved to incorporate 3D-printing technology into industrial applications and the emergence of nanocellulose as an ideal nanofiller candidate for 3D-printable materials due to their inherently desirable properties (such as shear-thinning rheology, renewability, high mechanical strength, biocompatibility, *etc.*). Moreover, strategies to produce nanocellulose composite materials with high printability and shape fidelity have been presented. Despite the consensus on the importance of parameters affecting the printability and shape fidelity over time, many researchers have only managed to base the optimization of their 3D-printed nanocellulosic products on a macroscopic qualitative screening methodology. Hence, the authors address the need for a more comprehensive study into the development of quantitative database for optimal printing parameters in specific applications and the elucidation of the material's process–structure–property relationships, which is so far lacking in the scientific literature. These fundamental understandings could accelerate the development of new preparation methods and the development of novel nanocellulose-based composites with high reproducibility and consistency for commercializing 3D-printing applications.

Conflicts of interest

There are no conflicts to declare.

Acknowledgements

The research grant (R-143-000-B24-592) is co-funded by Singapore National Additive Manufacturing – Innovation Cluster (NAMIC) and MIPS Innovations Pte. Ltd., with facility support from NUS Centre of Additive Manufacturing (AM.NUS). The author would like to acknowledge Singapore Ministry of Education (MOE) for providing a scholarship for his Ph.D. research programme in Chemistry at National University of Singapore.

References

1 Z. Kassab, S. Mansouri, Y. Tamraoui, H. Sehaqui, H. Hannache, A. E. K. Qaiss and M. El Achaby, *Ind. Crops Prod.*, 2020, **144**, 112035.
2 S. Kalia, A. Dufresne, B. M. Cherian, B. S. Kaith, L. Avérous, J. Njuguna and E. Nassiopoulos, *Int. J. Polym. Sci.*, 2011, **2011**, 1–35.
3 M. Jawaid, S. Boufi and H. P. S. Abdul Khalil, *Cellulose-Reinforced Nanofibre Composites: Production, Properties and Applications*, Woodhead Publishing, 2017.
4 V. Kumar, P. Pathak and N. K. Bhardwaj, *Waste Manage.*, 2020, **102**, 281–303.
5 F. N. M. Padzil, S. H. Lee, Z. M. A. Ainun, C. H. Lee and L. C. Abdullah, *Materials*, 2020, **13**, 1245.
6 D. N. S. Hon, *Cellulose*, 1994, **1**, 1–25.
7 B. Thomas, M. C. Raj, K. B. Athira, M. H. Rubiyah, J. Joy, A. Moores, G. L. Drisko and C. Sanchez, *Chem. Rev.*, 2018, **118**, 11575–11625.
8 F. Vilarinho, A. Sanches Silva, M. F. Vaz and J. P. Farinha, *Crit. Rev. Food Sci. Nutr.*, 2018, **58**, 1526–1537.
9 L. Jasmani and W. Thielemans, *Forest Res.*, 2018, **7**, 1000222.
10 J. M. Rieland and B. J. Love, *Resour., Conserv. Recycl.*, 2020, **155**, 104678.
11 X. Zhang, W. Yang and W. Blasiak, *Energy Fuels*, 2011, **25**, 4786–4795.
12 L. Liang, S. Bhagia, M. Li, C. Huang and A. J. Ragauskas, *ChemSusChem*, 2020, **13**, 78–87.
13 A. Sharma, M. Thakur, M. Bhattacharya, T. Mandal and S. Goswami, *Biotechnol. Rep.*, 2019, **21**, e00316.
14 J.-H. Kim, B. S. Shim, H. S. Kim, Y.-J. Lee, S.-K. Min, D. Jang, Z. Abas and J. Kim, *Int. J. Precis. Eng. Manuf.- Green Technol.*, 2015, **2**, 197–213.
15 F. V. Ferreira, A. Dufresne, I. F. Pinheiro, D. H. S. Souza, R. F. Gouveia, L. H. I. Mei and L. M. F. Lona, *Eur. Polym. J.*, 2018, **108**, 274–285.
16 J. Liu, L. Sun, W. Xu, Q. Wang, S. Yu and J. Sun, *Carbohydr. Polym.*, 2019, **207**, 297–316.
17 S. Mondal, *Carbohydr. Polym.*, 2017, **163**, 301–316.
18 H. V. Lee, S. B. Hamid and S. K. Zain, *Sci. World J.*, 2014, **2014**, 631013.
19 S. Ling, W. Chen, Y. Fan, K. Zheng, K. Jin, H. Yu, M. J. Buehler and D. L. Kaplan, *Prog. Polym. Sci.*, 2018, **85**, 1–56.
20 A. J. Benítez and A. Walther, *J. Mater. Chem. A*, 2017, **5**, 16003–16024.
21 D. Klemm, E. D. Cranston, D. Fischer, M. Gama, S. A. Kedzior, D. Kralisch, F. Kramer, T. Kondo, T. Lindström, S. Nietzsche, K. Petzold-Welcke and F. Rauchfuß, *Mater. Today*, 2018, **21**, 720–748.
22 M. C. Iglesias, D. Gomez-Maldonado, B. K. Via, Z. Jiang and M. S. Peresin, *For. Prod. J.*, 2020, **70**, 10–21.

23 M. Nasrollahzadeh, M. Sajjadi, S. Iravani and R. S. Varma, *Carbohydr. Polym.*, 2021, **251**, 116986.
24 H. Sehaqui, Q. Zhou and L. A. Berglund, *Compos. Sci. Technol.*, 2011, **71**, 1593–1599.
25 M. Mariano, N. El Kissi and A. Dufresne, *J. Polym. Sci., Part B: Polym. Phys.*, 2014, **52**, 791–806.
26 N. Lavoine, I. Desloges, A. Dufresne and J. Bras, *Carbohydr. Polym.*, 2012, **90**, 735–764.
27 A. G. de Souza, M. T. Junqueira, G. F. de Lima, V. K. Rangari and D. S. Rosa, *J. Polym. Environ.*, 2020, **28**, 1150–1159.
28 M. Dominic, R. Joseph, P. M. Sabura Begum, B. P. Kanoth, J. Chandra and S. Thomas, *Carbohydr. Polym.*, 2020, **230**, 115620.
29 A. A. Oun, S. Shankar and J. W. Rhim, *Crit. Rev. Food Sci. Nutr.*, 2019, 1–26, DOI: 10.1080/10408398.2018.1536966.
30 F. Rol, M. Billot, M. Bolloli, D. Beneventi and J. Bras, *Ind. Eng. Chem. Res.*, 2020, **59**, 7670–7679.
31 R. Soni, T. A. Asoh and H. Uyama, *Carbohydr. Polym.*, 2020, **238**, 116203.
32 X. Xu, F. Liu, L. Jiang, J. Y. Zhu, D. Haagenson and D. P. Wiesenborn, *ACS Appl. Mater. Interfaces*, 2013, **5**, 2999–3009.
33 D. G. Gray, *Botany*, 2020, **98**, 77–80.
34 D. Trache, M. H. Hussin, M. K. Haafiz and V. K. Thakur, *Nanoscale*, 2017, **9**, 1763–1786.
35 G. Jyoti and R. Adhikari, *Environ. Res.*, 2012, **9**, 81–87.
36 T. X. Yan, Master of Philosophy, University of Malaya, 2016.
37 M. Badiei, N. Asim, J. M. Jahim and K. Sopian, *APCBEE Proc.*, 2014, **9**, 170–174.
38 A. D. N. F. Júnior, M. I. Etchelet, A. F. M. Braga, L. Clavijo, I. Loaces, F. Noya and C. Etchebehere, *Fuel*, 2020, **266**, 117068.
39 Y. Sewsynker-Sukai, A. Naomi David and E. B. Gueguim Kana, *Bioresour. Technol.*, 2020, 123225, DOI: 10.1016/j.biortech.2020.123225.
40 D. M. dos Santos, L. Bukzem Ade, D. P. Ascheri, R. Signini and G. L. de Aquino, *Carbohydr. Polym.*, 2015, **131**, 125–133.
41 R. Koshani, T. G. M. van de Ven and A. Madadlou, *J. Agric. Food Chem.*, 2018, **66**, 7692–7700.
42 J. P. Oliveira, G. P. Bruni, K. O. Lima, S. Halal, G. S. D. Rosa, A. R. G. Dias and E. D. R. Zavareze, *Food Chem.*, 2017, **221**, 153–160.
43 J. Trifol, C. Sillard, D. Plackett, P. Szabo, J. Bras and A. E. Daugaard, *Cellulose*, 2016, **24**, 107–118.
44 J. Yao, H. Huang, L. Mao, Z. Li, H. Zhu and Y. Liu, *Fibers Polym.*, 2017, **18**, 2118–2124.
45 M. A. Mariño, C. A. Rezende and L. Tasic, *Cellulose*, 2018, **25**, 5739–5750.
46 G. Bali, X. Meng, J. I. Deneff, Q. Sun and A. J. Ragauskas, *ChemSusChem*, 2015, **8**, 275–279.
47 C. J. Chirayil, L. Mathew and S. Thomas, *Rev. Adv. Mater. Sci.*, 2013, **37**, 20–28.
48 M. N. Khan, N. Rehman, A. Sharif, E. Ahmed, Z. H. Farooqi and M. I. Din, *Int. J. Biol. Macromol.*, 2020, **153**, 72–78.
49 S. I. Mussatto, G. J. M. Rocha and I. C. Roberto, *Cellulose*, 2008, **15**, 641–649.
50 B. N. Kuznetsov, S. A. Kuznetsova, V. G. Danilov, O. V. Yatsenkova and A. V. Petrov, *React. Kinet., Mech. Catal.*, 2011, **104**, 337–343.
51 G. Rojith and I. S. B. Singh, *Int. J. Environ. Bioenergy*, 2012, **3**, 46–55.
52 C. A. Hubbell and A. J. Ragauskas, *Bioresour. Technol.*, 2010, **101**, 7410–7415.
53 A. Isogai and Y. Zhou, *Curr. Opin. Solid State Mater. Sci.*, 2019, **23**, 101–106.
54 H. Ito, M. Sakata, C. Hongo, T. Matsumoto and T. Nishino, *Nanocomposites*, 2019, **4**, 167–177.
55 A. Morone, G. Sharma, A. Sharma, T. Chakrabarti and R. A. Pandey, *Renewable Energy*, 2018, **120**, 88–97.
56 Y. Zhou, T. Saito, L. Bergstrom and A. Isogai, *Biomacromolecules*, 2018, **19**, 633–639.
57 J. Lopes, M. Bermejo, Á. Martín and M. Cocero, *ChemEngineering*, 2017, **1**, 10.
58 J. Zhang, J. Wu, J. Yu, X. Zhang, J. He and J. Zhang, *Mater. Chem. Front.*, 2017, **1**, 1273–1290.
59 N. Mohd, S. F. S. Draman, M. S. N. Salleh and N. B. Yusof, *AIP Conf. Proc.*, 2017, **1809**, 020035.
60 A. H. Bhat, I. Khan, M. A. Usmani, R. Umapathi and S. M. Z. Al-Kindy, *Int. J. Biol. Macromol.*, 2019, **129**, 750–777.
61 S. Zhu, Y. Wu, Q. Chen, Z. Yu, C. Wang, S. Jin, Y. Ding and G. Wu, *Green Chem.*, 2006, **8**, 325.
62 M. Isik, H. Sardon and D. Mecerreyes, *Int. J. Mol. Sci.*, 2014, **15**, 11922–11940.
63 A. J. Holding, Doctor of Philosophy, University of Helsinki, 2016.
64 M. Koel, T. Aid and F. Elhi, *Proc. Est. Acad. Sci.*, 2016, **65**, 255.
65 M. Jiang, M. Zhao, Z. Zhou, T. Huang, X. Chen and Y. Wang, *Ind. Crops Prod.*, 2011, **33**, 734–738.
66 W. Lan, C. F. Liu and R. C. Sun, *J. Agric. Food Chem.*, 2011, **59**, 8691–8701.
67 X. Wang, H. Li, Y. Cao and Q. Tang, *Bioresour. Technol.*, 2011, **102**, 7959–7965.
68 S. B. A. Hamid, M. A. Amin and M. E. Ali, *Adv. Mater. Res.*, 2014, **925**, 52–56.
69 J. K. Singh, R. K. Sharma, P. Ghosh, A. Kumar and M. L. Khan, *Front. Chem.*, 2018, **6**, 548.
70 J. Yang, X. Lu, Y. Zhang, J. Xu, Y. Yang and Q. Zhou, *Green Energy Environ.*, 2020, **5**, 223–231.
71 L. Berglund, I. Anugwom, M. Hedenström, Y. Aitomäki, J.-P. Mikkola and K. Oksman, *Cellulose*, 2017, **24**, 3265–3279.
72 P. Phanthong, S. Karnjanakom, P. Reubroycharoen, X. Hao, A. Abudula and G. Guan, *Cellulose*, 2017, **24**, 2083–2093.
73 Y.-L. Chen, X. Zhang, T.-T. You and F. Xu, *Cellulose*, 2018, **26**, 205–213.
74 S. Xia, G. A. Baker, H. Li, S. Ravula and H. Zhao, *RSC Adv.*, 2014, **4**, 10586–10596.
75 J. A. Sirviö, M. Visanko and H. Liimatainen, *Green Chem.*, 2015, **17**, 3401–3406.
76 T. Selkala, J. A. Sirvio, G. S. Lorite and H. Liimatainen, *ChemSusChem*, 2016, **9**, 3074–3083.

77 J. G. Lynam, N. Kumar and M. J. Wong, *Bioresour. Technol.*, 2017, **238**, 684–689.
78 Y. Liu, B. Guo, Q. Xia, J. Meng, W. Chen, S. Liu, Q. Wang, Y. Liu, J. Li and H. Yu, *ACS Sustainable Chem. Eng.*, 2017, **5**, 7623–7631.
79 T. Suopajarvi, J. A. Sirvio and H. Liimatainen, *Carbohydr. Polym.*, 2017, **169**, 167–175.
80 T.-M. Tenhunen, A. E. Lewandowska, H. Orelma, L.-S. Johansson, T. Virtanen, A. Harlin, M. Österberg, S. J. Eichhorn and T. Tammelin, *Cellulose*, 2017, **25**, 137–150.
81 J. A. Sirviö, *J. Mater. Chem. A*, 2019, **7**, 755–763.
82 A. Ibrahim, M. F. Abdullah and S. T. Sam, *IOP Conf. Ser.: Mater. Sci. Eng.*, 2018, **429**, 012059.
83 J. A. Sirvio, M. Visanko and H. Liimatainen, *Biomacromolecules*, 2016, **17**, 3025–3032.
84 W. Yu, C. Wang, Y. Yi, W. Zhou, H. Wang, Y. Yang and Z. Tan, *Cellulose*, 2019, **26**, 3069–3082.
85 Z. Ling, J. V. Edwards, Z. Guo, N. T. Prevost, S. Nam, Q. Wu, A. D. French and F. Xu, *Cellulose*, 2018, **26**, 861–876.
86 Y. Ma, Q. Xia, Y. Liu, W. Chen, S. Liu, Q. Wang, Y. Liu, J. Li and H. Yu, *ACS Omega*, 2019, **4**, 8539–8547.
87 S. Thi and K. M. Lee, *Bioresour. Technol.*, 2019, **282**, 525–529.
88 P. Li, J. A. Sirvio, B. Asante and H. Liimatainen, *Carbohydr. Polym.*, 2018, **199**, 219–227.
89 T. Suopajärvi, P. Ricci, V. Karvonen, G. Ottolina and H. Liimatainen, *Ind. Crops Prod.*, 2020, **145**, 111956.
90 A. K. Kumar, B. S. Parikh and M. Pravakar, *Environ. Sci. Pollut. Res.*, 2016, **23**, 9265–9275.
91 L. W. Lun, A. A. N. Gunny, F. H. Kasim and D. Arbain, *AIP Conf. Proc.*, 2017, **1835**, 020049.
92 W.-L. Lim, A. A. N. Gunny, F. H. Kasim, I. M. AlNashef and D. Arbain, *Cellulose*, 2019, **26**, 4085–4098.
93 J. A. Sirviö, J. Ukkola and H. Liimatainen, *Cellulose*, 2019, **26**, 2303–2316.
94 P. G. Gan, S. T. Sam, M. F. Abdullah, M. F. Omar and L. S. Tan, *BioResources*, 2020, **15**, 1154–1170.
95 Z. Chen, W. A. Jacoby and C. Wan, *Bioresour. Technol.*, 2019, **279**, 281–286.
96 O. Nechyporchuk, M. N. Belgacem and J. Bras, *Ind. Crops Prod.*, 2016, **93**, 2–25.
97 R. Abbasi and V. Baheti, *J. Text. Eng. Fash. Technol.*, 2018, **4**, 101–104.
98 H. L. Teo and R. A. Wahab, *Int. J. Biol. Macromol.*, 2020, **161**, 1414–1430.
99 A. K. Bharimalla, S. P. Deshmukh, P. G. Patil and N. Vigneshwaran, *World J. Nano Sci. Eng.*, 2015, **05**, 204–212.
100 L. Berglund, M. Noël, Y. Aitomäki, T. Öman and K. Oksman, *Ind. Crops Prod.*, 2016, **92**, 84–92.
101 T.-K. Fu, J.-H. Li, X.-Y. Wei, F. Wang, L.-H. Cui and Y.-H. Wang, *Presented in part at the 2nd Annual International Conference on Advanced Material Engineering*, China, 2016.
102 Y. Zhang, J. Chen, L. Zhang, P. Zhan, N. Liu and Z. Wu, *Mater. Res. Express*, 2020, **7**, 035010.
103 A. Kaushik, M. Singh and G. Verma, *Carbohydr. Polym.*, 2010, **82**, 337–345.
104 K. U. H. Yano, *Biomacromolecules*, 2011, **12**, 348–353.
105 P. Khawas and S. C. Deka, *Carbohydr. Polym.*, 2016, **137**, 608–616.
106 X. Kang, S. Kuga, C. Wang, Y. Zhao, M. Wu and Y. Huang, *ACS Sustainable Chem. Eng.*, 2018, **6**, 2954–2960.
107 M. Dilamian and B. Noroozi, *Cellulose*, 2019, **26**, 5831–5849.
108 M. Rahimi Kord Sofla, W. Batchelor, J. Kosinkova, R. Pepper, R. Brown and T. Rainey, *Cellulose*, 2019, **26**, 4799–4814.
109 J. Wu, X. Du, Z. Yin, S. Xu, S. Xu and Y. Zhang, *Carbohydr. Polym.*, 2019, **211**, 49–56.
110 M. F. Yazdanbakhsh and A. Rashidi, *J. Text. Inst.*, 2020, 1–12, DOI: 10.1080/00405000.2019.1709261.
111 P. Phanthong, P. Reubroycharoen, X. Hao, G. Xu, A. Abudula and G. Guan, *Carbon Resour. Convers.*, 2018, **1**, 32–43.
112 N. H. Abdul Rahman, B. W. Chieng, N. A. Ibrahim and N. Abdul Rahman, *Polymers*, 2017, **9**, 588.
113 S. M. L. Rosa, N. Rehman, M. I. G. de Miranda, S. M. B. Nachtigall and C. I. D. Bica, *Carbohydr. Polym.*, 2012, **87**, 1131–1138.
114 M. Martínez-Sanz, A. A. Vicente, N. Gontard, A. Lopez-Rubio and J. M. Lagaron, *Cellulose*, 2014, **22**, 535–551.
115 P. M. Tahir, L. H. Zaini, M. Jonoobi and H. P. S. Abdul Khalil, 2015, DOI: 10.1007/978-3-642-45232-1_52, 119–144.
116 P. Nascimento, R. Marim, G. Carvalho and S. Mali, *Mater. Res.*, 2016, **19**, 167–174.
117 S. Y. Ooi, I. Ahmad and M. C. I. M. Amin, *Ind. Crops Prod.*, 2016, **93**, 227–234.
118 Y. W. Chen and H. V. Lee, *Int. J. Biol. Macromol.*, 2018, **107**, 78–92.
119 S. Collazo-Bigliardi, R. Ortega-Toro and A. Chiralt Boix, *Carbohydr. Polym.*, 2018, **191**, 205–215.
120 S. Naduparambath, T. V. Jinitha, V. Shaniba, M. P. Sreejith, A. K. Balan and E. Purushothaman, *Carbohydr. Polym.*, 2018, **180**, 13–20.
121 T. Theivasanthi, F. L. Anne Christma, A. J. Toyin, S. C. B. Gopinath and R. Ravichandran, *Int. J. Biol. Macromol.*, 2018, **109**, 832–836.
122 J. Yang, Masters Degree, Aalto University, 2017.
123 K. Zhao, W. Wang, A. Teng, K. Zhang, Y. Ma, S. Duan, S. Li and Y. Guo, *Carbohydr. Polym.*, 2020, **227**, 115264.
124 M. Chen, J. Parot, A. Mukherjee, M. Couillard, S. Zou, V. A. Hackley and L. J. Johnston, *Cellulose*, 2019, **27**, 2015–2028.
125 M. Wakabayashi, S. Fujisawa, T. Saito and A. Isogai, *Front. Chem.*, 2020, **8**, 37.
126 B. Soni, E. B. Hassan and B. Mahmoud, *Carbohydr. Polym.*, 2015, **134**, 581–589.
127 A. Isogai, T. Saito and H. Fukuzumi, *Nanoscale*, 2011, **3**, 71–85.
128 A. A. Oun and J.-W. Rhim, *Cellulose*, 2018, **25**, 2143–2149.
129 M. T. Islam, M. M. Alam, A. Patrucco, A. Montarsolo and M. Zoccola, *AATCC J. Res.*, 2014, **1**, 17–23.

130 H. Xie, H. Du, X. Yang and C. Si, *Int. J. Polym. Sci.*, 2018, **2018**, 1–25.
131 J. P. de Oliveira, G. P. Bruni, S. L. M. El Halal, F. C. Bertoldi, A. R. G. Dias and E. D. R. Zavareze, *Int. J. Biol. Macromol.*, 2019, **124**, 175–184.
132 C. Alvarez, F. M. Reyes-Sosa and B. Diez, *Microb. Biotechnol.*, 2016, **9**, 149–156.
133 M. Marino, L. Lopes da Silva, N. Duran and L. Tasic, *Molecules*, 2015, **20**, 5908–5923.
134 Y. Tang, X. Shen, J. Zhang, D. Guo, F. Kong and N. Zhang, *Carbohydr. Polym.*, 2015, **125**, 360–366.
135 S. Cui, S. Zhang, S. Ge, L. Xiong and Q. Sun, *Ind. Crops Prod.*, 2016, **83**, 346–352.
136 S. Sun, S. Sun, X. Cao and R. Sun, *Bioresour. Technol.*, 2016, **199**, 49–58.
137 H. Lou, M. Zeng, Q. Hu, C. Cai, X. Lin, X. Qiu, D. Yang and Y. Pang, *Bioresour. Technol.*, 2018, **249**, 1–8.
138 A. Perzon, B. Jorgensen and P. Ulvskov, *Carbohydr. Polym.*, 2020, **230**, 115581.
139 C. S. Farinas, J. M. Marconcini and L. H. C. Mattoso, *J. Renewable Mater.*, 2018, **6**, 203–216.
140 R. S. A. Ribeiro, B. C. Pohlmann, V. Calado, N. Bojorge and N. Pereira, *Eng. Life Sci.*, 2019, **19**, 279–291.
141 X. Kang, P. Sun, S. Kuga, C. Wang, Y. Zhao, M. Wu and Y. Huang, *ACS Sustainable Chem. Eng.*, 2017, **5**, 2529–2534.
142 K. Pacaphol and D. Aht-Ong, *J. Cleaner Prod.*, 2017, **142**, 1283–1295.
143 J. S. Santana, J. M. do Rosário, C. C. Pola, C. G. Otoni, N. de Fátima FerreiraSoares, G. P. Camilloto and R. S. Cruz, *J. Appl. Polym. Sci.*, 2017, **134**, 44637.
144 B. Fan, Q. Yao, C. Wang, C. Jin, H. Wang, Y. Xiong, S. Li and Q. Sun, *Polym. Compos.*, 2018, **39**, 3869–3876.
145 U. Fillat, B. Wicklein, R. Martin-Sampedro, D. Ibarra, E. Ruiz-Hitzky, C. Valencia, A. Sarrion, E. Castro and M. E. Eugenio, *Carbohydr. Polym.*, 2018, **179**, 252–261.
146 A. Sinclair, L. Jiang, D. Bajwa, S. Bajwa, S. Tangpong and X. Wang, *J. Appl. Polym. Sci.*, 2018, **135**, 46304.
147 M. Guan, X. An and H. Liu, *Cellulose*, 2019, **26**, 2613–2624.
148 J. Henschen, D. Li and M. Ek, *Carbohydr. Polym.*, 2019, **213**, 208–216.
149 S. Jonasson, A. Bünder, T. Niittylä and K. Oksman, *Cellulose*, 2019, **27**, 185–203.
150 Y. Lu, J. Yu, J. Ma, Z. Wang, Y. Fan and X. Zhou, *Cellulose*, 2019, **26**, 3735–3745.
151 K. Uetani, H. Koga and M. Nogi, *ACS Macro Lett.*, 2019, **8**, 250–254.
152 L. Yue, F. Liu, S. Mekala, A. Patel, R. A. Gross and I. Manas-Zloczower, *ACS Sustainable Chem. Eng.*, 2019, **7**, 5986–5992.
153 H. Abral, J. Ariksa, M. Mahardika, D. Handayani, I. Aminah, N. Sandrawati, A. B. Pratama, N. Fajri, S. M. Sapuan and R. A. Ilyas, *Food Hydrocolloids*, 2020, **98**, 105266.
154 Z. Liu, D. Lin, P. Lopez-Sanchez and X. Yang, *Int. J. Biol. Macromol.*, 2020, **145**, 634–645.
155 J. A. Sirviö, K. Hyypiö, S. Asaadi, K. Junka and H. Liimatainen, *Green Chem.*, 2020, **22**, 1763–1775.
156 B. Sun, M. Zhang, Q. Hou, R. Liu, T. Wu and C. Si, *Cellulose*, 2015, **23**, 439–450.
157 K. Zhang, P. Sun, H. Liu, S. Shang, J. Song and D. Wang, *Carbohydr. Polym.*, 2016, **138**, 237–243.
158 S. Singh, K. K. Gaikwad, S. I. Park and Y. S. Lee, *Int. J. Biol. Macromol.*, 2017, **99**, 506–510.
159 K. Song, Y. Ji, L. Wang, Y. Wei and Z. Yu, *J. Cleaner Prod.*, 2018, **196**, 1169–1175.
160 R. H. Longaresi, A. J. de Menezes, M. A. Pereira-da-Silva, D. Baron and S. L. Mathias, *Ind. Crops Prod.*, 2019, **133**, 232–240.
161 C. Trilokesh and K. B. Uppuluri, *Sci. Rep.*, 2019, **9**, 16709.
162 H. Wang, J. Li, X. Zeng, X. Tang, Y. Sun, T. Lei and L. Lin, *Cellulose*, 2019, **27**, 1301–1314.
163 L. Amoroso, G. Muratore, M. A. Ortenzi, S. Gazzotti, S. Limbo and L. Piergiovanni, *Polymers*, 2020, **12**, 68.
164 H. Doh, M. H. Lee and W. S. Whiteside, *Food Hydrocolloids*, 2020, **102**, 105542.
165 Y. Esparza, T.-D. Ngo and Y. Boluk, *Colloids Surf., A*, 2020, 124823, DOI: 10.1016/j.colsurfa.2020.124823.
166 E. Hafemann, R. Battisti, D. Bresolin, C. Marangoni and R. A. F. Machado, *Waste Biomass Valorization*, 2020, **11**, 6595–6611.
167 Q. Jiang, X. Xing, Y. Jing and Y. Han, *Int. J. Biol. Macromol.*, 2020, **149**, 1318–1322.
168 S. Ford, L. Mortara and T. Minshall, *Technol Forecast. Soc. Change*, 2016, **102**, 156–159.
169 T. Pereira, J. V. Kennedy and J. Potgieter, *Procedia Manuf.*, 2019, **30**, 11–18.
170 B. C. Gross, J. L. Erkal, S. Y. Lockwood, C. Chen and D. M. Spence, *Anal. Chem.*, 2014, **86**, 3240–3253.
171 Q. Yan, H. Dong, J. Su, J. Han, B. Song, Q. Wei and Y. Shi, *Engineering*, 2018, **4**, 729–742.
172 W. Xu, Doctor of Philosophy, Åbo Akademi University, 2019.
173 S. D. Chhabra, *Int. J. Latest Trends Eng. Technol.*, 2017, **8**, 264–272.
174 J. A. Lewis, *Adv. Funct. Mater.*, 2006, **16**, 2193–2204.
175 J. Roleček, L. Pejchalová, F. J. Martínez-Vázquez, P. Miranda González and D. Salamon, *J. Eur. Ceram. Soc.*, 2019, **39**, 1595–1602.
176 J. Saroia, Y. Wang, Q. Wei, M. Lei, X. Li, Y. Guo and K. Zhang, *Int. J. Adv. Des. Manuf. Technol.*, 2019, **106**, 1695–1721.
177 R. Ajdary, S. Huan, N. Zanjanizadeh Ezazi, W. Xiang, R. Grande, H. A. Santos and O. J. Rojas, *Biomacromolecules*, 2019, **20**, 2770–2778.
178 S. Huan, R. Ajdary, L. Bai, V. Klar and O. J. Rojas, *Biomacromolecules*, 2019, **20**, 635–644.
179 3DHUBS, *Manufacturing Processes Explained*, https://www.3dhubs.com/knowledge-base/collection/material-processes-explained/, accessed 25 August, 2019.
180 Q. Wang, C. Ji, J. Sun, Q. Yao, J. Liu, R. M. Y. Saeed and Q. Zhu, *J. Appl. Polym. Sci.*, 2019, **137**, 48374.
181 T. Ambone, A. Torris and K. Shanmuganathan, *Polym. Eng. Sci.*, 2020, **60**, 1842–1855.
182 A. Giubilini, G. Siqueira, F. J. Clemens, C. Sciancalepore, M. Messori, G. Nyström and F. Bondioli, *ACS Sustainable Chem. Eng.*, 2020, **8**, 10292–10302.

183 L. A. E. Müller, T. Zimmermann, G. Nyström, I. Burgert and G. Siqueira, *Adv. Funct. Mater.*, 2020, **30**, 2002914.
184 T. Kuhnt and S. Camarero-Espinosa, *Carbohydr. Polym.*, 2021, **252**, 117159.
185 H. Luo, R. Cha, J. Li, W. Hao, Y. Zhang and F. Zhou, *Carbohydr. Polym.*, 2019, **224**, 115144.
186 T. D. Ngo, A. Kashani, G. Imbalzano, K. T. Q. Nguyen and D. Hui, *Composites, Part B*, 2018, **143**, 172–196.
187 X. Sun, P. Tyagi, S. Agate, M. G. McCord, L. A. Lucia and L. Pal, *Carbohydr. Polym.*, 2020, **234**, 115898.
188 S. Singh, S. Ramakrishna and F. Berto, *Mater. Des. Process. Commun.*, 2019, **2**, 97.
189 H. Wu, W. P. Fahy, S. Kim, H. Kim, N. Zhao, L. Pilato, A. Kafi, S. Bateman and J. H. Koo, *Prog. Mater. Sci.*, 2020, **111**, 100638.
190 Y. Teramoto, *Adv. Powder Technol.*, 2020, **31**, 528–532.
191 A. Kazemian, X. Yuan, E. Cochran and B. Khoshnevis, *Constr. Build. Mater.*, 2017, **145**, 639–647.
192 X. Wang, M. Jiang, Z. Zhou, J. Gou and D. Hui, *Composites, Part B*, 2017, **110**, 442–458.
193 A. Balea, E. Fuente, M. C. Monte, N. Merayo, C. Campano, C. Negro and A. Blanco, *Molecules*, 2020, **25**, 526.
194 D. Miyashiro, R. Hamano and K. Umemura, *Nanomaterials*, 2020, **10**, 186.
195 Q. Wang, J. Sun, Q. Yao, C. Ji, J. Liu and Q. Zhu, *Cellulose*, 2018, **25**, 4275–4301.
196 Y. Yang, Y. Zhou, X. Lin, Q. Yang and G. Yang, *Pharmaceutics*, 2020, **12**, 207.
197 L. Dai, T. Cheng, C. Duan, W. Zhao, W. Zhang, X. Zou, J. Aspler and Y. Ni, *Carbohydr. Polym.*, 2019, **203**, 71–86.
198 D. Gethin, A. Rees, L. Powell, G. Chinga-Carassco, T. Claypole, D. Deganello, K. Hill, D. Thomas and K. Syverud, *Presented in part at the Advances in Printing and Media Technology*, United Kingdom, 2014.
199 K. De France, Z. Zeng, T. Wu and G. Nystrom, *Adv. Mater.*, 2020, e2000657, DOI: 10.1002/adma.202000657.
200 B. P. Sutliff, A. Das, J. Youngblood and M. J. Bortner, *Carbohydr. Polym.*, 2020, **231**, 115735.
201 X. Zeng, H. Chen, L. Chen and B. Zheng, *Food Chem.*, 2020, 128362, DOI: 10.1016/j.foodchem.2020.128362.
202 A. C. Heidenreich, M. Pérez-Recalde, A. González Wusener and É. B. Hermida, *Polym. Test.*, 2020, **82**, 106297.
203 T. Ma, L. Lv, C. Ouyang, X. Hu, X. Liao, Y. Song and X. Hu, *Carbohydr. Polym.*, 2021, **253**, 117217.
204 J. Jiang, H. Oguzlu and F. Jiang, *Chem. Eng. J.*, 2021, **405**, 126668.
205 Q. Zhang, L. Zhang, W. Wu and H. Xiao, *Carbohydr. Polym.*, 2020, **229**, 115454.
206 F. Ferreira, I. Pinheiro, S. de Souza, L. Mei and L. Lona, *J. Compos. Sci.*, 2019, **3**, 51.
207 J. Wang, A. Chiappone, I. Roppolo, F. Shao, E. Fantino, M. Lorusso, D. Rentsch, K. Dietliker, C. F. Pirri and H. Grgtzmacher, *Angew. Chem., Int. Ed.*, 2018, **57**, 2353–2356.
208 A. Tang, Q. Wang, S. Zhao and W. Liu, *Rapid Prototyp. J.*, 2018, **24**, 1265–1271.
209 J. M. Koo, J. Kang, S.-H. Shin, J. Jegal, H. G. Cha, S. Choy, M. Hakkarainen, J. Park, D. X. Oh and S. Y. Hwang, *Compos. Sci. Technol.*, 2020, **185**, 107885.
210 N. V. Challagulla, V. Rohatgi, D. Sharma and R. Kumar, *Curr. Opin. Chem. Eng.*, 2020, **28**, 75–82.
211 A. I. Cernencu, A. Lungu, I. C. Stancu, A. Serafim, E. Heggset, K. Syverud and H. Iovu, *Carbohydr. Polym.*, 2019, **220**, 12–21.
212 K. Markstedt, A. Escalante, G. Toriz and P. Gatenholm, *ACS Appl. Mater. Interfaces*, 2017, **9**, 40878–40886.
213 Z. Wang, J. Xu, Y. Lu, L. Hu, Y. Fan, J. Ma and X. Zhou, *Ind. Crops Prod.*, 2017, **109**, 889–896.
214 A. Cataldi, D. Rigotti, V. D. H. Nguyen and A. Pegoretti, *Mater. Today Commun.*, 2018, **15**, 236–244.
215 L. Wang, J. Palmer, M. Tajvidi, D. J. Gardner and Y. Han, *J. Therm. Anal. Calorim.*, 2018, **136**, 1069–1077.
216 L. M. Mariani, W. R. Johnson, J. M. Considine and K. T. Turner, *Cellulose*, 2019, **26**, 2639–2651.
217 V. Klar, J. Pere, T. Turpeinen, P. Karki, H. Orelma and P. Kuosmanen, *Sci. Rep.*, 2019, **9**, 3822.
218 L. M. Mariani, J. M. Considine and K. T. Turner, 2019, DOI: 10.1007/978-3-319-95083-9_9, 43–45.
219 V. Li, Doctor of Philosophy, Georgia Institute of Technology, 2019.
220 M. K. Hausmann, P. A. Ruhs, G. Siqueira, J. Lauger, R. Libanori, T. Zimmermann and A. R. Studart, *ACS Nano*, 2018, **12**, 6926–6937.
221 B. Wang, G. Ding, K. Chen, S. Jia, J. Wei, Y. Wang, R. He and Z. Shao, *J. Appl. Polym. Sci.*, 2020, **137**, 49164.
222 J. Wei, B. Wang, Z. Li, Z. Wu, M. Zhang, N. Sheng, Q. Liang, H. Wang and S. Chen, *Carbohydr. Polym.*, 2020, **238**, 116207.
223 C. Fey, J. Betz, C. Rosenbaum, D. Kralisch, M. Vielreicher, O. Friedrich, M. Metzger and D. Zdzieblo, *Mater. Sci. Eng., C*, 2020, **109**, 110613.
224 C. Ghibaudo, Master of Science, Politecnico di Torino, 2018.
225 S. S. Athukoralalage, R. Balu, N. K. Dutta and N. Roy Choudhury, *Polymers*, 2019, **11**, 898.
226 D. Chimene, R. Kaunas and A. K. Gaharwar, *Adv. Mater.*, 2020, **32**, e1902026.
227 J. Leppiniemi, P. Lahtinen, A. Paajanen, R. Mahlberg, S. Metsa-Kortelainen, T. Pinomaa, H. Pajari, I. Vikholm-Lundin, P. Pursula and V. P. Hytonen, *ACS Appl. Mater. Interfaces*, 2017, **9**, 21959–21970.
228 E. B. Heggset, B. L. Strand, K. W. Sundby, S. Simon, G. Chinga-Carrasco and K. Syverud, *Cellulose*, 2018, **26**, 581–595.
229 V. Kuzmenko, E. Karabulut, E. Pernevik, P. Enoksson and P. Gatenholm, *Carbohydr. Polym.*, 2018, **189**, 22–30.
230 Z. M. Jessop, A. Al-Sabah, N. Gao, S. Kyle, B. Thomas, N. Badiei, K. Hawkins and I. S. Whitaker, *Biofabrication*, 2019, **11**, 045006.
231 J. Gohl, K. Markstedt, A. Mark, K. Hakansson, P. Gatenholm and F. Edelvik, *Biofabrication*, 2018, **10**, 034105.

232 W. Xu, B. Z. Molino, F. Cheng, P. J. Molino, Z. Yue, D. Su, X. Wang, S. Willfor, C. Xu and G. G. Wallace, *ACS Appl. Mater. Interfaces*, 2019, **11**, 8838–8848.
233 H. P. S. A. Khalil, F. Jummaat, E. B. Yahya, N. G. Olaiya, A. S. Adnan, M. Abdat, N. A. M. Nasir, A. S. Halim, U. S. U. Kumar, R. Bairwan and A. B. Suriani, *Polymers*, 2020, **12**, 2043.
234 N. B. Palaganas, J. D. Mangadlao, A. C. C. de Leon, J. O. Palaganas, K. D. Pangilinan, Y. J. Lee and R. C. Advincula, *ACS Appl. Mater. Interfaces*, 2017, **9**, 34314–34324.
235 G. Siqueira, D. Kokkinis, R. Libanori, M. K. Hausmann, A. S. Gladman, A. Neels, P. Tingaut, T. Zimmermann, J. A. Lewis and A. R. Studart, *Adv. Funct. Mater.*, 2017, **27**, 1604619.
236 R. E. Abouzeid, R. Khiari, D. Beneventi and A. Dufresne, *Biomacromolecules*, 2018, **19**, 4442–4452.
237 V. C. F. Li, A. Mulyadi, C. K. Dunn, Y. Deng and H. J. Qi, *ACS Sustainable Chem. Eng.*, 2018, **6**, 2011–2022.
238 V. C.-F. Li, X. Kuang, A. Mulyadi, C. M. Hamel, Y. Deng and H. J. Qi, *Cellulose*, 2019, **26**, 3973–3985.
239 F. V. Ferreira, C. G. Otoni, K. J. De France, H. S. Barud, L. M. F. Lona, E. D. Cranston and O. J. Rojas, *Mater. Today*, 2020, **37**, 126–141.
240 M. Bordoni, E. Karabulut, V. Kuzmenko, V. Fantini, O. Pansarasa, C. Cereda and P. Gatenholm, *Cells*, 2020, **9**, 682.
241 P. Thomas, T. Duolikun, N. P. Rumjit, S. Moosavi, C. W. Lai, M. R. Bin Johan and L. B. Fen, *J. Mech. Behav. Biomed. Mater.*, 2020, **110**, 103884.
242 L. Bacakova, J. Pajorova, M. Tomkova, R. Matejka, A. Broz, J. Stepanovska, S. Prazak, A. Skogberg, S. Siljander and P. Kallio, *Nanomaterials*, 2020, **10**, 196.
243 M. Tavakolian, S. M. Jafari and T. G. M. van de Ven, *Nano-Micro Lett.*, 2020, **12**, 73.
244 B. Ates, S. Koytepe, A. Ulu, C. Gurses and V. K. Thakur, *Chem. Rev.*, 2020, **120**, 9304–9362.
245 N. J. Kanu, E. Gupta, U. K. Vates and G. K. Singh, *RSC Adv.*, 2019, **9**, 38209–38226.
246 Y. Xing, Master of Science, Northeastern University, 2017.
247 S. Nie, N. Hao, K. Zhang, C. Xing and S. Wang, *Cellulose*, 2020, **27**, 4173–4187.
248 R. Reshmy, E. Philip, S. A. Paul, A. Madhavan, R. Sindhu, P. Binod, A. Pandey and R. Sirohi, *Rev. Environ. Sci. Bio/Technol.*, 2020, **19**, 779–806.
249 S. Tuukkanen, S. Lehtimaki, F. Jahangir, A. P. Eskelinen, D. Lupo and S. Franssila, 2014, DOI: 10.1109/estc.2014.6962740, 1–6.
250 Y. Li, H. Zhu, Y. Wang, U. Ray, S. Zhu, J. Dai, C. Chen, K. Fu, S.-H. Jang, D. Henderson, T. Li and L. Hu, *Small Methods*, 2017, **1**, 1700222.
251 W. Chen, H. Yu, S. Y. Lee, T. Wei, J. Li and Z. Fan, *Chem. Soc. Rev.*, 2018, **47**, 2837–2872.
252 D. Cao, Y. Xing, K. Tantratian, X. Wang, Y. Ma, A. Mukhopadhyay, Z. Cheng, Q. Zhang, Y. Jiao, L. Chen and H. Zhu, *Adv. Mater.*, 2019, **31**, e1807313.
253 D. Lasrado, S. Ahankari and K. Kar, *J. Appl. Polym. Sci.*, 2020, **137**, 48959.
254 Y. Zhang, N. Hao, X. Lin and S. Nie, *Carbohydr. Polym.*, 2020, **234**, 115888.
255 J. Han, H. Wang, Y. Yue, C. Mei, J. Chen, C. Huang, Q. Wu and X. Xu, *Carbon*, 2019, **149**, 1–18.
256 H. Zhang, C. Dou, L. Pal and M. A. Hubbe, *BioResources*, 2019, **14**, 7494–7542.
257 K. P. Y. Shak, Y. L. Pang and S. K. Mah, *Beilstein J. Nanotechnol.*, 2018, **9**, 2479–2498.
258 S. F. Jin, Y. Chen and M. Liu, *Adv. Mater. Res.*, 2013, **662**, 198–201.
259 H. Voisin, L. Bergstrom, P. Liu and A. P. Mathew, *Nanomaterials*, 2017, **7**, 57–69.
260 D. Wang, *Cellulose*, 2018, **26**, 687–701.
261 H. Gu, X. Zhou, S. Lyu, D. Pan, M. Dong, S. Wu, T. Ding, X. Wei, I. Seok, S. Wei and Z. Guo, *J. Colloid Interface Sci.*, 2020, **560**, 849–856.
262 C. Zhu, S. Monti and A. P. Mathew, *Carbohydr. Polym.*, 2020, **229**, 115510.
263 S. Sultan, H. N. Abdelhamid, X. Zou and A. P. Mathew, *Adv. Funct. Mater.*, 2019, **29**, 1805372.
264 M. L. Soriano and C. Ruiz-Palomero, *Nanotechnol. Environ. Sci.*, 2018, 579–597.
265 T. Syrový, S. Maronová, P. Kuberský, N. V. Ehman, M. E. Vallejos, S. Pretl, F. E. Felissia, M. C. Area and G. Chinga-Carrasco, *J. Appl. Polym. Sci.*, 2019, **136**, 47920.
266 E. Niinivaara and E. D. Cranston, *Carbohydr. Polym.*, 2020, **247**, 116664.
267 S. Huang, X. Liu, C. Chang and Y. Wang, *Cellulose*, 2020, **27**, 2991–3011.
268 H. Françon, Z. Wang, A. Marais, K. Mystek, A. Piper, H. Granberg, A. Malti, P. Gatenholm, P. A. Larsson and L. Wågberg, *Adv. Funct. Mater.*, 2020, **30**, 1909383.
269 M. Bunger and K. Kersh, *Pruning the Cost of Bio-Based Materials and Chemicals*, Lux Research, United States of America, 2012.
270 G. Hewage, R. Kozarsky and V. Oh, *Navigating the Web of Bio-based Performance Materials*, Lux Research, United States of America, 2016.
271 C. Willard, *Nanocellulose*, Lux Research, United States of America, 2018.
272 X. An, D. Cheng, J. Shen, Q. Jia, Z. He, L. Zheng, A. Khan, B. Sun, B. Xiong and Y. Ni, *J. Bioresour. Bioprod.*, 2017, **2**, 45–49.
273 B. Shen, O. Erol, L. Fang and S. H. Kang, *Multifunct. Mater.*, 2020, **3**, 012001.
274 Y. Li, F. Zhang, Y. Liu and J. Leng, *Sci. China: Technol. Sci.*, 2020, **63**, 545–560.
275 M. H. Ali, A. Abilgaziyev and D. Adair, *Int. J. Adv. Des. Manuf. Technol.*, 2019, **105**, 701–717.
276 J. Tang, M. U. Javaid, C. Pan, G. Yu, R. M. Berry and K. C. Tam, *Carbohydr. Polym.*, 2020, **229**, 115486.
277 R. Nasseri, C. P. Deutschman, L. Han, M. A. Pope and K. C. Tam, *Mater. Today Adv.*, 2020, **5**, 100055.
278 S. Ma, Y. Zhang, M. Wang, Y. Liang, L. Ren and L. Ren, *Sci. China: Technol. Sci.*, 2019, **63**, 532–544.

279 M. Hervy, S. Evangelisti, P. Lettieri and K.-Y. Lee, *Compos. Sci. Technol.*, 2015, **118**, 154–162.
280 H. Gu, R. Reiner, R. Bergman and A. Rudie, in *Proceedings of the Life Cycle Assessment XV Conference*, Vancouver, Canada, 2015, pp. 33–42.
281 R. Arvidsson, D. Nguyen and M. Svanstrom, *Environ. Sci. Technol.*, 2015, **49**, 6881–6890.
282 Q. Li, S. McGinnis, C. Sydnor, A. Wong and S. Renneckar, *ACS Sustainable Chem. Eng.*, 2013, **1**, 919–928.
283 F. Piccinno, R. Hischier, S. Seeger and C. Som, *J. Cleaner Prod.*, 2018, **174**, 283–295.
284 K. Sahoo, R. Bergman, S. Alanya-Rosenbaum, H. Gu and S. Liang, *Sustainability*, 2019, **11**, 4722.
285 J. Turk, P. Oven, I. Poljanšek, A. Lešek, F. Knez and K. Malovrh Rebec, *J. Cleaner Prod.*, 2020, **247**, 119107.
286 D. Haldar and M. K. Purkait, *Carbohydr. Polym.*, 2020, **250**, 116937.
287 S. Sinquefield, P. N. Ciesielski, K. Li, D. J. Gardner and S. Ozcan, *ACS Sustainable Chem. Eng.*, 2020, **8**, 9601–9615.
288 Z. Jiang, B. Diggle, M. L. Tan, J. Viktorova, C. W. Bennett and L. A. Connal, *Adv. Sci.*, 2020, **7**, 2001379.
289 X. Wang, Q. Wang and C. Xu, *Bioengineering*, 2020, **7**, 40.
290 S. C. Daminabo, S. Goel, S. A. Grammatikos, H. Y. Nezhad and V. K. Thakur, *Mater. Today Chem.*, 2020, **16**, 100248.